ABSTRACT

Title of Document:	PLATE HEAT EXCHANGER IMPROVEMENTS WITH SHAPE OPTIMIZATION
	Radia Mohamed Fekry Eldeeb Doctor of Philosophy, 2018
Directed By:	Professor Reinhard Radermacher, Department of Mechanical Engineering

Plate Heat Exchangers (PHXs) are used in a wide variety of applications including, but not limited to Heating, Ventilation, Air-Conditioning, and Refrigeration (HVAC&R). PHXs are favored by the HVAC&R industry due to their compactness, flexible sizing, close approach temperature, and good heat transfer performance. PHXs are increasingly utilized and becoming very competitive in two-phase flow applications due to their desirable thermal-hydraulic characteristics. Pillow plate heat exchanger (PPHX) is a type of PHXs that consists of wavy plates that are welded together with a certain pattern using spot welding, sealed at the edges, and then inflated in a hydroforming process. PPHXs have an economic advantage over other types of PHXs due to their simple manufacturing process. Additionally, the complex wavy structure of the pillow plates creates an excellent heat transfer medium and thus, if their performance is optimized, they can potentially replace other types of PHXs in a wide range of applications. However, very limited research is done regarding the use of PPHXs in the HVAC&R and no research on their optimization is found in literature.

The first objective of this thesis is the optimization of PPHXs using four design parameters including their basic geometry parameters using Parallel Parameterized Computational Fluid Dynamics (PPCFD) and Approximation Assisted Optimization (AAO). The potential improvement in thermal-hydraulic performance is expected to be at least 50% as compared to existing designs. The second objective is to perform a comprehensive multi-scale analysis with topology and shape optimization integrating Non-Uniform Rational B-Splines (NURBS) to obtain a novel PPHX design with at least 20% improvement in thermal-hydraulic performance as compared to optimal chevron PHXs designs. This will improve energy efficiency significantly on the component level and potentially on the system level.

Finally, a comprehensive literature survey shows a significant gap regarding PHXs modeling with respect to combining robustness, accuracy, flexibility, and convenient speed into a single model. A current PHX computer model in literature is significantly improved in the aforementioned aspects using a novel algorithm. The model is also used as a component on a system level modeling to evaluate the performance of PHXs on the system level.

PLATE HEAT EXCHANGER IMPROVEMENTS WITH SHAPE OPTIMIZATION

by

Radia Mohamed Fekry Eldeeb

Dissertation submitted to the Faculty of the Graduate School of the
University of Maryland, College Park, in partial fulfillment
of the requirements for the degree of
Doctor of Philosophy
2018

Advisory Committee:
Professor Reinhard Radermacher, Chair
Professor Jungho Kim
Professor Bao Yang
Professor Jelena Srebric
Professor James Baeder
Dr. Vikrant Aute

Dedication

To Mohamed, Amira, Huda,
my family and all my teachers.

Acknowledgements

I would like to express my sincere gratitude for Dr. Radermacher for believing in me and giving me the opportunity to be a graduate student on his research team. My deepest gratitude and appreciation also goes to Dr. Aute who taught me how to do objective research without missing a detail, and who also was there for me as my teacher, and my friend throughout the hardships in my graduate years. Their continuous encouragement, patience, and advice throughout my graduate years are the main reason this work has been completed. I am very fortunate to have had the opportunity to work at the Center for Environmental Engineering (CEEE) under the leadership of Dr. Radermacher and the Modeling and Optimization Consortium (MOC) group led by Dr. Aute who provided for me enormous computing resources, flexibility to work from anywhere, and flexible working hours, without which this dissertation would have not been completed.

I would like to express my appreciation to all my teachers during my graduate studies who are also the members on this committee: Dr. Jungho Kim, Dr. Bao Yang, Dr. Jelena Srebric, and Dr. James Baeder. Every course I attended, I carry life lessons with me. I will always owe my teachers.

I would like to thank Dr. Hongtao Qiao for taking the time and effort to walk me through his code that I then inherited when I first started my work; Dr. Mohamed Beshr for his help and guidance during my first years, as well as teaching me a whole lot about programming and conducting research; Dr. Daniel Bacellar for his help and guidance and taking the time and effort to teach me about CFD simulation and

approximation assisted optimization. Dr. Bacellar was a dear colleague during courses and the most difficult of exams, as well as a generous teacher during our research years.

I would also like to express my thanks to Dr. Abdullah Aladbulkarem, Ms. Bracha Mandel, and Dr. John Bush who provided me with the experimental work for validation as well as sharing their experience and advice with me in my early years.

I would like to express my deepest thanks to Lopamudra Vemulapalli for her patience and providing me with a rich programming experience; Dr. Jiazhen Ling who provided me with guidance, follow up, and help from the first day to the last in my studies.

I would like to express my great thanks and appreciation to Mr. James Tancabel who provided me with his own computational resources to help me complete this work on time. He is indeed a great selfless colleague. I would like to thank all my colleagues who helped me with any technical issue while I was working from another state during my last two years: James Tancabel, Ransisi Huang, Zhenning Li, and Rohit Dhumane.

I would also like to thank Mary Baugher and Tanya Pringle for their administrative support throughout the years.

Whatever I say, I will never be able to express how grateful I am to my parents. I grew up in a tough environment where success in basic life aspects is not something to be taken for granted. My parents gave me all the reasons not only to succeed but also to be distinguished. Without the encouragement of my father, Dr. Fekry Eldeeb, and my mother, Dr. Nashwah AbdelKhalick, I would not be presenting this work today. I would also like to express my thanks to my sisters; Dr. Rowayda Eldeeb and Miss Rania Eldeeb, for their continuous encouragement and always being there for me; my whole family, and my husband's family, especially my mother-in-law, who supported me

infinitely by every way she could. She passed away during my graduate years, but she will remain the best of my friends, and source of inspiration and optimism, and she will always be remembered. I would also like to express my love and gratitude to my close friends who always poured positive energy, encouraging words, and love into my life, Eman Ahdy, Ghada Abobakr, Marwa Ismail, and Dr. Nourhan Ayyad, and their families.

It takes a village to raise a child, and I was blessed by two beautiful girls during my graduate years, Amira and Huda, with my husband, colleague, and best friend, Dr. Mohamed Beshr. I would like to express my heartfelt appreciation to those who took care of my babies during the past three years, which was crucial for me to focus on my work, including my dearest best friend Eman Ahdy, who supported me during my hardest of times; Fouzeya, Amira's caregiver in Maryland; Samantha Waelchli, the girls' nanny in North Carolina; Aisha Khader, Amira's teacher in North Carolina.

Last, but not least, no words can express how grateful I am towards my husband, Dr. Mohamed Beshr, who is the greatest blessing of my life. He believes in me like no other, he generously gives me unlimited support, and he is a loving husband and father.

Table of Contents

List of Tables

List of Figures

List of Abbreviations

Acronyms

A	heat transfer area (m^2)
b	corrugation pitch (m)
Bo	Boiling number (dimensionless)
C_p	specific heat ($J \cdot kg^{-1} \cdot K^{-1}$)
Co	Convection number (dimensionless)
d	diameter (m)
d_h	hydraulic diameter (m)
e	relative error fraction (dimensionless)
f	Darcy friction factor (dimensionless)
Fr	Froude number (dimensionless)
Ga	Galileo number (dimensionless)
g	gravitational acceleration ($m \cdot s^{-2}$)
G	mass flux ($kg \cdot m^{-2} \cdot s^{-1}$)
h	convective heat transfer coefficient ($W \cdot m^{-2} \cdot K^{-1}$)
h_p	pillow height (m)
h_w	weld height (m)
Ja	Jacob number (dimensionless)
k	thermal conductivity, ($W \cdot m^{-1} \cdot K^{-1}$)
L	length (m)

M	molecular number
Nu	Nusselt number (dimensionless)
p	pressure (Pa)
Pr	Prandtl number (dimensionless)
Q	total heat transfer (W)
$q"$	heat flux ($W \cdot m^{-2}$)
Re	Reynolds number (dimensionless)
s	welding spot pitch (m)
T	temperature (K)
U	Overall heat transfer coefficient ($W \cdot m^{-2} \cdot K^{-1}$)
WHR	weld width-height ratio (-)
w_w	weld width (m)
u	velocity ($m \cdot s^{-1}$)
V	volume (m^3)
X_{tt}	Lockhart-Martinelli parameter
x	vapor quality

Greek Symbols

α	thermal diffusivity ($m^2 \cdot s$)
β	chevron angle ($^\circ$)
γ	latent heat of vaporization ($J \cdot kg^{-1}$)
ε_M	Eddy diffusivity ($m^2 \cdot s$)
Δ	difference

ν	kinematic viscosity ($m^2 \cdot s$)
ρ	density ($kg \cdot m^{-3}$)
ϕ	two-phase multiplier (dimensionless)
φ	surface enlargement factor (dimensionless)
μ	dynamic viscosity ($Pa \cdot s$)
ω	accentric factor

Subscripts

c	critical
cb	convective boiling
cr	critical
eq	equivalent
emp	empirical
g	Vapor
h	hydraulic
l	liquid
L	longitudinal
m	mean
nb	nucleate boiling
red	reduced
sat	saturation
sp	spot weld
T	transverse

tt	turbulent-turbulent
w	wetted
$wall$	wall

Abbreviations

AAO	Approximation Assisted Optimization
BPHX	Brazed Plate Heat Exchangers
CFC	Chloro-Fluoro-Carbons
CFD	Computational Fluid Dynamics
DoE	Design of Experiments
EIA	Energy Information Adminstration
FEM	Finite Element Modeler
FF	Fluid Flow
GA	Genetic Algorithm
GCI	Grid Convergence Index
GWP	Global Warming Potential
HFC	Hydro-Fluoro-Carbons
HVAC&R	Heating, Ventilation, Air Conditioning, and Refrigeration
MAS	Metamodel Acceptability Score
MOGA	Multi-Objective Genetic Algorithm
ODP	Ozone Depletion Potential
PHX	Plate Heat Exchanger
PPHX	Pillow Plate Heat Exchanger

SS	Static Structural

Chapter 1: Introduction

1.1. Motivation

The heating, ventilating, and air conditioning energy consumption accounts for a great portion of energy consumption in buildings. In 2016, according to the U.S. Energy Information Administration (EIA), about 40% of total U.S. energy was consumed in residential and commercial buildings, or about 39 quadrillion British thermal units, while this number is projected to increase by 6.7% in 2040 [1]. The HVAC&R industry is also under scrutiny for the negative environmental impact associated with the refrigerant production, disposal, and leakage in the equipment, which caused ozone layer depletion and global warming. Heat exchangers, being an essential part of the heat transfer process in HVAC&R equipment, play a crucial role in energy consumption and the consequent environmental impact. Designing heat exchangers with high heat transfer effectiveness can directly greatly reduce the total energy consumption by buildings.

Plate Heat Exchangers (PHXs) were introduced to the dairy industry in the late 1800s. Later improvements to the plate designs, sealing aspects, and other mechanical issues allowed them to gain success in many industries including, but not limited to, HVAC&R, food processing, chemical industry, marine, and energy generation systems. PHXs are highly compact and therefore require less refrigerant charge than

other heat exchangers. Turbulence is readily achieved due to flow separation which takes place as a result of the corrugated pattern and thus the required surface area for heat transfer is smaller than the surface area needed by other types of heat exchangers as well. Low charge is favored by the HVAC&R industry because it decreases the environmental impact of refrigerants and lowers inventory costs, while turbulence enhances heat transfer. Overall, PHXs are characterized by high effectiveness of heat transfer which is highly required in the competitive heat exchanger industry.

Brazed plate heat exchangers (BPHX) consist of a pack of thin metal or metal alloy (usually stainless steel) plates and two end plates, which are brazed together using a brazing material, such as copper or nickel for ammonia applications, where two or more fluids flow in between the plates and exchange thermal energy. BPHXs are favored by the HVAC&R industry due to concerns over refrigerant leakage and high compactness. They can be used for high temperature and high pressure applications, including water-cooled evaporators and condensers refrigeration applications, as well as process water heating and heat recovery in various applications [2].

It is however challenging to improve PHX design as they tend to be more expensive since the manufacturing process requires a special die for every new plate design. Pillow plate heat exchanger (PPHX), on the other hand, is a type of PHXs with complex wavy structure creating a flow channel with a fully developed turbulent flow that requires simple welding processes and a hydroforming process. Thus, the manufacturing process of PPHXs is simpler and way more economical than other types of PHXs. Additionally, PPHX has favorable high structural stability and a sealed

construction since it is fully welded. There is also more flexibility in the design of pillow plates which also makes it an excellent candidate for optimization and further miniaturization in order to reduce the material and refrigerant charge needed for the same thermal-hydraulic performance. PPHXs, therefore, have great potential to outperform existing types of PHXs such as chevron PHXs due to their compactness, easier more economic manufacturing process, lower capital cost, and close approach temperature. The thermal-hydraulic performance of the pillow plate is affected by the longitudinal and transverse pitches between the spot welds, the shape and size of the weld, the thickness of the plate, and the height of the pillow. Since the structure of the PPHX is fully welded, it has high structure stability and a sealed construction which is very favorable. There is also a great flexibility in the design of the plate geometry since the geometry of the plate can be varied easily using very similar equipment unlike chevron plate, for example, where every new design might need a special die to manufacture.

In order to find heat exchanger designs that significantly improve the energy consumption figure, while delivering the same performance, as well as minimize the environmental negative impact, it is highly desirable to miniaturize PHXs. This can be achieved by optimizing the performance of PPHXs using approximation techniques since it is computationally very expensive to numerically simulate the 3D volume of PHXs. This will allow for seizing the economic advantage while benefiting from the favorable characteristics. PPHXs are however in a very early stage of research and development, so it is desired to explore the optimization of their thermal-hydraulic

performance. This research proposes novel PPHX designs using multi-scale analysis with shape optimization.

1.2. Literature Review

1.2.1. Heat Transfer Coefficient and Pressure Drop Correlations

Due to the cost of building and testing PHX prototypes, it is desired to predict the performance of different PHX designs using numerical models. However, in order to be able to accurately predict the performance of PHXs, reliable heat transfer coefficient and pressure drop correlations are required to be used in such models. Several studies on single-phase heat transfer correlations, however specific in nature, are present in literature, while studies on two-phase heat transfer correlations are more limited. A summary of important single-phase correlations can be found in Ayub [3] and in Khan and Chyu [4]. Unlike single-phase heat transfer, two-phase heat transfer in PHXs is a function of various parameters such as the plate surface structure, heat flux, mass flux, vapor quality, film thickness, flow regime, dry out, and effects of lubricant oils. Thus, it is more challenging to obtain a general correlation that would take into account the effects of all these parameters.

Due to the negative impacts and serious destruction caused by CFC refrigerants to the ozone layer, and due to the global warming potential caused by other HFC refrigerants, lower GWP and natural refrigerants are becoming more favorable in air-conditioning and refrigeration applications. Ammonia is widely used in industrial processes in PHXs [3] as the ODP and the GWP of ammonia are zero. However, limited research has been

conducted for two-phase flow on natural refrigerants in PHXs and correlations on natural refrigerant mixtures are scarce.

1.2.1.1. Flow Boiling Heat Transfer

Evaporation heat transfer in PHXs is the result of nucleate boiling and forced convection boiling, each contributing to the heat transfer coefficient. In the nucleate boiling region, the heat transfer coefficient is mainly dependent on heat flux, while in the forced convection region the heat transfer coefficient is mainly dependent on the vapor quality and the mass flux. Since the data available on boiling heat transfer in PHXs is limited, it is still not clear which boiling mechanism is dominant in PHXs. Some of the current published work concluded that the main boiling mechanism is nucleate boiling [5, 6], while other work concluded that it is only forced convective boiling [7, 8]. Others considered both effects [9, 10, 11]. However, forced convective boiling has been associated with experiments carried out at high mass fluxes, typical in PHXs operating as flooded evaporators, while nucleate boiling is associated with experiments carried out at low mass fluxes, and high heat fluxes, typical in PHXs operating as direct expansion evaporators [12].

Studies on evaporation generally focus on the evaporation of pure refrigerants and near azeotropic mixtures for refrigeration and air-conditioning applications, while work on zeotropic mixtures is rather scarce. Panchal et al. [10] investigated the boiling of ammonia and R22 in various PHXs with different chevron angles and different geometries. They found that the overall heat transfer coefficient is higher when using

plates with higher chevron angles. Palmer et al. [13] measured the average Nusselt numbers during evaporation and condensation of R22, R290 (propane), R290/600a (propane/isobutane), and R32/152a in the presence of lubricant oils inside a BPHX at low mass fluxes. Two correlations are developed using typical system operating conditions allowing the correlations to be used for actual system designs.

The group of Lin investigated the evaporation heat transfer and pressure drop of R134a [14, 15], and R410A [9, 16] in a single-channel vertical BPHX with a chevron angle of 60°. They showed that even at a lower mass flux, the boiling heat transfer coefficient in BPHX is higher than that for a circular pipe with a higher mass flux obtained under similar operating conditions, especially at higher vapor quality, where forced convection is more dominant and the flow in the BPHX is highly turbulent. For R134a [14], the heat transfer coefficient increases almost exponentially with vapor quality, while it increases further with higher mass fluxes. For R410A [9], the boiling heat transfer coefficient and the frictional pressure drop increase with the refrigerant mass flux and vapor quality. The heat transfer coefficient increases significantly with imposed heat flux, and is slightly influenced by the system pressure. The frictional pressure drop increases with imposed heat flux, and decreases at higher system pressure.

Han et al. [7] conducted experiments on R410A and R22. Three chevron angles were used in their investigation: 20°, 35°, and 45°. The values of the heat fluxes used are much lower than those used by Hsieh and Lin [9]. They concluded that both the boiling heat transfer coefficient and pressure drop increases with mass flux and vapor quality,

while they decrease with saturation temperature and chevron angle. Ayub [3] used field data of ammonia and R22 to develop a heat transfer coefficient correlation using chevron angles in the range of 30˚ to 65˚. Park and Kim [17] experimentally investigated the effects of vapor quality, mass flux, average heat flux, and saturation temperature on the heat transfer characteristics of R134a in an oblong shell and plate heat exchanger, which has the same underlying flow configuration as conventional PHXs. They reported an increase in the heat tranfer coefficient with a mass flux at high vapor qualities, and with heat flux and correlated their results by using a modified Yan and Lin [14] correlation. Using the same heat exchanger, Kim et al. [18] investigated the evaporation heat transfer characteristics of R410A. In this case, the boiling heat transfer coefficient increased with both mass flux and average heat flux, with an increased effect of mass flux, and a decreased effect on saturation temperature. Longo and Gasparella [6] investigated the evaporation of R134a, which yield similar results and supports their conclusion about nucleate boiling domination.

Palm and Claesson [5] concluded that the heat transfer in PHXs is governed by heat flux rather than mass flux, indicating that nucleate boiling is dominant, and the chevron angle has no effect on evaporation. They also showed that the heat transfer performance can be predicted by the Cooper correlation [19], as well as other pool boiling correlations. This conclusion is also indicated by Longo [20]. Longo et al. [21] developed a numerical model for predicitng nucleate and convective boiling using 251 experiemtal data points obtained by their research group. The model is compared to 505 experiemntal data from different research groups showing an absolutle percentage

deviation of 20%. Sterner and Sunden [22] concluded that using an inlet flow distributor improves the heat transfer performance and makes it more stable, although it also increases the pressure drop. They developed three different correlations for the boiling of ammonia for three different PHXs. Ouazia [23] studied the upward flow boiling of R134a in PHXs with different chevron angles. It was concluded that the heat transfer performance is independent of the heat flux, while it is sensitive to flow conditions, such as vapor quality, mass velocity, and to the chevron angle used. The correlation provided contains various constants that are functions of plate geometry and inlet flow conditions. It is unclear how this correlation can be applied in practical situations. Djordjevic and Kabelac [24] studied the flow boiling of R134a and ammonia in a PHX, and reported that the heat transfer coefficient of ammonia is greater than that of R134a and that the heat transfer coefficient is dependent on both mass flux and heat flux indicating that both nucleate boiling and convective boiling take place. No correlation is developed. Arima et al. [8] investigated the local boiling heat transfer of ammonia in a vertical flat PHX with low mass fluxes. They concluded that forced convection boiling is dominant in their experiments and reassured this finding by fluid visualization. The local boiling heat transfer coefficient increases with vapor quality up to a vapor quality of 0.7. Then dry out takes place, and the heat transfer coefficient dramatically decreases. Unlike other findings [14], a change in mass flux shows no effect on boiling heat transfer. However, the mass fluxes used in their experiments are relatively low.

Khan and Chyu [4] and Khan et al. [25] investigated the evaporation of ammonia and ammonia with miscible oil in flooded, in corrugated PHXs with 30°, 60°, and mixed 30°/60° chevron angle configurations. The boiling heat transfer coefficient is found to increase with chevron angle and saturation temperature. The effect of mass flux is found to be negligible. Their data compared well with Ayub's [3] direct expansion correlation. The study also found that the pressure drop increases with mass flux and chevron angle, while decreases with saturation temperature. They concluded that both nucleate boiling and convective boiling mechanisms take place, with convective boiling dominating the higher heat flux and exit vapor quality regimes.

Huang et al. [26] investigated the evaporation of R134a and R507A in three different PHXs with different plate configurations. Based on data from their experiments and other field data for ammonia and R12, they developed empirical correlations for predictng the refrigerant boiling heat transfer coefficient and the two-phase frictional pressure drop. Their heat transfer data shows a strong dependence on heat flux and a weak dependence on mass flux, vapor quality, and chevron angle, concluding the domination of nucleate boiling process. The pressure drop data shows a strong dependence on mass flux and vapor quality. Pressure drop is also found to be higher in PHXs with higher chevron angles.

Táboas et al. [11] studied the evaporation of ammonia/water mixtures in a vertical PHX. The concentration of ammnoia varies from 0.42 to 0.62, a range in which no significant effects were shown. The study revealed that the heat transfer coefficient increases sharply with vapor quality at very low qualities, afterwhich the vapor quality

has little influence except for on higher mass fluxes, where it increases with quality more significantly. The results also showed little influence of heat flux on the heat transfer coefficient, while the mass flux has a significant effect which suggests forced convective boiling. Táboas et al. [27] used these experimental results to propose two correlations for nucleate and forced convective boiling. They set a criterion for the transition from nucleate boiling to forced convective boiling according to the superficial velocity of liquid and vapor.

Lee et al. [28] studied flow boiling of water in a PHX at low mass flux. They concluded that the dominant heat transfer regime is convective boiling due to a low $Bo \cdot X_{tt}$ number, and that the heat transfer coefficient decreases with increasing vapor quality unlike most of other studies. They proposed a pre-partial dry-out correlation and a post-partial dry-out correlation, in addition to a frictional pressure drop correlation. It is generally difficult to get local measurements in PHXs especially BPHX, thus, most of the evaporation correlations compute the average heat transfer coefficients except for Arima et al. [8] which computes the local heat transfer coefficient. Amalfi et al. [29] proposed a generalized correlation that is based on dimensional analysis. The proposed correlation is developed using 1903 data points and a wide range of operating conditions, plate geometries, and fluids, including ammonia and ammonia/water mixture. This correlation shows that the potential improvement and development of a generalized correlation for flow boiling in PHXs is possible. Most recently, Lee et al. [30] investigated the heat transfer coefficient and pressure drop in a corrugated BPHX using the refrigerant R1233zd(E). They concluded that the heat transfer coefficient of

this refrigerant is independent of heat flux concluding that convective boiling flow is in place. Instead, the heat transfer coefficient in their experiments is dependent on mass flux and vapor quality. On the other hand, the pressure drop is a function of the mass flux, vapor quality, and saturation pressure. They developed correlations for heat transfer coefficient and pressure drop for this refrigerant. This is apparently a continuous effort especially with new refrigerants emerging. All correlations are presented in Table 1.

Table 1: Boiling heat transfer and pressure drop correlations.

Investigator	Correlation	Comments
Yan and Lin [14]	$h = 1.926\left(\frac{k_l}{D_h}\right)\mathrm{Re}_{eq}\,\mathrm{Pr}_l^{1/3}\,Bo_{eq}^{0.3}\,\mathrm{Re}^{-0.5}$ $where\ \mathrm{Re}_{eq} = \frac{G_{eq}D_h}{\mu_l}, Bo_{eq} = \frac{q_w^{"}}{G_{eq}\cdot\gamma},$ $G_{eq} = G\left[(1-x_m) + x_m\left(\frac{\rho_l}{\rho_g}\right)\right]^{1/2}$ $h = 1.926\left(\frac{k_l}{D_h}\right)\mathrm{Re}_{eq}\,\mathrm{Pr}_l^{1/3}\,Bo_{eq}^{0.3}\,\mathrm{Re}^{-0.5}$ $where\ \mathrm{Re}_{eq} = \frac{G_{eq}D_h}{\mu_l}, Bo_{eq} = \frac{q_w^{"}}{G_{eq}\cdot\gamma},$ $G_{eq} = G\left[(1-x_m) + x_m\left(\frac{\rho_l}{\rho_g}\right)\right]^{1/2}$ $f = 6.947\times10^5\cdot\mathrm{Re}_{eq}^{-1.109}\cdot\mathrm{Re}^{-0.5},\ for\ \mathrm{Re}_{eq} < 6{,}000$ $f = 31.21\cdot\mathrm{Re}_{eq}^{0.04557}\cdot\mathrm{Re}^{-0.5},\ for\ \mathrm{Re}_{eq} \geq 6{,}000$	R134a, Chevron plate, based on plate effective corrugated area, $\beta = 60°$, 8.3% deviation for heat transfer coefficient and 7% deviation for friction factor. $2{,}000 < \mathrm{Re}_{eq} < 10{,}000,$ $55 \leq G \leq 70,$ $11 \leq q" \leq 15,$ $0.1 \leq x_m \leq 0.9$ $0.675 \leq p \leq 0.8$

Palmer et al. [13]	$h = 2.7\left(\frac{k_l}{D_h}\right)\mathrm{Re}_l^{0.55}\,\mathrm{Pr}_l^{0.5}$, (R22, R290, R290/600a) $h = \left(\frac{k_l}{D_h}\right)Nu_l^{0.42}Fr^{0.088}\omega^{1.5}Co^{1.5}M^{1.5}$ where for R32/R152a, $Nu_l = 0.16\,\mathrm{Re}_l^{0.89}\,\mathrm{Pr}_l^{0.4}$, $Fr = \frac{G^2}{\rho^2 g D_h}$, $Co = \left(\frac{\rho_g}{\rho_l}\right)^{0.5}\left\{\frac{(1-x)}{x}\right\}^{0.8}$, $\omega = -\log_{10}(p/p_{cr})$	R22, R290, R290/600a, R32/R152a, $13 < \mathrm{Re}_{eq} < 230$, $1.6 \le G \le 19$, $1.3 \le q'' \le 8.3$
Ouazia [23]	$h = a\frac{k_l}{D_h}\left(\frac{G(1-x)D_h}{\mu_l}\right)^b \mathrm{Pr}_l^{1/3}\left(\frac{\mu_l}{\mu_w}\right)^{0.17}\left[1 + C_1\left(\frac{1}{X_{tt}}\right)^{C_2}\right]$	R134a, based on developed surface area, $\beta = 0°, 30°, 60°$, 30% deviation a & b depend on plate geometry. C_1 & C_2 depend on inlet condition
Hsieh et al. [15]	$h = h_{l,emp}\left[1.2Fr^{0.75} + 13.5Bo^{1/3}Ja^{1/4}\right]$, $h_{l,emp} = 0.2092\left(\frac{k_l}{D_h}\right)\mathrm{Re}^{0.78}\,\mathrm{Pr}^{1/3}\left(\frac{\mu_m}{\mu_w}\right)^{0.14}$ $where,\ Fr = \frac{G^2}{\rho_l^2 g D_h},\ Ja = \frac{\rho_l C_p \Delta T_{sat}}{\rho_g \gamma}$	R134a, Chevron plate, based on plate effective corrugated area, $\beta = 60°$ Subcooled flow boiling $50 \le G \le 200,\ 8.5 \le q'' \le 30$

Hsieh and Lin [9]	$h = h_{l,emp}\left(88Bo^{0.5}\right)$ $f = 61{,}000\,\mathrm{Re}_{eq}^{-1.25}$ $where,$ $\mathrm{Re}_{eq} = \frac{G_{eq} D_h}{\mu_l},$ $G_{eq} = G\left[(1 - x_m) + x_m\left(\frac{\rho_l}{\rho_g}\right)^{1/2}\right]$	R410A, Chevron plate, based on plate effective corrugated area, $\beta = 60°$ $50 \le G \le 125,$ $5 \le q'' \le 35,$ $T_{sat} = 10°C,\ 15°C,\ 20°C$
Han et al. [7]	$h = Ge_1\left(\frac{k_l}{D_h}\right)\mathrm{Re}_{eq}^{Ge_2}\,\mathrm{Pr}^{0.4}\,Bo_{eq}^{0.3},$ $where \begin{cases} Ge_1 = 2.81\left(\frac{b}{D_h}\right)^{-0.041}\left(\frac{\pi}{2} - \beta\right)^{-2.83} \\ Ge_2 = 0.746\left(\frac{b}{D_h}\right)^{-0.082}\left(\frac{\pi}{2} - \beta\right)^{0.61} \end{cases}$ $f = Ge_3\,\mathrm{Re}_{eq}^{Ge_4},$ $where \begin{cases} Ge_3 = 64{,}710\left(\frac{b}{D_h}\right)^{-5.27}\left(\frac{\pi}{2} - \beta\right)^{-3.03} \\ Ge_4 = -1.314\left(\frac{b}{D_h}\right)^{-0.62}\left(\frac{\pi}{2} - \beta\right)^{-0.47} \end{cases}$ $and\ \ \mathrm{Re}_{eq} = \frac{G_{eq} D_h}{\mu_l}, G_{eq} = G\left[(1 - x_m) + x_m\left(\frac{\rho_l}{\rho_g}\right)^{1/2}\right]$	R410A, R22, $\beta = 20°, 35°, 45°$, heat transfer coefficient agreed within 25%, pressure drop agreed within 15%. $13 \le G \le 34,$ $2.5 \le q'' \le 8.5,$ $T_{sat} = 5°C,\ 10°C,\ 15°C$

Park and Kim [17]	$h = 532.2\left(\frac{k_l}{D_h}\right)\mathrm{Re}_{eq}^{0.3237}\, Bo_{eq}^{0.3}\,\mathrm{Pr}^{1/3}\,\mathrm{Re}^{-0.5}$ $where,$ $\mathrm{Re}_{eq} = \frac{G_{eq} D_h}{\mu_l},$ $Bo_{eq} = \frac{q''_w}{G_{eq}\cdot\gamma},$ $G_{eq} = G\left[(1-x_m) + x_m\left(\frac{\rho_l}{\rho_g}\right)^{1/2}\right]$	R134a, based on effective corrugated area, $\beta = 45°$ $45 \le G \le 55,$ $T_{sat} = 10°C,\ 15°C,\ 20°C$ $4 \le q'' \le 8,$ $0.1 \le x_m \le 0.8$ Oblong shell and plate heat exchanger
Ayub [3]	$h = C\left(\frac{k_l}{D_h}\right)\left[\frac{\mathrm{Re}_l^2\,\gamma}{L}\right]^{0.4124}\left(\frac{p}{p_{cr}}\right)^{0.12}\left(\frac{65}{\beta}\right)^{0.35}$ [Btu/hr-ft^2-°F] $f = 4\times\left[\left(n/\mathrm{Re}^m\right)\left(-1.89+6.56R-3.69R^2\right)\right],\ R = \beta/30$ $\begin{cases} C = 0.1121\ for\ flooded\ and\ thermo\text{-}syphon \\ C = 0.0675\ for\ direct\ \exp ansion \end{cases}$	Ammonia, R22, based on the projected area, $30° < \beta < 65°,$ $4{,}000 \le \mathrm{Re} < 16{,}000,$ US units
Sterner and Sunden [22]	$h = C\left(\frac{k_l}{D_h}\right)\mathrm{Re}_l^m\, Ja^n Co^p$ $Ja = \frac{C_{p,l}\rho_l \Delta T_{in}}{\gamma\rho_g},\ Co = \left(\frac{1-x}{x}\right)^{0.8}\left(\frac{\rho_g}{\rho_l}\right)^{0.5}$	Ammonia, $\beta = 59°,\ 65°,$ $50 < \mathrm{Re}_l < 225,$ $12 < q'' < 185$ $0.5 < G < 0.9,$ $0.05 < x < 1.0$ $-6°C < T_{sat} < -3°C$

Kim et al. [18]	$h = 5.323\left(\frac{k_l}{D_h}\right)\mathrm{Re}_{eq}^{0.42}\,\mathrm{Pr}^{1/3}$ $where\ \mathrm{Re}_{eq} = \frac{G_{eq} D_h}{\mu_l}, G_{eq} = G\left[(1 - x_m) + x_m\left(\frac{\rho_l}{\rho_g}\right)^{1/2}\right]$	R410A, based on effective corrugated area, $\beta = 45°$, $600 < \mathrm{Re} < 2{,}300$, $40 \le G \le 80$, $4 \le q'' \le 8$, $0.1 \le x_m \le 0.9$, $0°C \le T_{sat} \le 10°C$ Oblong shell and plate heat exchanger
Arima et al. [8]	$h = 16.4 h_{l,eq}\left(\frac{1}{X_{vv}}\right)^{1.08}$ $h_{l,eq} = 0.023\left(\frac{k_l}{D_h}\right)\left[\frac{G(1-x)D_h}{\mu_l}\right]^{0.8}\mathrm{Pr}_l^{0.4}$ $X_{vv} = \left(\frac{1-x}{x}\right)^{0.5}\left(\frac{\rho_g}{\rho_l}\right)^{0.5}\left(\frac{\mu_l}{\mu_g}\right)^{0.5}$ (laminar-laminar)	Ammonia, local heat transfer coefficient, flat plate, agreed within 25% of their data, $40 < \mathrm{Re} < 3600$, $7.4 \le G \le 15$, $15.4 \le q'' \le 24.5$, $0.1 \le x \le 0.9$, $0.7 \le p \le 0.9$ Dry out at $x > 0.7$
Khan and Chyu [4], and	$h = \left(-173.52\frac{\beta}{60} + 257.12\right)\left(\frac{k_l}{D_h}\right)\left(\mathrm{Re}_{eq}\, Bo_{eq}\right)^{\left(-0.09\frac{\beta}{60} + 0.0005\right)} p^{*\left(0.624\frac{\beta}{60} - 0.822\right)}$	Ammonia, Chevron plate, based on

Khan et al. [25]	$f = 4 \times 305{,}590\,\mathrm{Re}_{eq}^{-1.26}\, p^{*0.9}$ $where,$ $p^* = \frac{p}{p_c},$ $\mathrm{Re}_{eq} = \frac{G_{eq} D_h}{\mu_l},$ $G_{eq} = G\left[(1 - x_m) + x_m\left(\frac{\rho_l}{\rho_g}\right)\right]^{1/2}$	effective heat transfer area, heat transfer coefficient over predicts data for symmetric plates by 6% and under predicts data for mixed configuration by 10%, error band of ±10%. $30° \le \beta \le 60°$ $500 < \mathrm{Re} < 2{,}500,$ $3.5 < \mathrm{Pr} < 6,$ $1{,}225 < \mathrm{Re}_{eq} < 3{,}000,$ $5.5 < G < 27$ $20 \le q'' \le 70,$ $0.1 \le x \le 0.9$ $-2°C \le T_{sat} \le -25°C$
Táboas et al. [27]	$h = \begin{cases} h_{nb} = 5Bo^{0.15} h_l, & \text{for } u_g < -111.88u_l + 11.848 \\ \max(h_{nb}, h_{cb}), & \text{for } u_g > -111.88u_l + 11.848 \end{cases}$ $u_g = \frac{G \cdot x}{\rho_g}, u_l = \frac{G \cdot (1 - x)}{\rho_l},\ h_{cb} = (\phi^2_{Chisholm})^{0.2} h_l$ $\phi^2_{Chisholm} = 1 + \frac{C}{X_{tt}} + \frac{1}{X_{tt}^2},\ C = 3$ $0.42 \le \text{Ammonia Concentration} \le 0.62$	Ammonia/water mixture, based on nominal area, $70 \le G \le 140,$ $20 \le q'' \le 50,$ $0.0 \le x_m \le 0.22,$ $0.7 \le p \le 1.5$

Huang et al. [26]	$h = 1.87\times10^{-3}\cdot\left(\frac{k_l}{D_h}\right)\left(\frac{q''d_0}{k_l T_{sat}}\right)^{0.56}\left(\frac{\gamma d_0}{\alpha_l^2}\right)\mathrm{Pr}_l^{0.33}$, $\alpha = \frac{k}{\rho C_p}, d_0 = 0.0146\theta\left[\frac{2\sigma}{g(\rho_l-\rho_g)}\right]^{0.5}, \theta = 35°$ $f = \frac{3.81\times10^4\cdot F_{R,f}}{\mathrm{Re}_{tp}^{0.9}(\rho_l/\rho_g)^{0.16}}$, $\mathrm{Re}_{tp} = \frac{GD_h}{\mu_{tp}}$, $\mu_{tp} = \rho_m\left[\frac{x_m\mu_g}{\rho_g}+(1-x_m)\frac{\mu_l}{\rho_l}\right], \rho_m = \left[\frac{x_m}{\rho_g}+\frac{(1-x_m)}{\rho_l}\right]^{-1}$ $F_{R,f} = 0.183R^2 - 0.275R + 1.10, R = \beta/30°$	Mainly R134a, and R507A, and few with Ammonia, and R12 (222 data points) $28° < \beta < 60°$ $5.6 \le G \le 52.3,$ $1.8 \le q'' \le 6.9$ $5.9°C \le T_{sat} \le 13°C$
Lee et al. [28]	$h = 98.7\left(\frac{k_l}{D_h}\right)\left(\frac{\mathrm{Re}_g}{\mathrm{Re}_l}\right)^{-0.0848} Bo^{-0.0597} X_{tt}^{0.0973}, \frac{\mathrm{Re}_g}{\mathrm{Re}_l} < 9.0$ $h = 234.9\left(\frac{k_l}{D_h}\right)\left(\frac{\mathrm{Re}_g}{\mathrm{Re}_l}\right)^{-0.576} Bo^{-0.275} X_{tt}^{0.660}, \frac{\mathrm{Re}_g}{\mathrm{Re}_l} > 9.0$ $where\ \frac{\mathrm{Re}_g}{\mathrm{Re}_l} = \frac{x}{1-x}\frac{\mu_l}{\mu_g}, \mathrm{X}_{tt} = \left(\frac{1-x}{x}\right)^{0.875}\left(\frac{\rho_g}{\rho_l}\right)^{0.5}\left(\frac{\mu_l}{\mu_g}\right)^{0.125}$ $f = 4\times49.13\mathrm{Re}_{eq}^{-0.4386}\mathrm{Re}^{-0.4074}$ $where\ \mathrm{Re}_{eq} = \frac{G_{eq}D_h}{\mu_l}, G_{eq} = G\left[(1-x_m)+x_m\left(\frac{\rho_l}{\rho_g}\right)^{1/2}\right]$	Water, Chevron plate, based on effective heat transfer area, $\beta = 60°$ $14.5 \le G \le 33.6$ $15.0 \le q'' \le 30.0$

Longo et al. [21]	Nucleate Boiling, $BoX_{tt} > 0.15\times10^{-3}$ $h = 0.58\varphi h_0 \left(\frac{\varepsilon}{\varepsilon_0}\right)^{0.1333} \left[1.2p^{*0.27} + \left(2.5 + \frac{1}{1-p^*}\right)p^*\right] \left(\frac{q''}{q_0}\right)^{0.467}$, where h_0 is specific for each rerigerant at: $p_0^* = 0.1, q_0 = 20{,}000\ \mathrm{W\,m^{-2}},\ \varepsilon_0 = 0.4\mu m$ Convective Boiling, $BoX_{tt} < 0.15\times10^{-3}$ $h = 0.122\varphi \left(\frac{k_l}{D_h}\right) \mathrm{Re}_{eq}^{0.8} \mathrm{Pr}_l^{1/3}$, where $Bo = \frac{q''}{G\gamma}, X_{tt} = \left(\frac{1-x_m}{x_m}\right)^{0.9} \left(\frac{\rho_g}{\rho_l}\right)^{0.5} \left(\frac{\mu_l}{\mu_g}\right)^{0.1}, p^* = \frac{p}{p_c}$ $where\ \mathrm{Re}_{eq} = \frac{G_{eq}D_h}{\mu_l}, G_{eq} = G\left[(1-x_m) + x_m\left(\frac{\rho_l}{\rho_g}\right)^{1/2}\right]$	R134a, R410A, R507A, R22, isobutane, propane, propylene, R236fa, R1234yf, based on plate projected area, Herringbone plate, 20% mean absolute deviation, $5.7 \le G \le 125$ $28° \le \beta \le 70°$ $2.7 \le q \le 36.5$
Amalfi et al. [29]	$For\ Bd < 4,$ $h = 982\left(\frac{k_l}{D_h}\right)\left(\frac{\beta}{\beta_{max}}\right)^{1.101} \left(\frac{G^2 D_h}{\rho_m \sigma}\right)^{0.315} \left(\frac{\rho_l}{\rho_g}\right)^{-0.224} Bo^{0.320}$ $For\ \mathrm{Bd} \ge 4,$ $h = 18.495\left(\frac{k_l}{D_h}\right)\left(\frac{\beta}{\beta_{max}}\right)^{0.248} \left(\frac{xGD_h}{\mu_g}\right)^{0.135} \left(\frac{GD_h}{\mu_l}\right)^{0.351} \left(\frac{\rho_l}{\rho_g}\right)^{0.223} Bd^{0.235} Bo^{0.198}$ $where,$ $Bd = \frac{(\rho_l - \rho_g) g D_h^2}{\sigma}$ $Bo = \frac{q''}{G\gamma}, \beta_{max} = 70°$	Based on dimensional analysis, developed from 1903 data points. Wide range of operating conditions, plate geometries and fluids including R134a, ammonia, R236fa, R600a, R290, R1270, R1234yf, R410A,

	$f = 4 \times C \cdot 15.698 \left(\frac{G^2 D_h}{\rho_m \sigma} \right)^{-0.475} \left(\frac{(\rho_l - \rho_g) g D_h^2}{\sigma} \right)^{0.255} \left(\frac{\rho_l}{\rho_g} \right)^{-0.571}$, where, $C = 2.125 \left(\frac{\beta}{\beta_{max}} \right)^{9.993} + 0.955$	R507A, ammonia/water, and air/water)
Lee et al. [30]	$h = 0.9243 \left(\frac{k_l}{D_h} \right) \mathrm{Re}_{eq}^{0.6151} \mathrm{Pr}_l^{0.33}$ where $\mathrm{Re}_{eq} = \frac{G_{eq} D_h}{\mu_l}, G_{eq} = G \left[(1 - x_m) + x_m \left(\frac{\rho_l}{\rho_g} \right)^{1/2} \right]$ $f = 6.25 \times 10^{-4} \mathrm{Re}_{eq}^{1.427} \left(\frac{G D_h}{\mu_l} \right)^{-0.7098} \mathrm{Pr}_l^{0.4036}$	R1233zd(E), Chevron plate, $\beta = 60°$ $32 \le G \le 58$ $3.8 \le q'' \le 10.4$ $60°C \le T_{sat} \le 80°C$ $0.17 \le x \le 1.0$

1.2.1.2. Condensation Heat Transfer

There are fewer correlations developed for heat transfer and fluid flow characteristics for condensation than for evaporation in PHXs. Condensation in PHXs is recognized as gravity-controlled or shear-controlled. The first theoretical study undertaken on laminar condensation over cooled metal surfaces is the pioneering work of Nusselt [31], in which a correlation is developed. The correlation is further developed by including the effect of heat capacity [32], accounting for non-linear temperature distribution within the condensate film [33], and adding the effect of shear stress by including a non-zero negative velocity gradient at the liquid-vapor interface [34]. However, this

correlation is only applicable to gravity-controlled laminar film condensation with no waves, and cannot be applied in wavy or turbulent condensation regions, which is the case in most practical PHX applications.

Similar to evaporation, condensation in PHX is a function of various parameters such as quality, mass flux, heat flux, fluid property, plate surface geometry, local flow regimes, and oil effect. Therefore, theoretical performance evaluation is very challenging, and more experimental effort is required. Shah [35] developed a correlation for condensation in horizontal, vertical, and inclined pipes. This correlation is widely accepted in engineering calculations of PHXs perhaps because the correlation is developed from a wide range of experimental data [36]. Obtaining a similar general correlation for a wide range of conditions and refrigerants that accurately predicts the performance while taking the PHX geometry and thermal characteristics into account is desired.

The group of Lin investigated the condensation heat transfer and pressure drop of the refrigerants R134a [37] and R410A [38] experimentally in the same single-channel BPHX used for their evaporation experiments. Similar to their conclusion about evaporation, they showed that even at lower mass flux, the heat transfer coefficient for PHXs is about 25% higher than that for a circular pipe with a higher mass flux, obtained in similar measuring conditions by Eckels and Pate [39]. They concluded that the condensation heat transfer coefficient increases with mass flux, increases linearly with vapor quality, especially for lower mass flux for R134a, increases with average imposed heat flux, and shows almost no affect from condensation pressure.

Wang et al. [40] studied the condensation of steam in different PHXs. Although they did not take any local measurements, they proposed a modified Boyko-Kruzhilin [41] equation to predict the local heat transfer coefficient. However, the correlation does not effectively account for the effect of vapor quality on the heat transfer performance and its local accuracy is not verified by the authors as no local measurements were taken. Palmer et al. [13] developed two condensation correlations in their previously mentioned study as well. Thonon and Bontemps [42] investigated the condensation of pentane, butane, propane, and mixtures of butane and propane in a welded plate heat exchanger in operating conditions that are representative for some industrial cases. They concluded that the heat transfer coefficient of pure fluids increases with the Reynolds number, indicating a transition to turbulent regime, while for mixtures they are lower than that of pure fluids at lower Reynolds numbers, and almost the same at higher Reynolds numbers. However, the pattern of the heat transfer coefficient in their figures is not clear.

Han et al. [43] conducted experiments on R410A and R22 with chevron angles of 45˚, 35˚, and 20˚. Unlike the previous correlations, they included the effects of the plate geometry in their correlations. They concluded that both the heat transfer coefficient and the pressure drop increase with mass flux and vapor quality, while they decrease with saturation temperature and chevron angle.

Longo [44] performed experimental tests on R134a condensation inside a small BPHX with herringbone plates with a corrugation angle of 65˚. As previously concluded [37, 38], the heat transfer coefficient showed weak sensitivity to the change in the

condensation temperature. It is concluded that Nusselt correlation can be applied for a refrigerant mass flux under 20 $kg \cdot m^{-2} \cdot s^{-1}$ as condensation is mainly gravity-controlled, and the heat transfer coefficient is unaffected by an increase in the mass flux. However, for higher mass fluxes the heat transfer coefficient increases 30% by doubling the mass flux indicating forced convection condensation. Similar results were obtained using R410A [45], isobutane, propane, propene (HC-1270) [46], R236fa [47], R1234yf [48], R1234ze [49], and R404A [50]. Longo et al. [51, 52] developed a numerical model obtaining two correlations representing gravity-controlled condensation for equivalent Reynolds numbers below 1600 and forced convection condensation for equivalent Reynolds numbers higher than 1600 using 338 experimental data points obtained by the authors. The model is compared to 516 experimental data points obtained by different research groups showing an absolute mean percentage deviation of 16%.

Mancin et al. [53] studied the partial condensation of R410A and R407C inside two BPHX geometries with different aspect ratios and number of channels. Their experimental results showed that the heat transfer coefficient increases with vapor quality, and decreases with the wall to saturation temperature difference. They introduced a model for calculating the heat transfer coefficient as a function of mass velocity, vapor quality, local temperature difference, and fluid properties. Mancin et al. [54] investigated the partial condensation of R32 using similar procedures, and a model with 4.7% absolute deviation was also developed. They concluded that the condensation heat transfer coefficient increases with superheating, mass velocity, and vapor quality, while it decreases with increasing saturation-to-wall temperature

difference. All condensation correlations given in Table 2 compute the average heat transfer coefficients, except for Wang et al. [40].

Table 2: Condensation heat transfer and pressure drop correlations.

Investigator	Correlation	Comments
Shah [35]	$h = h_l \left[(1-x)^{0.8} + \frac{3.8 x^{0.76} (1-x)^{0.04}}{p^{0.38}} \right]$	Wide variety of refrigerants in horizontal, inclined, and vertical pipes
Yan *et al.* [37]	$h = 4.118 \left(\frac{k_l}{D_h} \right) \mathrm{Re}_{eq}^{0.4} \mathrm{Pr}_l^{1/3}$ $f = 94.75 \left(\frac{p_m}{P_c} \right)^{0.8} Bo^{0.5} \mathrm{Re}^{-0.4} \mathrm{Re}_{eq}^{-0.0467}$ $where\ \mathrm{Re}_{eq} = \frac{G_{eq} D_h}{\mu_l}, G_{eq} = G \left[(1-x_m) + x_m \left(\frac{\rho_l}{\rho_g} \right)^{1/2} \right]$	R134a, Chevron plate, based on plate effective corrugated area, $\beta = 60°$, heat transfer coefficient agreed within 15%, friction factor agreed within 13.3%. $500 < \mathrm{Re} < 1000,$ $60 \le G \le 120,$ $10 \le q'' \le 16,$ $0.1 \le x_m \le 0.9$ $0.7 \le P_m \le 0.9$

Palmer et al. [13]	$h = \left(\frac{k_l}{D_h}\right) \mathrm{Nu}_l^{0.387}\, \phi_l^{0.0824}\, \mathrm{Ga}^{0.346} \mathrm{P}_{red}^{1.5}\, \omega^{1.5}$, for (R22, R290, R290/600a) $h = \left(\frac{k_l}{D_h}\right) Nu_l^{0.298} Ga^{0.346} P_{red}^{1.5} \omega^{1.5}$ $where \begin{cases} Nu_l = 0.16\, \mathrm{Re}_l^{0.89}\, \mathrm{Pr}_l^{0.4},\ Ga = \dfrac{\rho_l \left(\rho_l - \rho_g\right) g D_h^3}{\mu_l^2} \\ \omega = -\log_{10}(p / p_{cr}) \\ \text{for (R32/R152a)} \end{cases}$,	R22, R290, R290/600a: correlated 95% of the data within 25%, R32/R152a: correlated 80% of the data within 25%. $13 < \mathrm{Re}_{eq} < 230$, $1.6 \le G \le 19$, $1.3 \le q'' \le 8.3$
Wang *et al.* [40]	$h = h_l \left(\frac{\rho_l}{\rho_m}\right)^{\left(a + b \cdot \mathrm{Re}_l^c\right)}$ *where,* $h_l = 0.023 \left(\frac{k_l}{D_h}\right) \mathrm{Re}_l^{0.8}\, \mathrm{Pr}_l^{0.4}$	Water, Chevron plate, local heat transfer coefficient, $\beta = 30°, 45°, 60°$ $300 < Re < 2000$, $20 < G < 120$

Thonon and Bontemps [42]	$h = 1564 h_{lo}\, \mathrm{Re}_{eq}^{-0.76}$, for pure hydrocarbons $h_{lo} = 0.347 \left(\frac{k_l}{D_h}\right) \mathrm{Re}^{0.653}\, \mathrm{Pr}^{0.33}$ (Thonon *et al.*1999) $where\ \mathrm{Re}_{eq} = \frac{G_{eq} D_h}{\mu_l}, G_{eq} = G\left[(1 - x_m) + x_m \left(\frac{\rho_l}{\rho_g}\right)^{1/2}\right]$	Pure hydrocarbons, mixtures of hydrocarbons Chevron plate, based on projected area, $\beta = 45°$, $100 < Re < 2000$
Han *et al.* [43]	$h = Ge_1 \left(\frac{k_l}{D_h}\right) \mathrm{Re}_{eq}^{Ge_2}\, \mathrm{Pr}^{1/3}$, $where$ $\begin{cases} Ge_1 = 11.22 \left(\frac{b}{D_h}\right)^{-2.83} \left(\frac{\pi}{2} - \beta\right)^{-4.5} \\ Ge_2 = 0.35 \left(\frac{b}{D_h}\right)^{0.23} \left(\frac{\pi}{2} - \beta\right)^{1.48} \end{cases}$ $f = Ge_3\, \mathrm{Re}_{eq}^{Ge_4}$, $where$ $\begin{cases} Ge_3 = 3521.1 \left(\frac{b}{D_h}\right)^{4.17} \left(\frac{\pi}{2} - \beta\right)^{-7.75} \\ Ge_4 = -1.024 \left(\frac{b}{D_h}\right)^{0.0925} \left(\frac{\pi}{2} - \beta\right)^{-1.3} \end{cases}$ $where\ \mathrm{Re}_{eq} = \frac{G_{eq} D_h}{\mu_l}, G_{eq} = G\left[(1 - x_m) + x_m \left(\frac{\rho_l}{\rho_g}\right)^{1/2}\right]$	R410A, R22, Chevron plate, $\beta = 20°, 35°, 45°$, heat transfer coefficient agreed within 20% of their experimental results. $10 \le G \le 35$, $4.7 \le q'' \le 5.3$, $T_{sat} = 20°C,\ 30°C$

Kuo *et al.* [38]	$h = 0.2092\left(\frac{k_l}{D_h}\right)\mathrm{Re}_l^{0.78}\,\mathrm{Pr}_l^{1/3}\left(\frac{\mu_m}{\mu_w}\right)^{0.14}\left(0.25Co^{-0.45}Fr_l^{0.25}+75Bo^{0.75}\right)$ $where\ Co=\left(\frac{\rho_g}{\rho_l}\right)\cdot\left(\frac{1-x_m}{x_m}\right)^{0.8}$ $f = 21{,}500\,\mathrm{Re}_{eq}^{-1.14}\,Bo^{-0.085}$ $where\ \mathrm{Re}_{eq}=\frac{G_{eq}D_h}{\mu_l}, G_{eq}=G\left[(1-x_m)+x_m\left(\frac{\rho_l}{\rho_g}\right)^{1/2}\right]$	R410A, Chevron plate, based on plate effective corrugated area, $\beta = 60°$ $50 \le G \le 150,$ $10 \le q'' \le 20,$ $0.1 \le x_m \le 0.9,$ $1.44 \le P_m \le 1.95$
Mancin et al. [53]	$h=\left(h_{Nu}^2+h_{shear}^2\right)^{1/2}\left[1.074\left(T_{sat}-T_w\right)^{-0.386}\right],$ $where\ \begin{cases} h_{Nu}=0.943\left[\frac{\rho_l\left(\rho_l-\rho_g\right)g\gamma k_l^3}{\mu_l L\left(T_{sat}-T_w\right)}\right] \\ h_{shear}=h_l\left[1+1.128x^{0.817}\left(\frac{\rho_l}{\rho_g}\right)^{0.3685}\left(\frac{\mu_l}{\mu_g}\right)^{0.2363}\left(1-\frac{\mu_g}{\mu_l}\right)^{2.144}\mathrm{Pr}^{-0.1}\right] \end{cases}$	R410A, R407C, herringbone plate, partial condensation based on the effective embossed area, 15 K superheat, 5.9% absolute deviation. $15 \le G \le 40,$ $0.01 < x < 0.58$

Longo et al. [51, 52]	$h = 0.943\varphi\left[\frac{\left(k_l^3\rho_l^3 g\gamma\right)}{\mu_l L\left(T_{sat}-T_w\right)}\right]^{1/4}, \quad \mathrm{Re}_{eq} < 1600$ $h = h_{sat} + F\left(h_l + \frac{C_p \cdot q''}{\gamma}\right), \quad \mathrm{Re}_{eq} \geq 1600$ $where \begin{cases} h_{sat} = 1.875\varphi\left(\frac{k_l}{D_h}\right)\mathrm{Re}_{eq}^{0.445}\,\mathrm{Pr}_l^{1/3} \\ h_l = 0.2267\left(\frac{k_g}{D_h}\right)\mathrm{Re}_g^{0.631}\,\mathrm{Pr}_g^{1/3} \\ F = \frac{T-T_{sat}}{T_{sat}-T_w} \end{cases}$ $where \ \mathrm{Re}_{eq} = \frac{G_{eq}D_h}{\mu_l}, G_{eq} = G\left[(1-x_m) + x_m\left(\frac{\rho_l}{\rho_g}\right)^{1/2}\right]$	R134a, R410A, isobutane, propane, propylene, R236fa, R22, R1234yf, R1234ze, CO_2, R32, based on plate projected area, Herringbone plate, 16% mean absolute deviation, $2.6 \leq G \leq 150$ $30° \leq \beta \leq 65°$ $2.0 \leq q \leq 35.2$

1.2.2. Pillow Plate Heat Exchangers

The manufacturing process of PPHXs consists of two thin metal sheets welded together using a certain pattern of spot welding that can be in-line or staggered. The two sheets are then sealed at the edges using seam welding. The plates are then inflated in a hydroforming process creating a pillow shape. The inflated plates are finally stacked together to form the channels of the PPHX. The weld pattern, longitudinal and transverse pitches between the welds, weld shape and size, plate thickness, and pillow height are all factors altering the thermal-hydraulic performance of the PPHX. PPHXs

are commonly used in chemical and process industry in single-phase and two-phase applications. However, research on the utilization of PPHXs in HVAC&R applications is limited. Mitrovic and Peterson [55] claim to be the first to study what they call a thermoplate. A thermoplate goes through the same manufacturing process as a pillow plate, and possesses very similar geometrical characteristics as pillow plates. They studied experiments with single phase and two-phase condensation heat transfer and pressure drop using isopropanol as the working fluid. Using their experiments results, they developed heat transfer coefficient and pressure drop correlations. However, they noted in their study that the correlations developed are only valid for isopropanol for the range of parameters specific to their experiments. Mitrovic and Maletic [56] performed numerical simulations on thermoplates as well using CFD with water as the working fluid. The Reynolds number investigated ranged from 50-3800 for which they proposed a heat transfer coefficient correlation. The CFD simulations used a laminar flow model although the Reynolds range covered part of the turbulent region which led to the underestimation of the heat transfer rate and pressure drop compared to their experimental results. They also used an approximation for the pillow plate surface geometry using a three-dimensional trigonometric function to describe the wavy surface which resulted in significant inaccuracies as mentioned by Piper et al. [57].

Piper et al. [57] adopted an alternative approach based on numerical forming simulations to determine the geometrical characteristics of PPHXs. The approach developed is described as flexible, and it well predicts the actual hydroforming process during the manufacture of the PPHXs. They developed correlations to calculate the

pillow plate channel volumetric mean hydraulic diameter, wetted heat transfer area, channel cross-sectional area, and channel volume. However, the correlations are developed based on a limited number of geometries which might have caused some inaccuracies in the model developed. It will be shown later in Chapter 4 that using a similar approach but a different platform, the results show good agreement with the volume calculation only for some of the geometries, whereas the heat transfer area only agreed within 20%. It is concluded that the correlations developed by Piper et al. [57] can be very useful as an initial attempt to calculate PPHXs geometric parameters, however, as also mentioned in their work and shown in the current study, more accurate design methods must be developed for a detailed design of a PPHX surface in order to reduce the design uncertainty. Piper et al. [58] performed a CFD study using a turbulent single-phase water flow in PPHXs with Reynolds number ranging from 1000-8000. In their study, the PPHX surface is obtained using forming simulations as well. In order to define the thermal-hydraulic performance of the PPHX, they defined an efficiency based on the total heat transfer divided by the total pumping power required. By comparing this defined efficiency, they concluded that a lower Reynolds number, larger pillow height, and transverse weld pattern result in better performance. They also concluded that a smaller weld diameter and an oval weld shape can significantly reduce the pumping power leading to a higher efficiency, although the heat transfer area is reduced as well. Piper et al. [59] later used these simulations to develop and verify heat transfer coefficient and pressure drop correlations. The correlations developed agree with their numerical simulations within ±15% and cover a wide range of Prandtl

number of 1-150. The correlations, however, do not capture lower Reynolds numbers and are developed using a limited number of plate geometries. Further discussion about these correlations is presented in Chapter 5. In order to obtain a more accurate correlation, more cases might need to be investigated to cover a greater range of geometric parameters as well as Reynolds number. Finally, another study by Tran et al. [60] shows that the heat transfer coefficient values in PPHXs are higher as compared to vertical tubes in coupled condensation-evaporation applications. This further reveals the great potential of using PPHXs in HVAC&R applications.

1.2.3. Modeling Tools

In order to predict the performance of heat exchangers in general, three scientific approaches are used in most engineering applications: 1) experimental; 2) analytical; and 3) numerical analysis. Although experimental investigation is the best approach to determine the actual performance, it is also the most expensive approach and usually preferred as the last step after analytical and/or numerical investigation is done. The analytical approach, on the other hand, yields partial differential equations that cannot be solved without either many assumptions that yield a very simplified model that inherits high uncertainty, or otherwise solved using a numerical method.

For PHXs in general, some modeling tools were developed over the last few decades employing both implicit and explicit numerical approaches as will be discussed in the following section. The heat transfer coefficient and pressure drop correlations developed for PHXs (Section 1.2.1) are usually employed in these tools to predict the

performance, otherwise empirical correlations based on individual experiments can be also applied [61]. However, PPHXs are still in a very early research stage. As mentioned in the previous section, more accurate design methods are required for describing the detailed geometrical characteristics and thermal-hydraulic characteristics of PPHXs over a wide range of conditions. In order to predict the performance of PPHXs, especially novel surfaces, robust numerical methods such as Computational Fluid Dynamics (CFD) are employed. The performance is predicted through first resembling the manufacturing process of PPHX to obtain the detailed structure of the surface using forming simulations, then studying the flow inside the surface by using suitable boundary conditions.

1.2.4. Plate Heat Exchanger Models

Computer models are essential for design and development of state of the art heat exchangers. It is widely accepted that they significantly reduce design and development time, as well as capital and operational costs. Additionally, it allows for evaluating the performance on a system level showing the overall benefit that will reflect directly on energy consumption. With the encouraging characteristics of PHXs, it is highly desirable to use computer models to develop and optimize PHX designs in order to maximize energy efficiency. However, there are limited computer models available for PHXs. The PHX problem is complex in nature. The number of unknowns in a PHX problem is equal to two times the number of channels minus one or $2 \times (N - 1)$, where N is the number of channels. With phase change and more complex flow

configurations, the problem becomes even more challenging. If the PHX is further divided into a number of segments M , this will result in a matrix of $2 \times (N-1) \times M$ unknowns which requires extensive thermos-physical property calculations and great computational effort to be solved. Numerically, the problem can also be unstable depending on the quality of the discretization method and due to the interdependence between the heat transfer and pressure drop calculations.

Kandlikar and Shah [62], Zaleski and Klepacka [63], Georgiadis and Macchietto [64], Ribeiro & Caño Andrade [65], and Gut and Pinto [66], developed various models for plate heat exchangers. Some literature proposed procedures to solve parallel flow, series flow, or flow with predefined configurations. Some propose algorithms to solve general configurations with no phase change with constant heat transfer coefficient all over the PHX due to lack of information on correlations at the time. Flow maldistribution was not accounted for in most of the studies. The algorithm developed by Ribeiro & Caño Andrade [65] was used in an industrial milk pasteurization simulation tool which is only used for single-phase heat transfer flow. In single-phase flow, the heat transfer and pressure drop equations can be decoupled, unlike the two-phase flow which is the common case in HVAC&R applications.

The finite volume semi-explicit method for wall temperature linked equations (SEWTLE) approach developed by Corberán et al. [67] was employed by Gullapalli [61] in a generalized rating method used in a specific industrial tool for the selection of brazed PHXs. However, the developed model is not fully implemented in the commercial PHX selection software due to speed limitations and to improve stability.

Instead, the detailed geometry of the plate is read from a product database. In-house empirical constants for single-phase and two-phase heat transfer coefficient and pressure drop correlations are also read from a product database. Also, all boundary temperatures must be specified by the user. This makes the tool good for the commercial purpose it was developed for, but negates its flexibility to design or simulate any PHX that is outside this product database. There are other very few commercial PHX simulation tools, but there is no enough information available to reveal information about these tools, such as flexibility, whether empirical factors for certain databases are used, speed, or the robustness of the tool.

Qiao et al. [68] developed a mathematical model that is employed in a PHX simulation tool which distinguishes itself by providing the greatest flexibility and pass configuration generality using the concept of "Junction-Channel Connectivity Matrix". The tool developed also allows customization features such as using a user-defined heat transfer coefficient or pressure drop correlation, in addition to built-in correlations from literature. The tool has the most up to date and comprehensive libraries of working fluids and allows for user-defined mixtures as well. However, with the generality comes the challenges of stability and speed limitations. It is thus desired to improve the robustness, and the speed of this model in order to provide an accurate, robust, flexible, and conveniently fast tool for modeling and designing PHXs.

1.2.5. CFD

The evolution of CFD in heat exchanger design added a new dimension for the design of new heat exchanger surfaces which in turn contributed to the improvement of heat exchanger performance and energy efficiency, and even became routine in some industrial applications [69]. CFD is still however viewed by some with high uncertainty due to the essential inherited numerical uncertainty. In 2006, Shah [69] concluded that CFD at the time did not provide accurate Nusselt numbers and friction factors versus Reynolds number as the latest publication back then showed a prediction uncertainty of 15-20%, while ideally an uncertainty of 5% is required. However, the same publication [69] predicted CFD will advance to the extent of conducting full 3D analysis of flows, and accurately designing complete compact heat exchangers, eliminating the need for experimental analysis. Although the need of experimental investigation is still required as a final step of design, but great advances took place in the last decade in computational power allowing faster CFD simulations and more accurate models to be developed.

Abdelaziz et al. [70] compared the air side capacity of CFD simulations of a novel heat exchanger using micro tubes against experimental data and obtained an uncertainty of +/-10%. Xioping et al. [71] also found 10% deviation when comparing air side heat transfer coefficient of a louvered fin microchannel heat exchanger. More recently, Taler and Oclon [72] obtained 4% deviation for a plate fin-and-tube heat exchanger when compared to experimental data. CFD simulations with the current available computational power is essentially the most efficient, low capital, fast method to

investigate novel heat exchanger surfaces with acceptable accuracies, especially as the complexity of the heat exchanger surface increases. The literature shows numerous examples of novel heat transfer surfaces studied using CFD [73, 74, 75, 76, 77, 78, 58]. In order to have a thorough optimization study to obtain the ultimate best design for a heat exchanger surface, geometry topology change is required which means numerous CFD simulations must be studied. Using conventional CFD analysis in this case inherently means a high engineering time cost which might be impractical. Thus, the automation of the CFD simulation procedure must be applied. Abdelaziz et al. [79, 70] developed an automated method for CFD simulation called Parallel Parametrized CFD (PPCFD). The PPCFD method consists of a code that automatically reads the Design of Experiment (DoE) input parameters and creates journal files for geometry, mesh, and CFD problem settings. An executable batch file is created to sequentially execute the simulations for the entire DoE. The sequential runs can be done in parallel depending on the number of processors available. Finally, the CFD output is processed to get the final results for thermal-hydraulic performance. Another automation technique is also available in literature [80]. However, automation comes with challenges as the number of components in a system increase as well as the geometry complexity. But generally, if automation is achieved, more than 90% of engineering computational time can be saved using this automation technique [79].

1.2.6. Optimization

Heat exchanger optimization design problem has been undertaken for more than half a century. The first systematic methodology for heat exchangers was presented by Fax and Mills [81] in optimizing plate-fin gas turbine heat exchanger based on analytical solutions. Hedderich et al. [82] used a numerical optimization scheme for air-cooled heat exchanger. Huang et al. [83] categorized optimization techniques as: 1) Basic Search (Exhaustive, random, parametric); 2) Lagrange's Multiplier [84]; 3) Gradient-based Algorithms [84]; 4) Heuristic Methods, e.g. Genetic Algorithms (GA); and 5) Approximation Assisted Optimization (AAO). The level of expertise required for each category and the computational cost, given by Aute [85], are shown in Table 3.

Table 3: Summary of heat exchanger categories adapted from Aute [85].

Category	Expertise	Relative Computational Cost
Exhaustive Search	Low	100000
Random Search	Low	10000
Parametric Analysis	Low	1000
Gradient-based Methods	Medium	100
Heuristic Methods (GA, MOGA)	Medium-High	100
Approximation Assisted Optimization (AAO)	High	1

Exhaustive search relies on simulating all possible combinations of design variables and then selecting the design that best meets the performance requirements. Although such an approach is very comprehensive, it is very computationally expensive and practically non-feasible. Deb [86] demonstrated the challenges with the first three categories from Huang et al. [83] which include the requirement of an initial point by some methods; some algorithms tend to find a suboptimal solution and becomes limited to it; they cannot be used in parallel computing; and they are not efficient when handling discrete variables.

Heuristic algorithms, such as Genetic Algorithms (GA), overcome these challenges with a relatively lower computational cost. GA is defined as a "search algorithm based on natural selection and natural genetics" [87]. GA is described in [88] and [89]. GA can simultaneously handle continuous, and discrete variables, can find global optimum solution, and it has been successfully applied to various engineering optimization problems in literature [83]. Although GA's have proven to be powerful and computationally less expensive than traditional methods, there is an increasing demand for computational time reduction, especially for more complex problems. In order to reduce computational time, Approximation Assisted Optimization (AAO) is created.

AAO simply creates a computationally cheap simplified model for predicting CFD results in order to avoid building and simulating a CFD model for every single design evaluated by the optimizer. This predictive model is essentially created using a fixed number of expensive CFD simulations which compromise the DoE which should provide the performance information scattered in the design space studied. The

predictive model can be as simple as curve fits or sophisticated metamodels such as Kriging [90]. The simplified model is verified using actual CFD simulations. Once verified, the optimization can be run unlimited times using this simplified predictive model. The DoE can be determined using a sampling method such as Latin Hypercube Sampling (LHS) [91] and Maximum Entropy Sampling (MES) [92]. Abdelaziz [79] studied the coupling of CFD into optimization and concluded that coupling PPCFD into AAO offered the most cost-effective method for heat exchanger optimization.

Saleh et al. [93] compared different multi-objective optimization approaches to optimize the thermal-hydraulic performance of turbulent single-phase flow in a chevron PHX. Exhaustive search, offline AAO, and online AAO were compared. In the online AAO, the optimum solutions are filtered in order to select the best designs and update the metamodel accordingly. This process is iterative and carried out until a certain stopping criterion is reached. Kriging metamodels were developed for heat transfer coefficient and pressure drop. The study found that the online AAO approach, compared to the other two approaches, predicted better optimum designs with high accuracy. In the online AAO study, only few hundreds CFD simulations were required to build and update the metamodels, compared to thousands of CFD simulations required when a conventional gradient-based method is used, which means a significant reduction in computation time. No similar effort is done for PPHX in the literature.

1.2.7. Summary of Literature Gaps

The main background for the current work and the potential literature gaps that the current research intends to fill are presented in the preceding sections. There are three main gaps summarized in the subsequent subsections.

1.2.7.1. PPHX Design and Optimization

The literature on PPHXs is very limited, especially in HVAC&R. It is desired to bring the thermal-hydraulic and economic advantages of PPHX into the spotlight in this field with optimized geometry which can give it a strong competitive advantage. The optimization of the basic PPHX geometry, with spot welds, can place the PPHX in HVAR&R as a competitive heat exchangers. Although some CFD analysis and a parametric study are recently performed on PPHXs, no optimization effort has been done on them before. Also, no previous comparison to an existing other type of PHXs has been done before to show their thermal-hydraulic advantage.

1.2.7.2. Multi-Scale and Weld Shape Optimization for PPHX

Only one study in literature shows the weld shape effect on the overall performance of PPHX using only one other shape with few sizes. It is desired to study the effect of changing the weld shape and size on the multi-scale analysis of PPHXs. Shape optimization allows the optimizer to find the best weld shape and size while optimizing the PPHX performance. The shape can be varied using mathematical approaches such

as Non-Uniform Rational B-Splines leading to innovative designs. This will lead to an even more distinguished PPHX.

1.2.7.3. Improved Modeling Algorithms for PHXs

The most flexible, robust, and general modeling tool for PHXs is presented by Qiao et al. [68]. However, it has some speed and robustness limitations due to the complex nature of the PHX geometry. If it is to be used on a system level, which is highly required to find system level performance, it will get even more challenging. Since it is very expensive to manufacture PHXs, it is crucial to find algorithms that will improve the calculations challenges inherited with this type of heat exchanger in order to be able to seize its favorable thermal-hydraulic characteristics. It is desired to develop algorithms that will further improve the robustness and the speed significantly such that a PHX will solve in a fraction of the time, without giving up on the generality and design flexibility advantages.

Chapter 2: Research Objectives

This dissertation will investigate the design of PPHX with its basic geometry as well as with multi-scale shape optimization. In addition, it will improve existing PHX modeling tools. In the light of what has been presented in the literature review, this research has the following objectives:

1. Optimization of PPHX basic geometry with circular spot welds using PPCFD and AAO with four design parameters. It is important to achieve at least 50% or similar improvement in thermal-hydraulic performance of PPHX compared to existing current designs. It is also crucial to compare this performance to optimal designs of existing other types of PHXs especially those that are widely used in HVAC&R, such as chevron type PHX, in order to prove the potential thermal-hydraulic competitiveness of PPHX in addition to its economic advantage.
2. Multi-scale analysis and weld shape optimization of PPHX to further add to the heat transfer enhancement potential as well as the hydraulic performance improvement. To build on the improvement achieved in the first objective, a more comprehensive optimization study using similar techniques of PPCFD and AAO but using eleven design parameters that include weld shape parameterization is undertaken. Smaller more streamlined weld shapes have a significant effect on the flow pattern inside PPHX reducing the pressure drop

significantly while at least maintaining the heat transfer performance. The weld shape and size are the most promising geometric parameters for potential performance improvement and thus, optimization can yield a novel weld shape for a novel PPHX design. The second objective is to obtain a novel PPHX design that possesses a 20% or similar thermal-hydraulic performance improvement when compared to optimal designs of chevron PHXs obtained from literature. The economic advantage will still be in place and therefore, PPHX will possess a distinguished advantage in this field.

3. The third objective is to improve the modeling of PHXs significantly, while preserving the generality and flexibility of the existing modeling tool developed by Qiao et al. [68]. This will be done through developing the tool by applying a new solution algorithm which will have a significantly improved robustness. The algorithm will also be more time efficient. The speed improvement is important to be at least two times faster than the existing solver in terms of both iteration count as well as time. Additionally, it is also desired to add a solver that is able to account for flow maldistribution that takes place at the inlet of the PHX due to the different types of pressure drop that takes place at the inlet and the exit of the PHX. This solver can seize the advantage of the new algorithm such that the outcome is a developed solver that is general, flexible, robust, fast, and more accurate, taking all different types pressure drop into consideration, such that the outcome is a reliable efficient design tool allowing for potential improved PHX performance and energy efficiency.

The objectives are developed and achieved in the next four chapters of this dissertation.

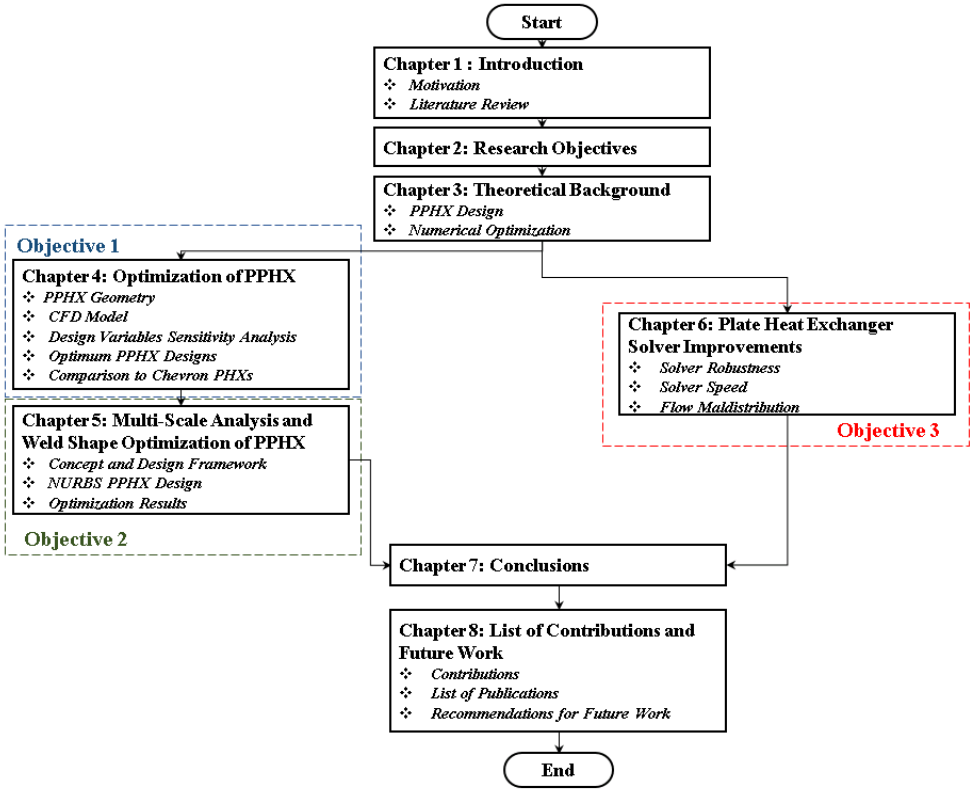

Figure 1: Dissertation organization workflow.

Figure 1 shows the dissertation organization workflow which summarizes the following chapter general outline:

Chapter 2:

- The research objectives of this dissertation are represented in this chapter.

Chapter 3:

- In this chapter all the fundamental and technical background required for this dissertation is covered.

Chapter 4:

- The PPHX geometry is presented in this chapter with all details related to its manufacturing and how to attain the complex 3D geometry numerically.
- The complete CFD model to simulate the fluid flow in the PPHX geometry is presented.
- The automation process details of the CFD simulation to create the PPCFD code is explained in detail.
- The metamodel verification metrics is shown using a set of random simulations.
- Sensitivity analysis of all four design parameters is presented showing the parameters with the least and the most significant effect on the performance.
- The optimum designs and the improvement in thermal-hydraulic performance compared to the baseline is presented.
- A comparison with optimum chevron PHX designs obtained from literature is presented showing the significant improvement obtained.

Chapter 5:

- The concept of design of PPHX with NURBS weld shape is presented.
- The framework of the multi-scale analysis for PPHX with weld shape optimization is demonstrated.
- NURBS PPHX optimization problem with 11 design variables is discussed.
- CFD results are discussed with sensitivity analysis for selected parameters.

- Optimization results including optimum designs, and a comparison with the previously obtained optimum designs without shape optimization as well as a comparison to chevron PHX optimum designs are discussed.

Chapter 6:

- Multiple solver improvements are discussed in this chapter
- Solver robustness improvement through an improved guess wall temperature and a slice routine is discussed.
- A novel algorithm is presented and the significant improvement in solver speed is examined.
- A flow maldistribution solver is presented in order to improve the accuracy of the model.

Chapter 7:

- The conclusions from the whole dissertation are presented in this chapter

Chapter 8:

- Summary of the dissertation research contributions, publications outcome from this work, and some recommendations for future work are presented in this chapter.

Chapter 3: Theoretical Background

3.1. Pillow Plate Heat Exchanger Design

The following steps are the main framework of the design methodology for PPHX:

1. Define the design problem: this step includes specifying the PPHX application (single-phase, e.g. radiator, two-phase, e.g. condenser... etc.), the baseline operating conditions, required capacity, and problem constraints.
2. Thermal-hydraulic design: this is the core of the procedure and includes defining the CFD modeling approach including how the geometry would be obtained, mesh size, and other problem physics, and the verification of the CFD code using standard procedures such as the computation of the Grid Convergence Index (GCI) [94].
3. Execute the Parallel Parametrized CFD (PPCFD) simulations for the selected Design of Experiments (DoE) and use the results from the simulations to generate metamodels for heat transfer coefficient and pressure drop. In this step, mechanical stress and fatigue analysis are conducted. This is a pass/fail check. In case of failure to pass this check, the simulation is not executed.
4. Run multi-objective optimization problem to obtain the optimal PPHX designs and compare them against the baseline and against the optimal chevron PHX designs.

5. Evaluate the PPHX full scale performance using the modeling tool developed by Qiao et al. [68] with the model developments presented in Chapter 6.
6. Manufacturing evaluation: the manufacturing options, costs, and constraints must be evaluated and passed.
7. System evaluation: the PPHX must be evaluated in a system context.
8. Experimental validation: the PPHX should be finally built and tested experimentally and the experimental results should be validated.

The execution of steps 5-8 is left as future work. In this work the performance of the PPHX plate is evaluated using the LMTD method [95] using post processed results from the CFD simulations, which is further explained in Section 3.1.2, while the thermal-hydraulic characteristics of PHXs is evaluated using the existing correlations from literature presented in Chapter 2 as will be mentioned in Chapter 6.

3.1.1. CFD Modeling and Simulation

Numerical analysis of PPHX employs 3-dimensional computational domains in order to be able to capture all the physics which is computationally very expensive. Thus, it is desired to reduce the computational cost by adequately reducing the computational domain while no physical meaning is lost in a similar manner as the method proposed by Patankar [96]. Typically, the end effects are neglected and the thermal-hydraulic performance is determined using a segment of the heat exchanger where all the boundaries are assumed periodic or symmetric. All CFD simulations are performed

using ANSYS Structure 17.0 for geometry construction, and ANSYS Fluent® 17.0 [97] for meshing and thermal-hydraulic simulations.

3.1.1.1. Governing Equations

The basic governing equations are the continuity, momentum (Navier-Stokes), and energy equations. The following assumptions are used in this design problem:

a) Steady state flow,

b) There is no mass source or sink, no energy source or sink, and no external forces

c) Negligible gravitational forces

d) Constant physical properties

e) Kinetic energy and pressure work are negligible

The resulting governing equations are thus

$$\nabla \left(\rho \bar{u} \right) = 0 \tag{1}$$

$$\left(\bar{u} \cdot \nabla \right) \left(\rho \bar{u} \right) = -\nabla P + \mu \nabla^2 \bar{u} \tag{2}$$

$$\bar{u} \cdot \nabla \left(\rho c_p T \right) - k \cdot \nabla^2 T = 0 \tag{3}$$

There is no analytical way to determine the critical Reynolds number for PPHX, especially using novel weld shapes. Thus, the transition from laminar to turbulent flow regime is unknown and must be solved for by the CFD simulation. The turbulence model used in this work is the $k - \varepsilon$ realizable model [98, 99]. This model is originally developed for high Reynolds numbers and it also has shown high accuracy and robustness in different applications. However, it should be noted that the mesh quality

near the wall boundary must be sufficiently fine for the sake of accuracy of this model. The reliability of this method is tested using the realizability conditions [100] for Reynolds stresses given by

$$\begin{aligned} \left\langle u_a', u_a' \right\rangle &\geq 0 \\ \left|\left\langle x, y \right\rangle\right|^2 &\leq \left\langle x, x \right\rangle \cdot \left\langle y, y \right\rangle \end{aligned} \tag{4}$$

These conditions must be satisfied to ensure that the solutions are physically and mathematically consistent. The conditions state that the turbulent normal stresses should be non-negative, and that the Cauchy-Schwarz inequality is satisfied. These conditions are imposed in the simulations of the current work.

A very important aspect of the CFD simulation is the near wall meshing as thermal diffusion is a function of the temperature at the surface deduced from the momentum equation

$$h_x \left(T_\infty - T_{wall} \right) = -k \left. \frac{\partial T}{\partial y} \right)_{wall} \tag{5}$$

The viscous resistance within the boundary layer is also a function of temperature as well as velocity gradient near the surface as given by the skin friction coefficient

$$C_f = \frac{\tau_{wall}}{0.5 \rho u_\infty^2} = \frac{1}{0.5 \rho u_\infty^2} \left(\alpha + \varepsilon_M \right) \left. \frac{\partial \bar{u}}{\partial y} \right)_{wall} \tag{6}$$

Subsequently, a very fine mesh near the wall must be considered in order to more accurately capture the boundary layer physics. Additionally, in order to capture the physics in the entire 3D domain, it is also necessary to sweep the mesh across the edges of the computational domain. The meshing scheme used in the current work is hence

sweep meshing and a finer mesh is used near the edges as well. Figure 2 and Figure 3 show the 3D computational domain for PPHX with circular spot weld, and for NURBS shaped welded PPHX, respectively.

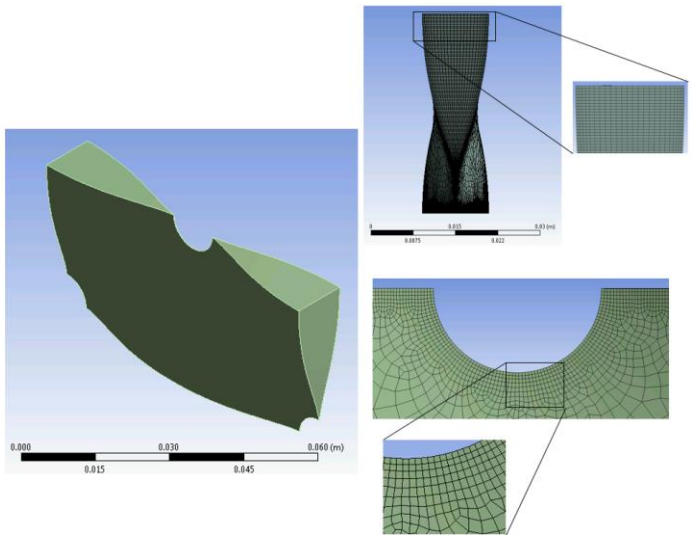

Figure 2: Typical three-dimensional computational domain with circular spot weld.

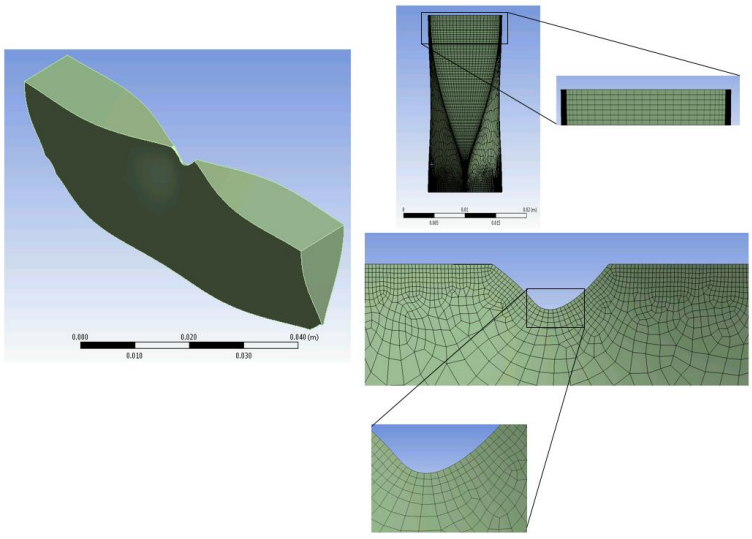

Figure 3: Typical three-dimensional computational domain with NURBS weld shape.

3.1.1.2. CFD Settings

The pressure-velocity coupling scheme used in this work is the SIMPLEC solver available in ANSYS FLUENT® [97]. All space discretization schemes are second order degree upwind. This is done to obtain good accuracy with relatively low computational cost, as the 3D CFD simulations of PPHX plates are very computationally expensive. The simulation convergence criteria are set to maximum residual of 10^{-5} for momentum and continuity, 10^{-6} for energy, and 10^{-3} for turbulence. The maximum number of iterations is set to 2000 iterations which is found sufficient to reach a steady state in the solution. If the simulation does not meet the criteria but still stabilizes through the 2000 iterations, it is assumed that if the standard deviation of the last 100 iterations is less than 5% of the average of those same 100 iterations, then the solution is converged. Additionally, a check is done for every simulation in order to make sure that the first and second law of thermodynamics are not violated.

3.1.2. CFD Data Reduction

No-slip boundary condition and constant wall temperature are applied. Single phase, incompressible, turbulent, steady-state water flow is studied. The Reynolds number in this study is defined by the following equation

$$\mathrm{Re} = \frac{u d_h}{\nu}, \ where \ d_h = \frac{4V}{A_w} \tag{7}$$

The heat transfer coefficient is calculated using the LMTD method using the equation

$$h = \frac{Q}{A_w LMTD} \tag{8}$$

The friction factor is calculated using the following equation

$$f = \frac{d_h}{2\rho u^2}\left(\frac{\Delta P}{L}\right) \tag{9}$$

The outlet boundary pressure is assumed to be uniform and at atmospheric pressure (0.0 guage).

3.1.3. CFD Grid Uncertainty

It is required to determine the optimal grid resolution that provides both minimal inaccuracies in the simulation results and minimal additional computational cost as well. In order to obtain this grid resolution, a grid independence study is undertaken. The Grid Convergence Index (GCI) [101] is developed based on the Richardson extrapolation to estimate the grid convergence error [102]. The GCI method is applied through implementing the following five steps [94]:

Step 1: Define a relative grid size, β. For three-dimensional computational domains, as for the current problem, the relative grid size is defined such that

$$\beta = \left[\frac{\sum_{i=1}^{N} \Delta V_i}{N}\right]^{1/3} \tag{10}$$

Where N is the total number of cells in the computational domain, while ΔV_i is the volume of the i^{th} cell in the domain.

Step 2: Select three grid resolutions which are significantly different such that the grid refinement factor, $r = \beta_{coarse} / \beta_{fine}$, should be equal to or greater than 1.3. This value is only recommended based on experience [94].

Step 3: Calculate the apparent order of accuracy, p, such that

$$p = \left(1 / \ln r_{21} \right) \left(\ln \left| \varepsilon_{32} / \varepsilon_{21} \right| + \ln \left(\frac{r_{21}^{p} - s}{r_{32}^{p} - s} \right) \right) \tag{11}$$

$$s = 1 \cdot sign \left(\varepsilon_{32} / \varepsilon_{21} \right) \tag{12}$$

where $\varepsilon_{32} = \varphi_3 - \varphi_2, \varepsilon_{21} = \varphi_2 - \varphi_1$, and φ is the physical quantity of interest, e.g. heat transfer coefficient, and pressure drop.

Step 4: Calculate the extrapolated values such that

$$\varphi_{ext}^{21} = \frac{r_{21}^{p} \varphi_1 - \varphi_2}{\left| r_{21}^{p} - 1 \right|} \tag{13}$$

Step 5: Calculate the approximate relative error and the extrapolation error estimates and the grid convergence index (GCI)

$$e_a^{21} = \left| \frac{\varphi_1 - \varphi_2}{\varphi_1} \right| \tag{14}$$

$$e_{ext}^{21} = \left| \frac{\varphi_{ext}^{21} - \varphi_1}{\varphi_{ext}^{21}} \right| \tag{15}$$

$$GCI_{fine}^{21} = \frac{F_s \cdot e_a^{21}}{r_{21}^{p} - 1} \tag{16}$$

The factor of safety F_s was originally assigned a value of 3.0 when two grids are only studied. Roache [101], however, has undertaken empirical studies using three grid studies arriving at the conclusion that a value of 1.25 results in a GCI with a 95% confidence interval. Many studies later supported this study [103, 104, 105]. Since three grid studies are used in the current study, a factor of safety value of 1.25 is generally used. However, a conservative value of 3.0 is also used to make sure under both values the mean GCI is under 5% for each parameter in order to be confident about the optimum grid resolution.

3.1.4. Non-Uniform Rational B-Splines

Non-Uniform Rational B-Splines (NURBS) is implemented to describe the weld shape using a set of parameters. The implementation of NURBS [106] is very common in shape optimization problems [80, 107]. The most efficient NURBS algorithm is presented by Piegl and Tiller [106] and consequently utilized in the current work. NURBS can be applied to curves (2D) as well as surfaces (3D). For the weld shape, a 2D curve is required. A NURBS curve is usually presented in a vector format and represented by control points, P_i, described by the rational piecewise base functions defined on $u \in [0,1]$, which is given by

$$C(u) = \sum R_{i,p}(u) P_i = \sum \frac{N_{i,p} w_i}{\sum N_{j,p}(u) w_j} P_i, \quad a \le u \le b \tag{17}$$

P_i are the control points, w_i are the weight vector points, and N_i are the p^{th} degree B-Spline base functions on the non-uniform knot vector U [106]. An example of a NURBS curve is shown from Piegl and Tiller [106] in Figure 4.

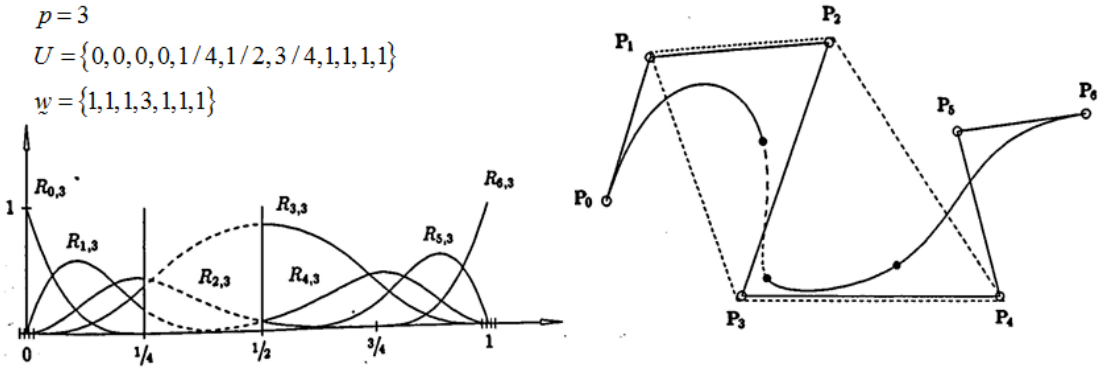

Figure 4: A 3rd degree curve plotted using NURBS example from Piegl and Tiller [106].

Out of the 14 properties of NURBS curves stated by Piegl and Tiller [106], the following are important to the current design problem:

- The first and last point on a NURBS curve coincide with the first and last control point, respectively, such that $C(0) = P_0$ and $C(1) = P_n$.
- If the weight vector is unitary, the rational base functions are simply B-Spline base functions. If the B-Spline degree is equal to the number of control points minus one, then it is simply a Bezier curve, which has the base functions as the Bernstein polynomials. This property shows that NURBS contains both rational and non-rational B-Splines and Bezier curves, thus allowing one to describe almost any type of curve.

- Local approximation: changing a single control point or a single weight affects only portion of the curve.

In the current work, 2D 4th order NURBS curves are considered where the coordinates of the control points are normalized between 0 and 1. The leading edge (le) is fixed at point (0,0), and the trailing edge (te) is fixed at point (1,0), while three mid-points are in between and each of the mid-points coordinate represent a shape design variable. The x-coordinates of the mid-points are bounded by equally spaced ranges in order to avoid over intersection between them. The parameterization is shown in Figure 5, showing only the upper half of the weld shape. The weld shape is symmetric around the x-axis.

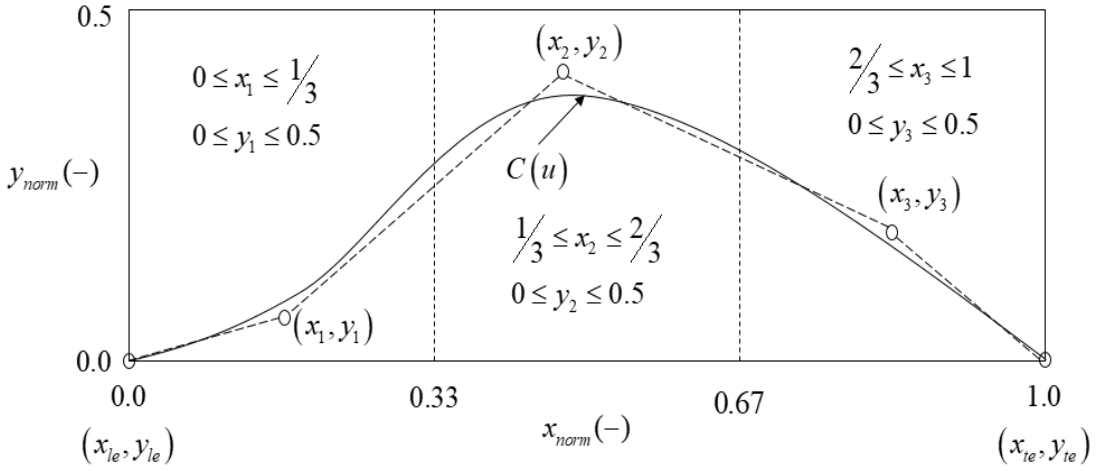

Figure 5: Weld shape parameterization.

3.2. Numerical Optimization

The current work is based on the multi-scale analysis and optimization method introduced by Abdelaziz et al. [70]. The method introduced consists of employing Approximation Assisted Optimization (AAO) using Parallel Parameterized CFD (PPCFD) [70] using Kriging metamodeling [90], and Multi-Objective Genetic Algorithm (MOGA). The optimization procedure is shown in Figure 6.

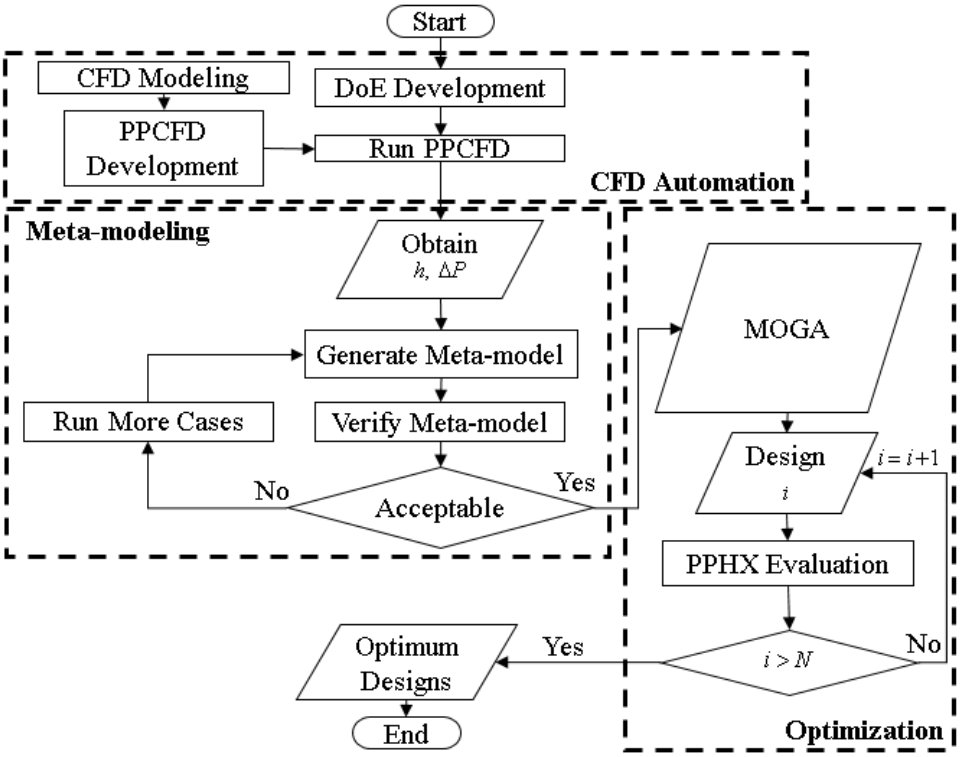

Figure 6 Optimization procedure.

3.2.1. CFD Simulations Automation

The first step in the optimization procedure is to automate the CFD simulations as shown in the framework (Figure 6). This is done through writing a Python script which executes the main workbench in ANSYS and calls JavaScript for each part in every component. The Python code execution workflow is shown in Figure 7. For each single simulation/design, one Python script, and four JavaScripts are written (in addition to two text files for NURBS curves coordinates for shape optimization) as follows

a) DesignModeler® JavaScript (SS component) for drawing the geometry
b) Mechanical simulation JavaScript (SS component) in which the mechanical deformation is simulated resembling the manufacturing process in order to get the pillow shape
c) DesignModeler® JavaScript (FF component) in which the Parasolid is exported from the FEM component, reassembled, and the computational domain is extracted
d) Meshing JavaScript (FF component) for meshing the computational domain

The Python script execution, as shown in Figure 7, is responsible for the following executions:

a) Opening a new workbench, adding a new SS component, and opening the DesignModeler® component
b) Running the geometry JavaScript, closing the component and opening the Mechanical component

c) Executing the mechanical JavaScript, closing the Mechanical component, then adding a new FEM component and a new FF component to the workbench
d) Updating the FEM component with the geometry exported from the SS component, which transforms the pillow plate geometry into a disassembled parasolid geometry
e) Opening the DesignModeler® in the FF component, running the geometry JavaScript, closing and opening the Mesh component
f) Executing the Mesh JavaScript, and
g) Finally executing the FLUENT® simulation.

For each CFD simulation, five scripts are written. For simulations of PPHX with weld shape optimization, two additional text files are written for the NURBS curve coordinates, one for each geometry component. The PPCFD code and all scripts are written using an external C# code which also writes an executable batch file to run the simulations. Figure 8 shows the three main components of a single PPHX CFD simulation in ANSYS. Post processing data from CFD simulations is also done using an external C# code.

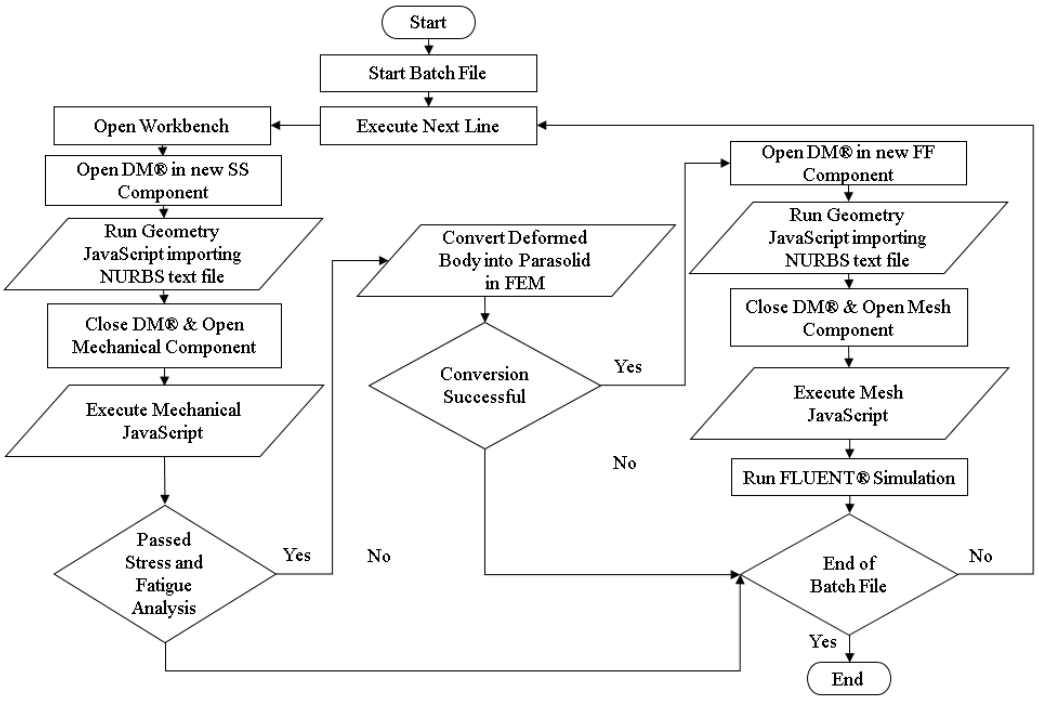

Figure 7: Python script execution within an executable batch file.

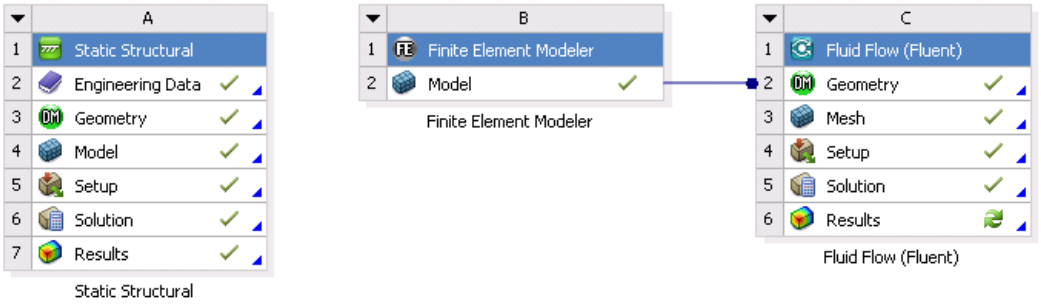

Figure 8: A single CFD simulation components for a PPHX plate [97].

3.2.2. Design of Experiments

In order to develop an unbiased metamodel with the highest quality of information which accurately portrays the impact of each design variable has on the simulation responses, it is necessary to select the right Design of Experiments (DoE). DoE is a systematic approach for sampling the appropriate designs from the design space to achieve this goal. In the current work, Latin Hypercube Sampling (LHS) [91] is used. The DoE space sampling includes the design space extreme points, which includes the lower and upper bounds of all design variables, the center point and space filling designs.

3.2.3. Metamodeling

Metamodels are essentially computationally inexpensive simplified models that are capable of capturing the behavior of the underlying system as a function of the independent parameters. The metamodel uses a limited number of expensive CFD simulations based on a finite set of parameterized initial designs in a DoE space. The developed metamodel can accurately predict the outcome of CFD simulation for any given design within the design space. Kriging metamodeling [90] is utilized in the current work in order to predict the thermal-hydraulic performance of the PPHX plate. The Kriging technique is a stochastic metamodel which predicts the responses of an unknown design based on its linear distance from known designs through a random/stochastic process. This technique is recommended with design space of 50 variables or less which is the case in the current work.

In order to verify the accuracy of the metamodel, it is required to evaluate the ability of the metamodel to accurately predict responses from random design, n. The number of random designs is usually taken as about 20% of the number of cases used to obtain the metamodel. The standard metrics to compare the accuracy of a metamodel prediction $\tilde{y}(x_i)$ with the response obtained by actually running the random design $y(x_i)$ are the following

a) Root mean square error ($RMSE$) given by

$$RMSE = \sqrt{\frac{1}{n}\sum_{i=1}^{n}[y(x_i) - \tilde{y}(x_i)]^2} \tag{18}$$

b) Maximum Absolute error (MAE) given by

$$MAE = \max(|y(x_i) - \tilde{y}(x_i)|), \quad i = 1,...,n \tag{19}$$

c) Relative $RMSE$ ($RRMSE$) given by

$$RRMSE = \sqrt{\frac{1}{n}\sum_{i=1}^{n} e_i^2} \tag{20}$$

$$e_i = \frac{y(x_i) - \tilde{y}(x_i)}{y(x_i)} \tag{21}$$

d) Relative MAE ($RMAE$)

$$RMAE = \max(|e_i|) \tag{22}$$

The acceptability of the metamodel can be established using the Metamodel Acceptability Score (MAS) [108]. The MAS value indicates the fraction of predicted responses by the metamodel in which the absolute relative error $|e_i|$ is equal to or less

than an established threshold e_{MAS}. This established threshold is typically less than or equal to 10%. Typically the metamodel is acceptable when the $MAS \geq 1 - e_{MAS}$.

3.2.4. Multi-Objective Optimization

Genetic algorithms [86] for multi-objective optimization problems (MOGA) is utilized in this work. Two conflicting objectives are analyzed. The tradeoff between the two objectives is represented by the set of optimum designs in a Pareto set.

In conclusion, the AAO framework is this divided into three parts, as shown in Figure 6, namely

1) PPCFD which consists of the DoE development and the CFD simulations
2) Metamodel development
3) Optimization using MOGA

Chapter 4: Optimization of Pillow Plate Heat Exchanger

4.1. PPHX Geometry

The geometry of PPHX is a complex 3D geometry that requires accurate prediction. One way to predict the PPHX geometry is to perform forming simulations as denoted by Piper et al. [57] who also, based on their own numerical simulations, introduced correlations that describe the geometrical characteristic of pillow plates. The pillow surface in this study is attained by simulating two thin metal plates made of stainless steel of material 1.4541 (AISI 321), bonded together at the welding spots, and undergoing a hydroforming process in ANSYS Static Structural component [97]. Figure 9 shows a portion of the pillow surface that results from this process, while Figure 10 shows the computational domain which consists of a periodic element of the pillow plate. The periodic element is repeated five times to ensure steady state is reached within the computational domain. The geometric parameters are defined as shown in Figure 10. The diameter of the spot weld in given by d_{sp}, the height of the pillow is given by h_p , and s_T, and $2s_L$ are the transverse and longitudinal pitches of the smallest cell, respectively.

Although numerical simulations have some drawbacks as an accurate reliable design method for PPHXs, they can also have several advantages. First, the resemblance of the actual manufacturing process gives an acceptable initial prediction of the geometry

as compared to other methods such as obtaining coordinates using numerical methods which poorly describe the complex 3D pillow surface. Second, it allows for stress analysis and shows if the maximum stress or even failure is reached at any part of the pillow plate especially at the welding spots. The area surrounding the welding spot is the most vulnerable to failure even before attaining the maximum stress due to the necking of the metal sheet as shown by Piper et al. [57]. Thus, numerical simulation can act as an initial failure test and give a very informative initial insight of the design of the PPHX. However, many uncertainties are embedded and more reliable prediction methods are highly desired. The PPHXs studied in this work have staggered circular welds with water as the refrigerant.

Figure 11 shows the heat transfer (wetted) area of the PPHXs simulated in this study plotted against the heat transfer area calculated using correlations from Piper et al. [57] which are developed using forming simulations using another commercial finite element tool. Two sets of data are plotted in Figure 11. The first set is for a conventional PPHX geometry like the one shown in Figure 10, while the second geometry is what Piper et al. [57] call "untypical" geometry. An example of an "untypical" geometry is shown in Figure 12 where the pillow has two maximum heights within the same periodic element. It has to be noted that all PPHXs in this optimization study have conventional/typical geometry. Although some of the predicted heat transfer areas using the correlations are very well predicted within less than 5%, as shown in Figure 11, however, the correlations greatly over predict the heat transfer area for both types of geometry up to about 40%.

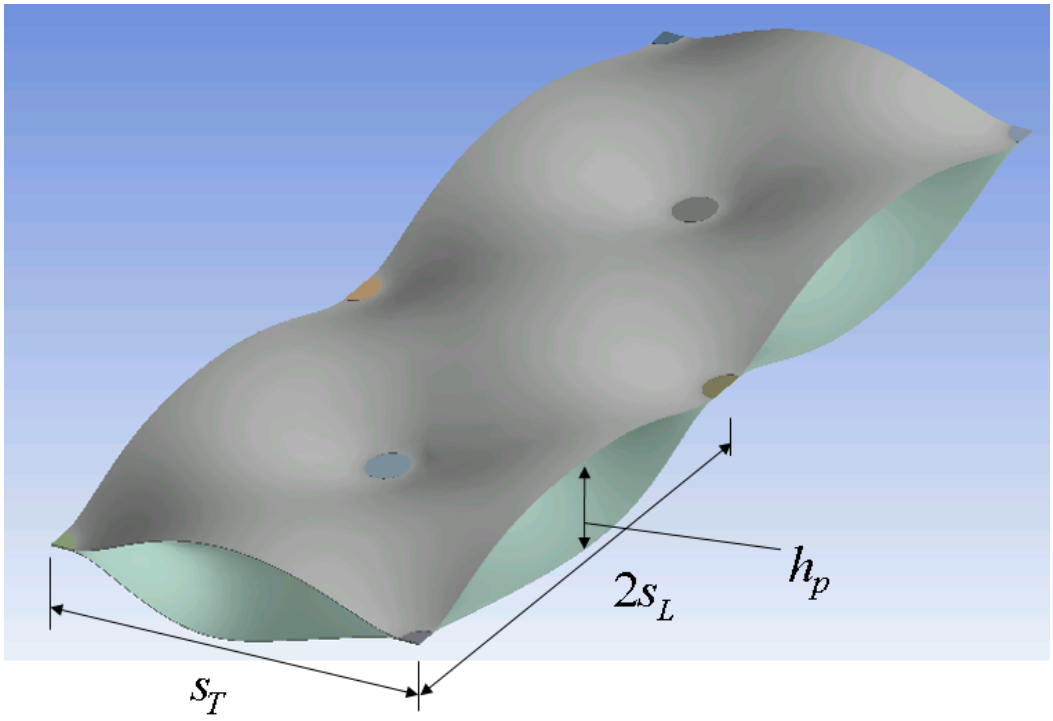

Figure 9: Pillow plate surface.

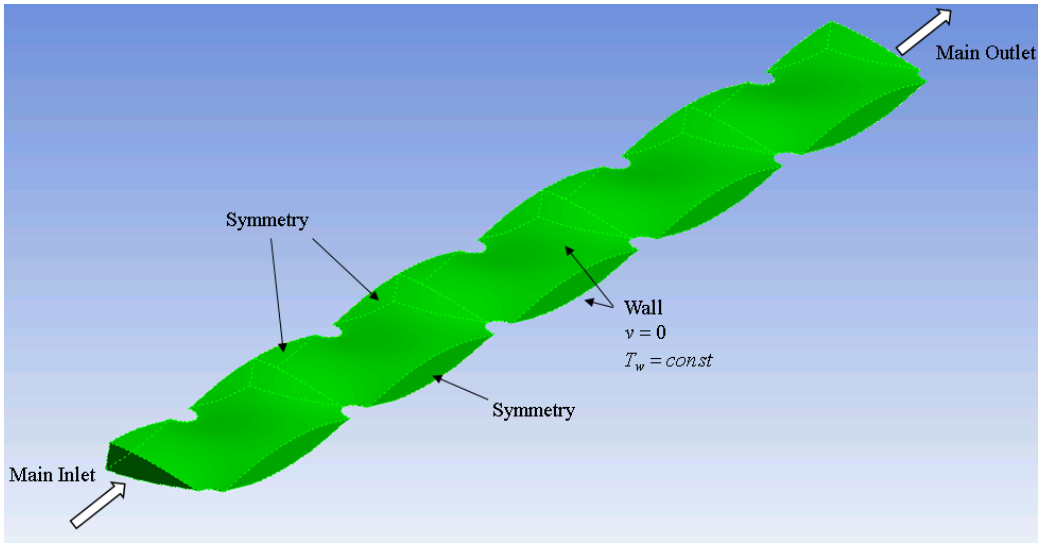

Figure 10: Computational domain of PPHX geometry.

Figure 13 shows the pillow plate volume calculated in the current study against values calculated using volume correlation from Piper et al. [57]. Unlike the heat transfer area, the volume is very well predicted within 5% but only for the conventional geometry. For the atypical geometry, the volume is greatly under predicted by up to 40%.

It is concluded that although, as an initial attempt to calculate PPHXs geometric parameters, the correlations developed by Piper et al. [57] can be very useful, but as mentioned in their work and shown in the current study, more accurate design methods are required for a detailed design of a PPHX geometry in order to reduce design uncertainty.

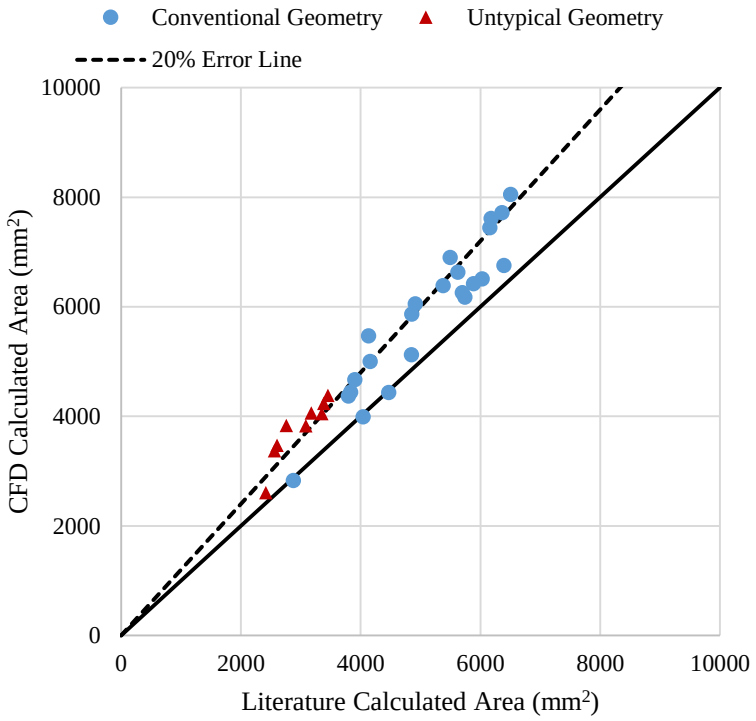

Figure 11: Heat transfer area calculated using forming simulations compared to heat transfer area calculated using correlations from Piper et al. [57].

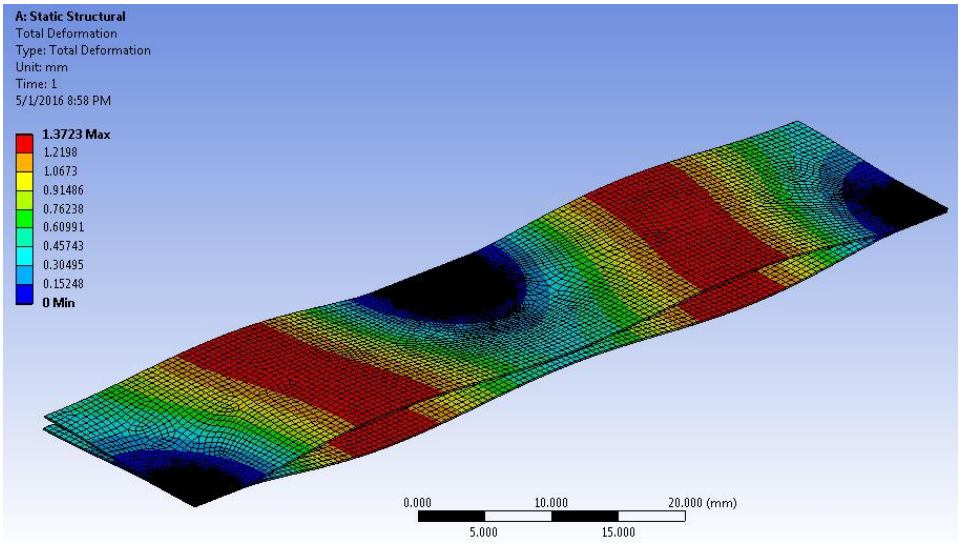

Figure 12: An "untypical" PPHX geometry simulated using forming simulation.

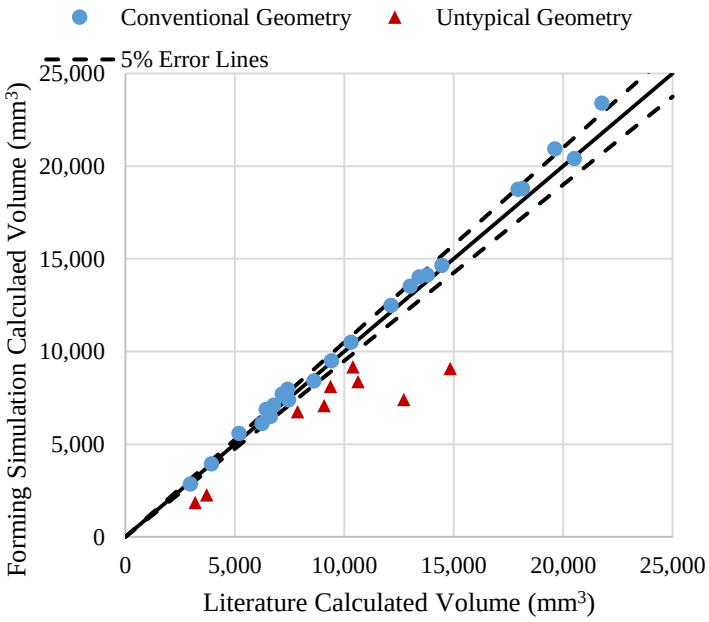

Figure 13: Volume calculated using forming simulations compared to volume calculated using correlations from Piper et al. [57].

In the current optimization problem, it is desired to maximize the heat transfer coefficient, and minimize the pressure drop per unit length. The design space has four design parameters shown with their upper and lower bounds in Table 4. The plate thickness is not a design parameter and is fixed at a value of 0.15 mm. The plate length, $2s_L$ is also fixed at a value of 72 mm.

Table 4: Optimization design space.

Design Variable	Unit	Lower Bound	Upper Bound
Ratio of transverse pitch and longitudinal pitch $\left(s_T / 2s_L\right)$	dimensionless	0.58	1.73
Spot weld diameter $\left(d_{sp}\right)$	mm	3.0	10.0
Pillow height $\left(h_p\right)$	mm	3.0	12.0
Inlet velocity $\left(v_{in}\right)$	m/s	0.1	2.0

4.2. CFD Model

Single phase, incompressible, turbulent, steady-state water flow is studied. The 3D computational domain is shown in Figure 10 consisting of five segments of the basic periodic symmetrical cell of the pillow surface in order to capture both the entrance region as well as the steady state region. A homogeneous inlet velocity, constant outlet atmospheric pressure (0.0 Pa gauge), and symmetrical pillow sides are assumed. A no-

slip boundary condition and constant wall temperature boundary conditions are applied. The Reynolds number in this study is defined using Equation (7), the heat transfer coefficient is calculated using the logarithmic mean temperature difference using Equation (8), and the friction factor is calculated using Equation (9). The baseline case corresponding to one of the geometries studied in Piper et al. [58] is shown in Table 5. The inlet temperature is 295 K and the wall temperature is 300 K. The GCI analysis results is shown in Figure 14.

Table 5: PPHX Baseline case geometrical parameters.

Case	$s_T / 2s_L$ (-)	h_i (mm)	d_{sp} (mm)	d_h (mm)
Baseline	0.58	3.0	10	4.1

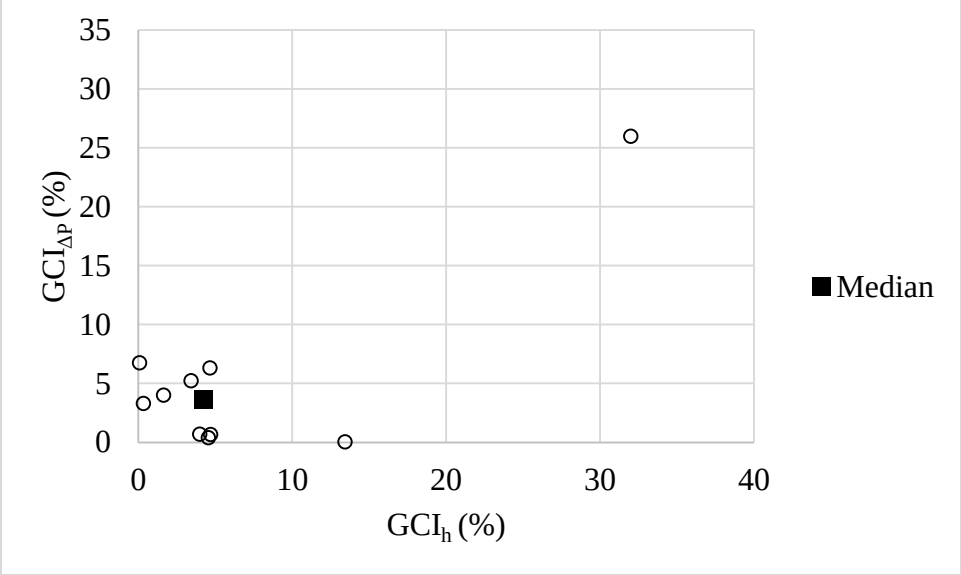

Figure 14: CFD GCI Analysis for PPHX.

In order to gain more confidence in CFD simulations results, it is desired to compare the CFD simulation results with correlations describing the thermal-hydraulic behavior in PPHXs. However, such correlations are scarce in the literature and the development of such correlations is still an ongoing process. A recent study by Piper et al. [59] developed correlations for predicting the heat transfer and pressure drop performance in PPHXs using numerical simulations some of which are validated against experimental results [58], using about 22 different geometries. The correlations are developed using a Reynolds number and Prandtl number ranges of $1000 \leq Re \leq 8000$, and $1 \leq Pr \leq 150$, respectively. Generally, the pattern of dependency of geometrical parameters reported in Piper et al. [59] is similar to that reported in the current work. Two correlations are developed to predict the Nusselt number based on two models. The first model is the Dittus-Boelter power-law approach [109], while the second model in developed by the authors for what they call the "meandering core flow" which is the core zone in the PPHX fluid flow volume excluding the recirculation zones that take place behind the welds. The Darcy friction factor, on the other hand, is predicted using a power-law function using the Reynolds number. Three correlations are developed for each of three cases corresponding to values of $2s_L/s_T$ approximately equal to 0.58, 1, and 1.71. Figure 15 and Figure 16 show the current work CFD simulation results compared to Piper et al. [59] correlations for the Nusselt number using the two models they developed, and for the Darcy friction factor, respectively. For the Nusselt number, 54% of the CFD data fall within 30% error lines using the correlations from model 1, while 36% of the CFD data fall within the same error lines

using correlations from model 2. For the Darcy friction factor, about 60% of the data lie within the 35% error lines.

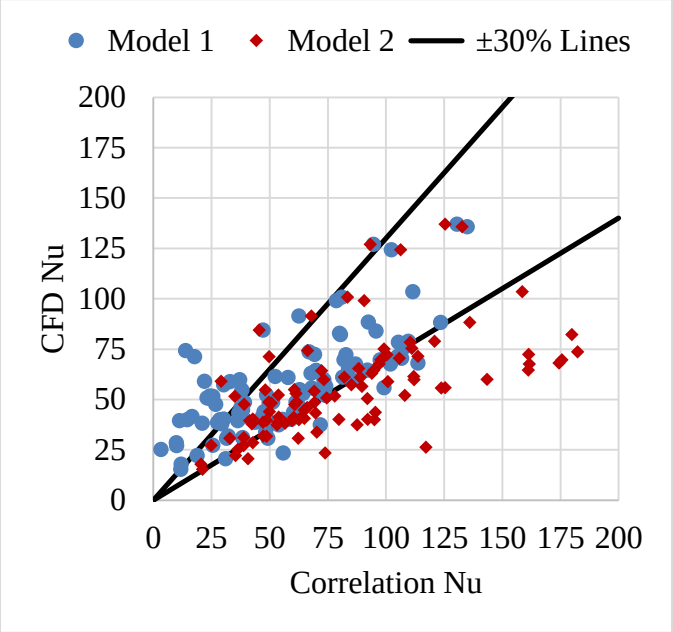

Figure 15: Comparison between CFD simulation and Piper et al. [59] correlation prediction of Nusselt number.

Since the weld pitch ratios in the current work is not constant at the values at which the correlations are developed (0.58, 1, and 1.71), and also these values are approximations to values falling within similar range resembling similar flow patterns, broader ranges are used in these calculations. For the correlations at a value of 0.58, values up to 0.75 are used which still lie in the transverse pattern range, while for those at a value of 1.71, a range of 1.5 to 1.73 is used which still lie in the longitudinal pattern range. Other reasons causing the discrepancies might be:

1. The correlations assume that the heat transfer coefficient and the friction factor are not a function of the pillow height while this assumption is not validated neither experimentally nor numerically and it is included in their future work. This might be true to a certain extent, but in their work the pillow height used ranges between 3-6 mm, while in the current work the range is between 3-12 mm which includes higher values of pillow height which might have a greater impact on performance.
2. The Reynolds number in their work is calculated based on the mean velocity in the channel, while in the current work it is calculated based on the inlet velocity. It is unclear what methodology is used to calculate the mean velocity, and at what section of the pillow plate it is calculated.
3. The channel length in model 2 is described as the arc length of a sin curve which might not be very accurate and might have caused an over prediction of the Nusselt numbers as compared to model 1 as can be seen in Figure 15.
4. The correlations are developed using a limited number of geometries which might have induced other sources of inaccuracies.
5. Correction factors are used for the hydraulic diameter and the mean velocity in order to account for a necessary extrusion of the welding spot for meshing reasons. The factors are determined using correlations from Piper et al. [57]. On the other hand, the volumes and areas in the current work are directly determined from the CFD simulations some of which vary significantly from the correlations in Piper et al. [57] as is presented in the previous section

(Section 4.1) , especially the surface area which lie within 20% from the value calculated from the correlation. This might also have introduced a compound error.

Although there is a fair agreement between the CFD simulations and the correlations, more experimental and numerical effort is required in order to more accurately predict the heat transfer coefficient and pressure drop in PPHXs.

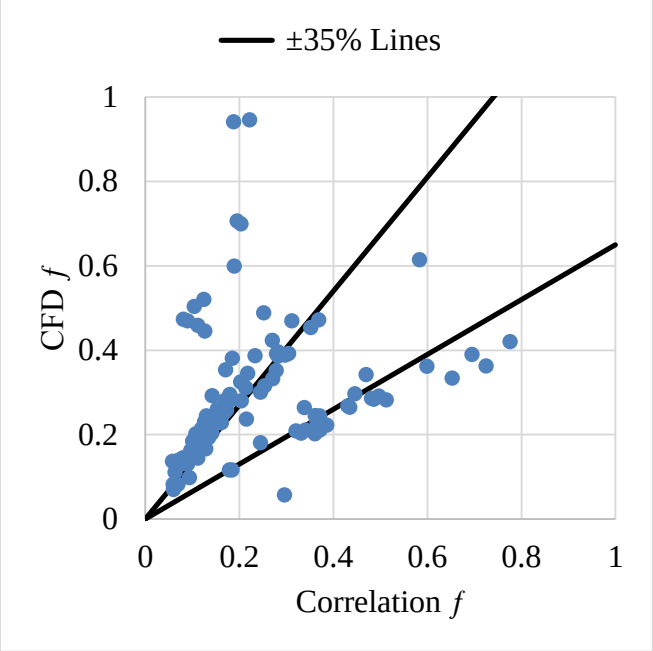

Figure 16: Comparison between CFD simulation and Piper et al. (2017) correlation prediction of Darcy friction factor.

4.3. Optimization

The optimization problem with four design parameters is given by

$$\begin{aligned} &\max \ h \\ &\min \ \Delta P / L \\ &s.t. \begin{cases} 0.58 \le \dfrac{s_T}{2 s_L} \le 1.73 \\ 3.0 \le h \le 12.0 \\ 3.0 \le d_{sp} \le 10.0 \\ 0.1 \le v_{in} \le 2.0 \end{cases} \end{aligned} \tag{23}$$

The metamodel is formed using 408 simulations and verified using 103 random samples yielding a MAS value of 94.17% for heat transfer coefficient and 90.29% for pressure drop. The metamodel verification metrics [110] are shown in Table 6.

Table 6: PPHX metamodel verification metrics.

Interpolated variable	Heat Transfer Coefficient	$\Delta P / L$
Number of samples	408	
Number of random samples	103	
Correlation	Spherical	Spherical
Regression model	Polynomial 2nd order	Polynomial 2nd order
Root Mean Square Error (RMSE)	15.6	0.8
Relative RMSE (%)	1.83	2.15
MAS threshold (%)	10	10
MAS (%)	94.17	90.29

4.4. Design Variables Sensitivity Analysis

After it is verified, the metamodel is used to conduct a sensitivity analysis on each of the four design parameters to investigate and verify the impact of changing each design variable on the thermal-hydraulic performance. For each parametric study, a single variable is changed while all other variables are fixed. The reference values used for each design variable in all studies are 0.58 pitch ratio, 3.0 mm pillow height, 10.0 mm spot weld diameter, and 0.95 $m \cdot s^{-1}$ inlet velocity. Figure 17 shows the results of the parametric analysis. The spot weld pattern is transverse up to a pitch ratio of 1, and longitudinal for pitch ratios greater than 1. Longitudinal pitch ratio shows higher heat transfer coefficient as well as higher pressure drop values. This can be explained by the recirculation that takes place behind the weld occupying most of the narrow path between the welds. This leads to enhanced mixing but higher pressure drop as well. Figure 17(b) shows the results of the sensitivity study for the pillow height. It is found that a larger pillow height has a desirable effect on both higher heat transfer coefficient as well as a lower pressure drop per unit length. This is because a larger pillow height means a larger hydraulic diameter and thus the average channel velocity will be lower leading to lower pressure drop. It also implies a slightly larger heat transfer area which leads to a slight overall enhancement in the heat transfer coefficient as well.

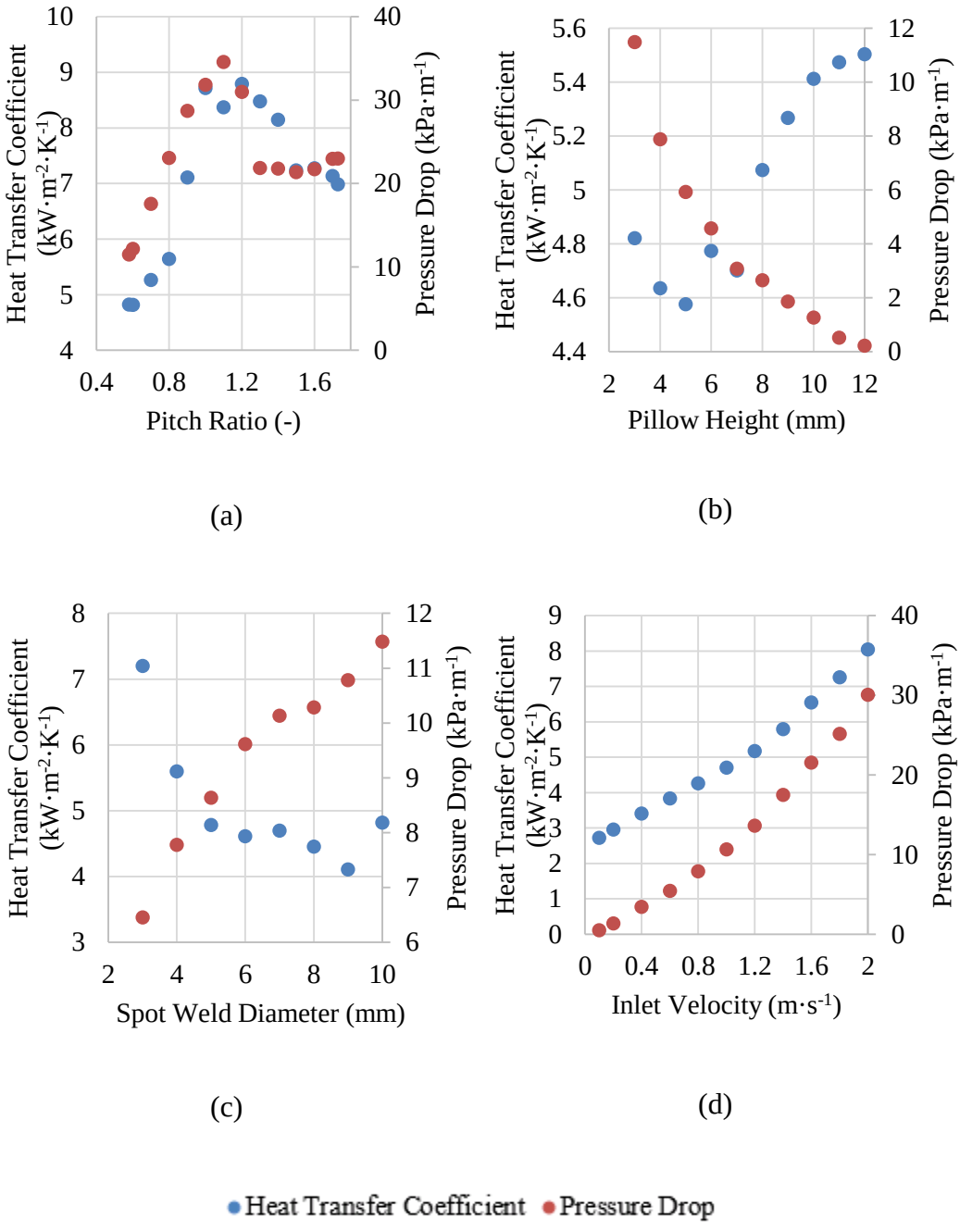

Figure 17: Sensitivity analysis for (a) pitch ratio, (b) pillow height, (c) spot weld diameter, and (d) inlet velocity.

Figure 17(c) shows the results of the spot weld diameter sensitivity study. The results show that a smaller weld diameter is desirable for both enhanced heat transfer and reduced pressure drop. It is especially noted that the size of the weld greatly affect the hydraulic performance.

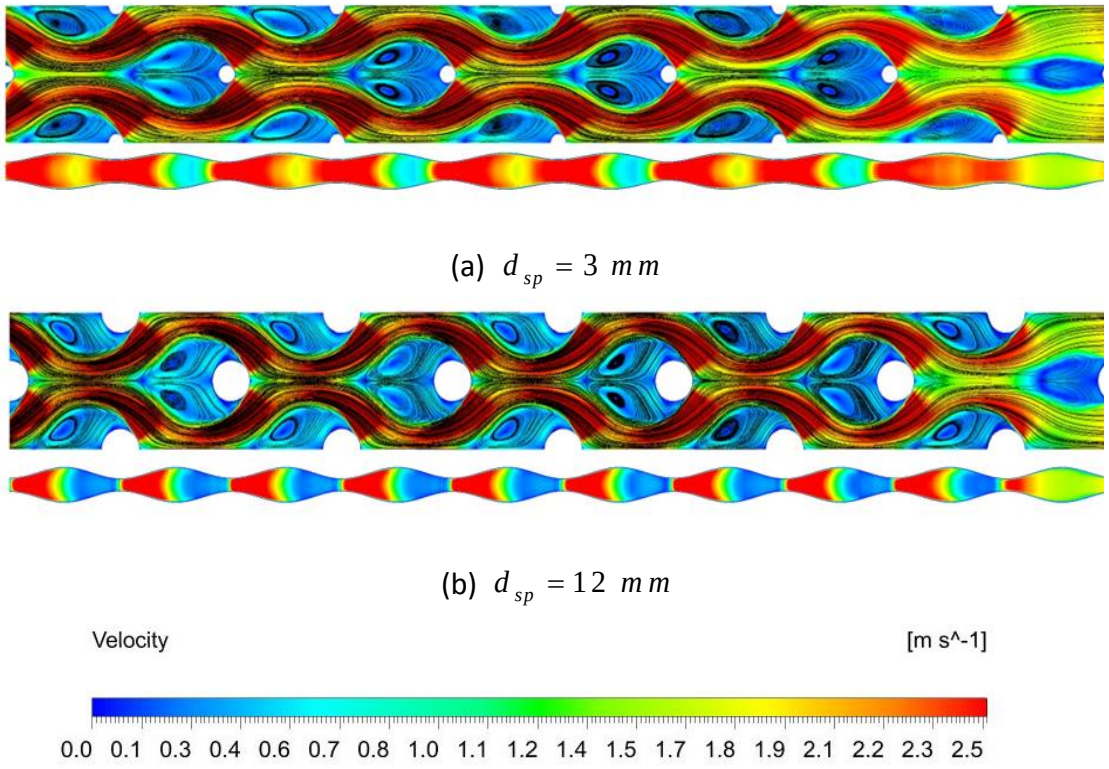

Figure 18: Velocity profile for different spot weld diameter.

Figure 18 shows the velocity profiles of two PPHX designs with different spot weld diameters. It can been seen from the velocity profiles that the PPHX design with larger weld diameter has a more restricted core flow zone yielding higher velocities due to the huge wake region behind the weld which not only deprives the design from heat transfer area required for higher heat transfer, but also lead to a higher pressure drop.

This becomes well established and more obvious especially when steady state flow is attained. Finally, Figure 17(d) shows the results of the velocity sensitivity analysis. The inlet velocity greatly affects the thermal-hydraulic performance of PPHXs. The higher the inlet velocity the higher the heat transfer coefficient and also the higher the pressure drop which also increases at an even higher rate at very high inlet velocity values.

4.5. Optimum PPHX Designs

The verified metamodel is also used to run a MOGA to optimize the thermal-hydraulic performance of PPHX. Figure 19 and Figure 20 present the optimum designs for the PPHX in comparison to the baseline. The baseline used for comparison in this study is one of the designs investigated by Piper et al. [58] given in Table 5 and calculated at an inlet velocity of 1.2 $m \cdot s^{-1}$. PPHX Optimum designs dimensions are given in Appendix A. The spot weld diameter for the optimum designs ranged from 3 mm to 9.6 mm. The small diameters yield a higher heat transfer coefficient as well as a higher pressure drop, while the larger diameters yield a lower heat transfer coefficient and a lower pressure drop. However, at lower inlet velocities both heat transfer coefficient and pressure drop are low with larger spot diameter. Some of the best designs right at the middle of the Pareto have the smallest spot diameters balancing between higher heat transfer coefficient and moderate pressure drop values.

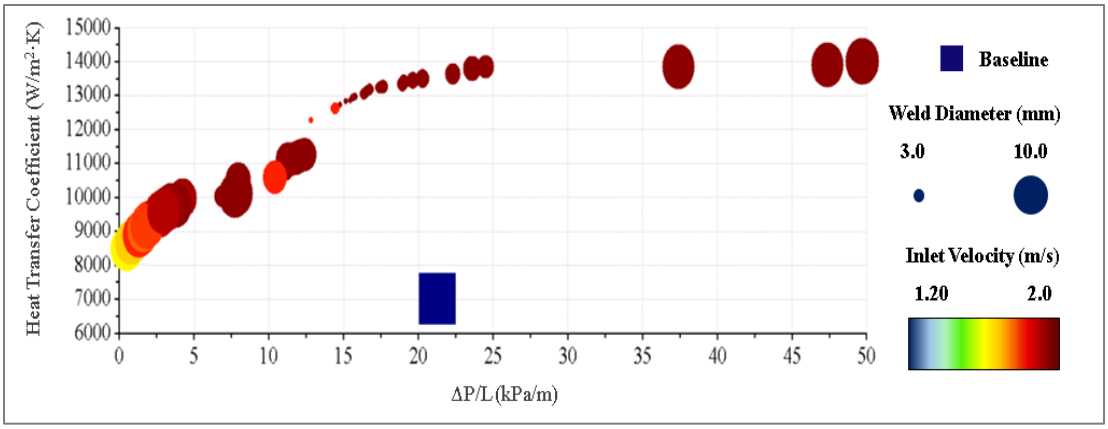

Figure 19: Optimum PPHX designs at different weld diameters and inlet velocity.

The optimum PPHX designs have pitch ratios ranging from 0.58-1.4. A pitch ratio of less than one constitutes a transverse weld pattern and is characterized by low heat transfer coefficient and low pressure drop as shown in Figure 20 with the blueish dots, while that of values greater than 1 constitutes a longitudinal weld pattern and is characterized by high heat transfer coefficient and high pressure drop as shown in Figure 20 by the reddish dots. The pillow height and the inlet velocity for the optimum designs are both in their respective high ranges of 11.5 mm to 12 mm, and 1.7 $m \cdot s^{-1}$ to 2 $m \cdot s^{-1}$, respectively. This is quite expected as per the sensitivity analysis in spite of the fact that pressure drop increases as well at higher values of inlet velocities. The optimization results show a significant improvement in heat transfer coefficient ranging from at least 33.1% at high Reynolds numbers and up to the double with respect to the baseline. The optimization results also show a significant reduction in pressure drop per unit length ranging from at least 11% at low Reynolds numbers and up to 98% reduction relative to the baseline.

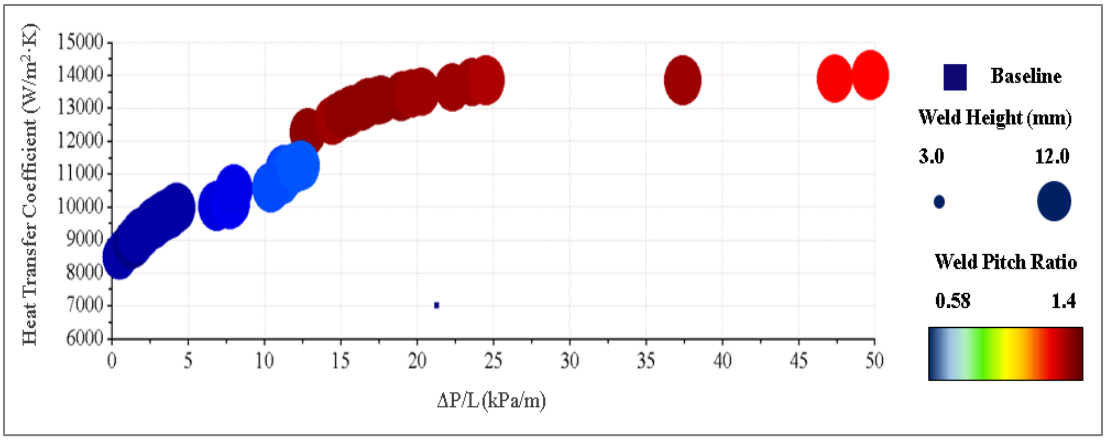

Figure 20: Optimum PPHX designs at different weld pitch ratios and weld height.

4.6. Comparison with Chevron Plate Heat Exchangers

Saleh et al. [111] studied the optimization of chevron PHXs using different optimization techniques. Figure 21 shows the optimum designs obtained by Saleh et al. [111] for chevron PHXs using offline AAO in comparison to the optimum design obtained for PPHX in the current study. Although chevron PHXs have higher heat transfer coefficient values at higher pressure drop per unit length values, but in the area of the plot where both types of PHXs have comparable values, PPHX is showing more favorable results. At a pressure drop of 2 kPa/m, for example, the heat transfer coefficient of PPHX is about three times greater than that of the chevron PHX. At a pressure drop of 25 kPa/m, the heat transfer coefficient is about 23% greater than that of the chevron PHX. On the other hand, at a heat transfer coefficient value of 14,000 $W/m^2 \cdot K$, the pressure drop of PPHX is 0.7 times that of the chevron PHX or about 30%

lower. This places PPHX in a very good position compared to chevron PHXs and gives it a great potential to outperform chevron PHXs.

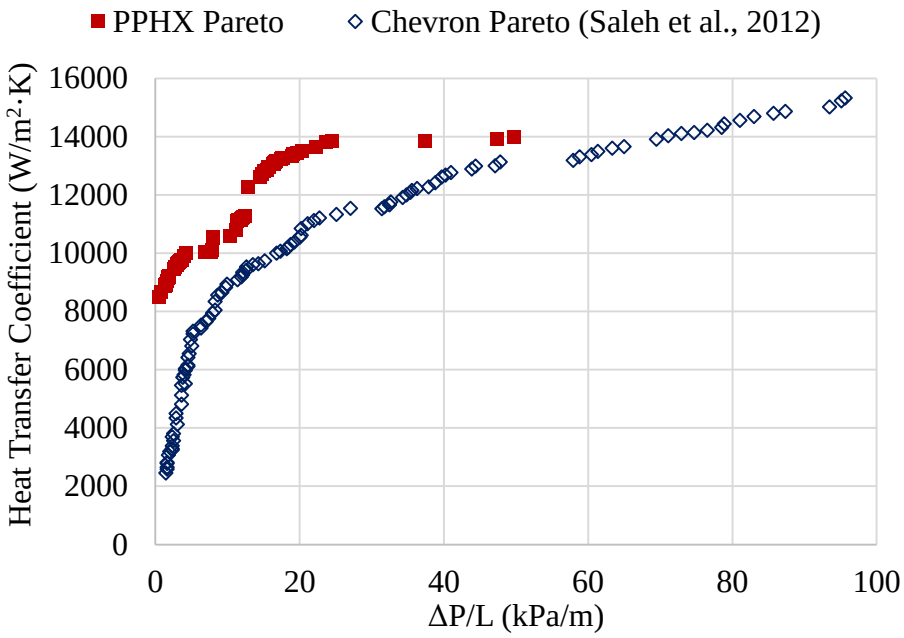

Figure 21: PPHX optimum designs compared to Chevron PHX optimum designs from Saleh et al. (2012).

Chapter 5: Weld Shape Optimization of Pillow Plate Heat Exchanger

5.1. Concept and Design Framework

The results from the preceding chapter can be summarized in two main findings. First, PPHXs can perform better than chevron PHXs by at least 23% (Figure 21) which is a significant improvement in addition to their economic advantage. Second, in order to further improve the performance of PPHXs and place it in a distinct position with respect to other types of PHXs, the weld size and shape have the most significant effect on the thermal-hydraulic performance as shown in Figure 17.

Given these findings, optimization of PPHXs including a larger set of design variables, to describe the weld shape, is undertaken. The weld shape used in the current problem varies from the previous problem which only used a circular spot weld shape with a fixed diameter. The more streamlined weld shapes will allow the wake region behind the weld spot to shrink and thus improving the pressure drop significantly (Figure 18). However, it is also desired to have a similar heat transfer area in order to at least maintain the heat transfer improvement previously attained. This is where optimization plays in. The current optimization problem has the same objectives of maximizing the heat transfer coefficient while minimizing the pressure drop per unit length with a set of 11 design variables that include shape variables that describe the weld shape and

size in addition to design variables describing the pillow height, weld pitch ratios, and the inlet fluid velocity.

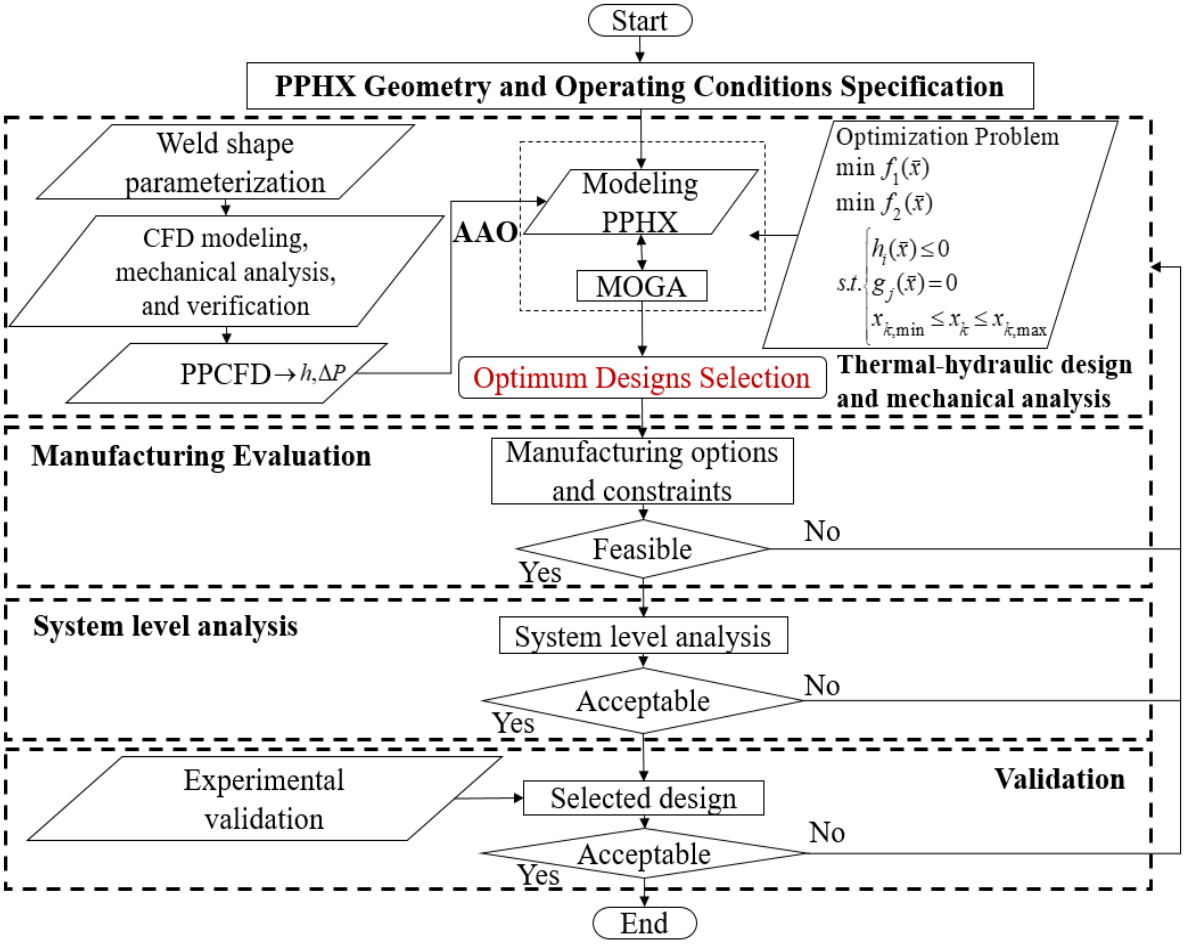

Figure 22: Design framework.

The design framework employed in the current work is shown in Figure 22 consisting of five main steps or subgroups. The first - PPHX geometry and operating conditions specification - includes the surface concept of the pillow plate and the parameters range specification. The second subgroup - thermal-hydraulic design and mechanical analysis - includes the main steps from the numerical optimization (Figure 6) which includes

the actual design and optimization using AAO methodology. This step also includes the mechanical evaluation of the pillow plate as the mechanical stress analysis is included in this step in the CFD SS component as mentioned in the preceding chapter. The following step includes the reality check of the manufacturing feasibility of the optimal designs. This potentially includes multi-physics analysis such as mechanical stress evaluation, noise, vibration, etc., as well as the ability to produce the desired weld shape and size. The fourth step is investigated in the case it is desired to evaluate the selected optimum designs for a system level application where the system performance is evaluated. Finally, the selected designs are manufactured and evaluated experimentally for validation. The last three steps are left for future work, however, this framework will serve as the guideline.

5.2. NURBS Weld Shape PPHX (NPPHX)

The NURBS wels shape Pillow Plate Heat Exchanger (NPPHX) concept is essentially equivalent to the PPHX with the addition of the shape variables that describe the weld shape of the pillow. The design space consists of 11 design variables from which 6 are the x and y normalized coordinates of the control points used to describe the weld NURBS curve. Additional two fixed control points denote the leading edge and the trailing edge of the NURBS curve as previously shown in Figure 4. The result is a 4^{th} order NURBS curve shown in Figure 23. The front view of the NPPHX computational domain and the 3D view are shown in Figure 24. The design space of the NPPHX is shown in Table 7.

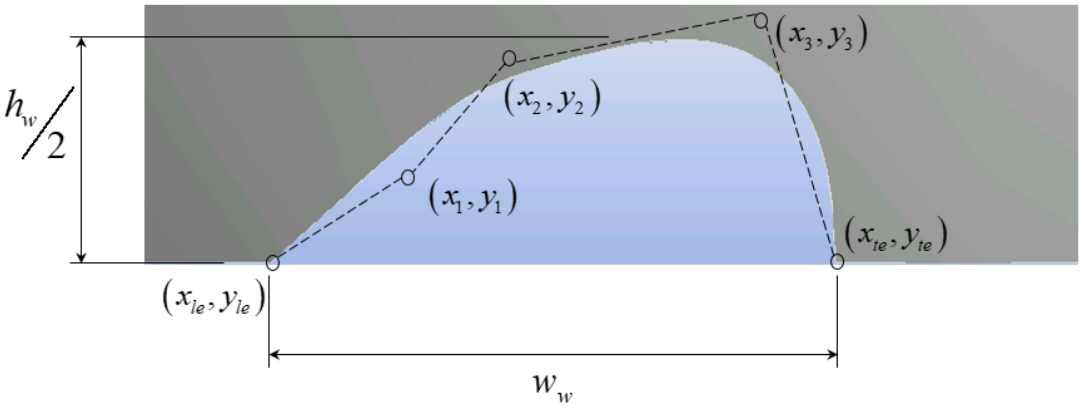

Figure 23: NPPHX weld profile parameterization.

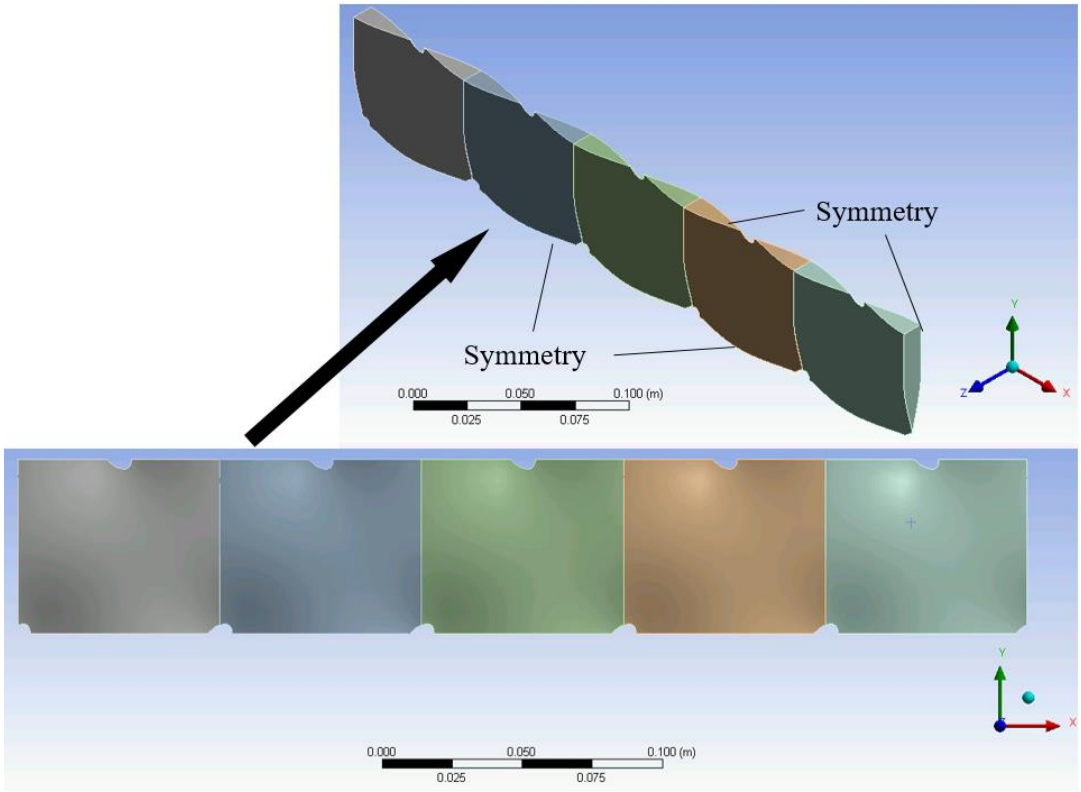

Figure 24: Front and 3D views of a NPPHX computational domain.

Table 7: NPPHX design space.

Variable Type	Design Variable	Unit	Range
Scaling	h_w	mm	3.0 – 10.0
	w_w / h_w	–	1.0 – 2.0
Topology	$2s_L / s_T$	–	0.58 – 1.73
	h_p	mm	3.0 – 12.0
Shape	x_i $where\ i = 1,2,3$	–	0.0 – 1.0
	y_i $where\ i = 1,2,3$	–	0.0 – 1.0
Fluid	v_{in}	$m \cdot s^{-1}$	0.1 - 2.0

5.3. CFD Model

The CFD automation procedure is similar to the automation procedure for the main PPCFD code explained in Section 3.2.1 with some additional geometrical operations related to the NURBS curve as shown in Figure 7. Thus, a new PPCFD code is written for this problem with the same platform that includes additional methods to write two extra text files for each design that contains the coordinates of the NURBS curve. Each NURBS curve consists of 1000 coordinates to ensure it is smooth enough for the geometric operations. Multiple geometric operations are undertaken for the NURBS curve to merge it into the PPHX geometry in DesignModeler® of the SS component

including transforming the curve into a surface, extrusion, rotation, translation, and slicing.

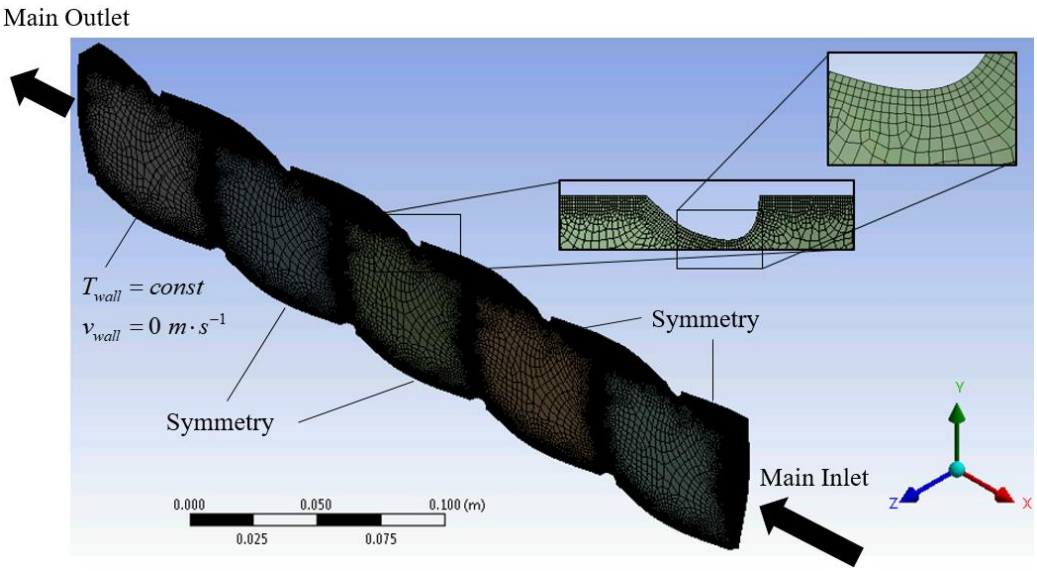

Figure 25: NPPHX meshed computational domain.

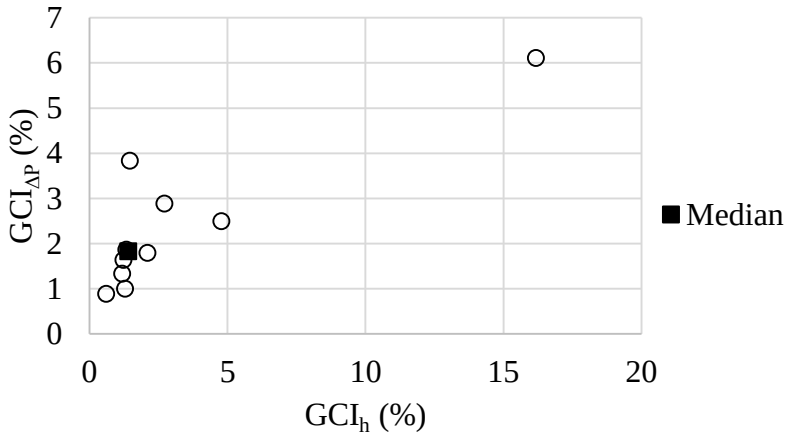

Figure 26: GCI analysis for NPPHX.

The CFD model for the NPPHX consists of a 3D computational domain with symmetric boundaries on top and bottom as shown in Figure 25. The GCI analysis results is shown in Figure 26. The GCI analysis uses a constant refinement ratio of 1.3 and a factor of safety of 3.0 for all samples.

5.4. Metamodel Verification

A Design of Experiments (DoE) containing 3615 samples generated using the Latin Hypercube Sampling (LHS) is simulated using the developed PPCFD code. Due to geometry/mesh fails or simulation divergence an effective 1764 samples are successful and used to create the metamodel. The metamodel is verified using 354 random designs shown in Figure 27 for the heat transfer coefficient and in Figure 28 for the pressure drop per unit length. The metamodel verification metrics are shown in Table 8.

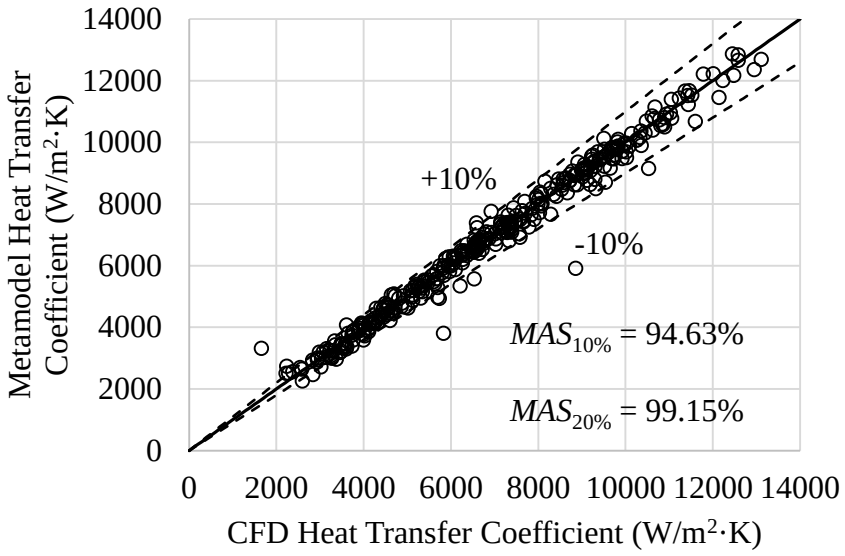

Figure 27: NPPHX metamodel verification for heat transfer coefficient against 354 random designs.

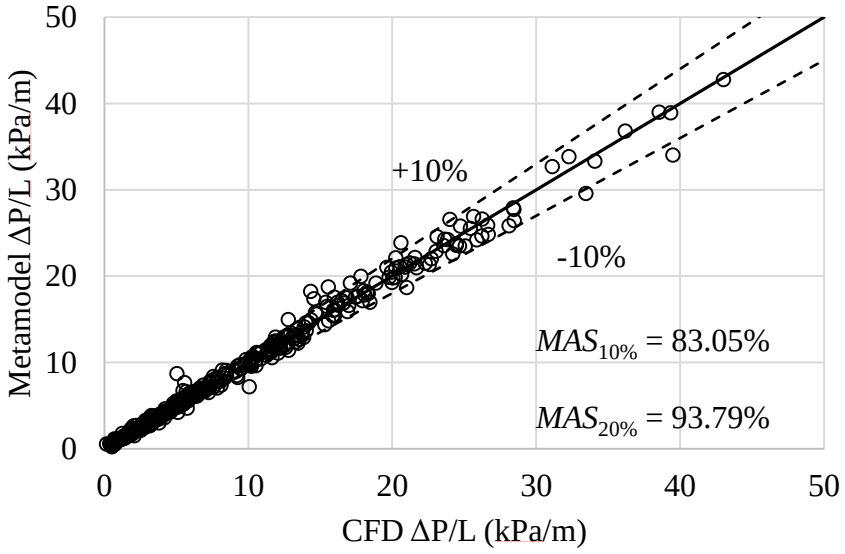

Figure 28: NPPHX metamodel verification for pressure drop against 354 random designs.

Table 8: NPPHX metamodel verification metrics.

Interpolated variable	Heat Transfer Coefficient	$\Delta P / L$
Number of samples	1764	
Number of random samples	354	
Correlation	Gaussian	Spline
Regression model	Polynomial 2nd order	Polynomial 2nd order
Root Mean Square Error (RMSE)	14.78	0.713
Relative RMSE (%)	1.92	2.69
MAS' threshold (%)	10	10
MAS (%)	94.63	83.05

5.5. CFD Results and Sensitivity Analysis

The verified metamodel is used to conduct a sensitivity analysis on some of the design variables to investigate and verify their impact on the thermal-hydraulic performance. For each parametric study, a single variable is changed while all other variables are fixed. The reference values used for each design variable in all studies are 1.73 pitch ratio, 12.0 mm pillow height, 5.0 mm weld height, 2.0 WHR, 2.0 $m \cdot s^{-1}$ inlet velocity, and the same weld shape. Figure 29 shows the results of the parametric analysis run on the weld height, WHR, pillow height, pitch ratio, and inlet velocity. All parameters are normalized.

As concluded from the previous sensitivity analysis in Figure 17 that the longitudinal pitch ratio is more favorable in terms of heat transfer, however yields higher pressure drop than transverse patterns. This is probably as a result of enhanced mixing in the core region of the channel, while flow separation and wake region formation is more probable even at low Reynolds numbers. Figure 30 shows an example of two typical designs and typical inlet conditions with the sole difference of pitch ratio. The fluid enters from the far right end in all figures.

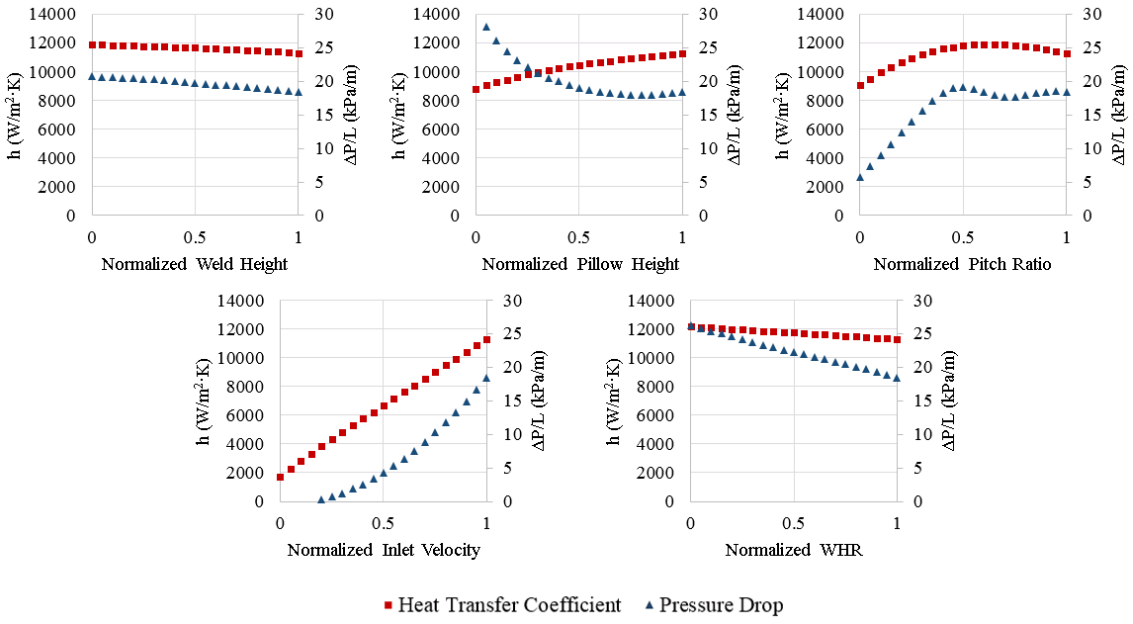

Figure 29: NPPHX sensitivity analysis for some normalized design parameters.

The parametric analysis results are also consistent for the pillow height and the inlet velocity such that it is highly desirable to design a PPHX with a large pillow height for both higher heat transfer coefficient and lower pressure drop per unit length. The inlet velocity also increases both the heat transfer coefficient and the pressure drop.

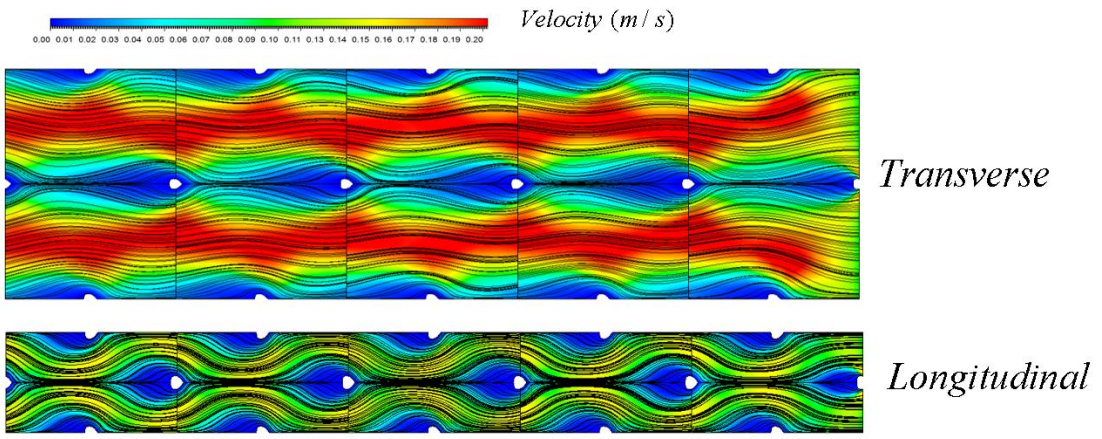

Figure 30: Velocity profile for transverse and longitudinal weld pitch ratio.

The effect of the inlet velocity on the wake region volume can be seen in the velocity profiles in Figure 31 where the two designs are typical except for the inlet velocity.

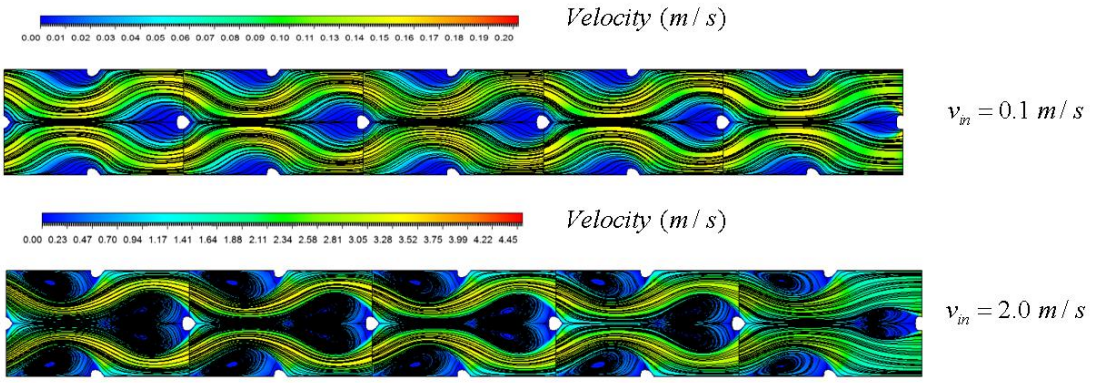

Figure 31: Velocity profile for different inlet velocity.

Eight parameters describe the weld shape and size in this problem, six of which are the control points coordinates and they are fixed for this parametric analysis, while the other two, the WHR and the weld height, are varied independently. Figure 32 shows the velocity profile of different NPPHX designs with different weld shapes. Generally

smaller more streamlined welds yield lower pressure drop values. The thermal-hydraulic performance is almost affected in a similar pattern by changing any of these two parameters, with the WHR reducing the pressure drop more sharply since the pressure drop is high for smaller values of WHR. As the size of the weld increases, the heat transfer area is reduced, and thus the heat transfer coefficient decreases as well. However, if the increase in size means a more streamlined weld as well, with higher WHR values, the pressure drop is significantly reduced as a result as well since the wake region behind the weld is reduced. Figure 33 shows the velocity profile for two different NPPHX designs. The wake region behind the NPPHX design with the lower WHR value is obviously larger than the design with the more streamlined weld shape with a higher WHR value, thus yielding a lower pressure drop.

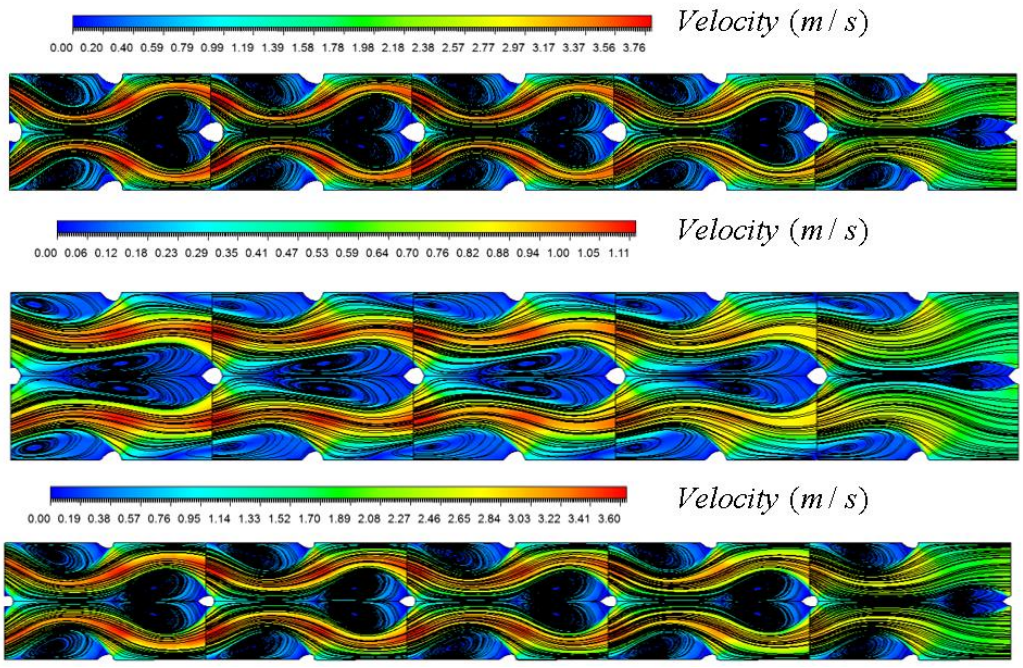

Figure 32: Velocity profile of NPPHX designs with different weld shapes

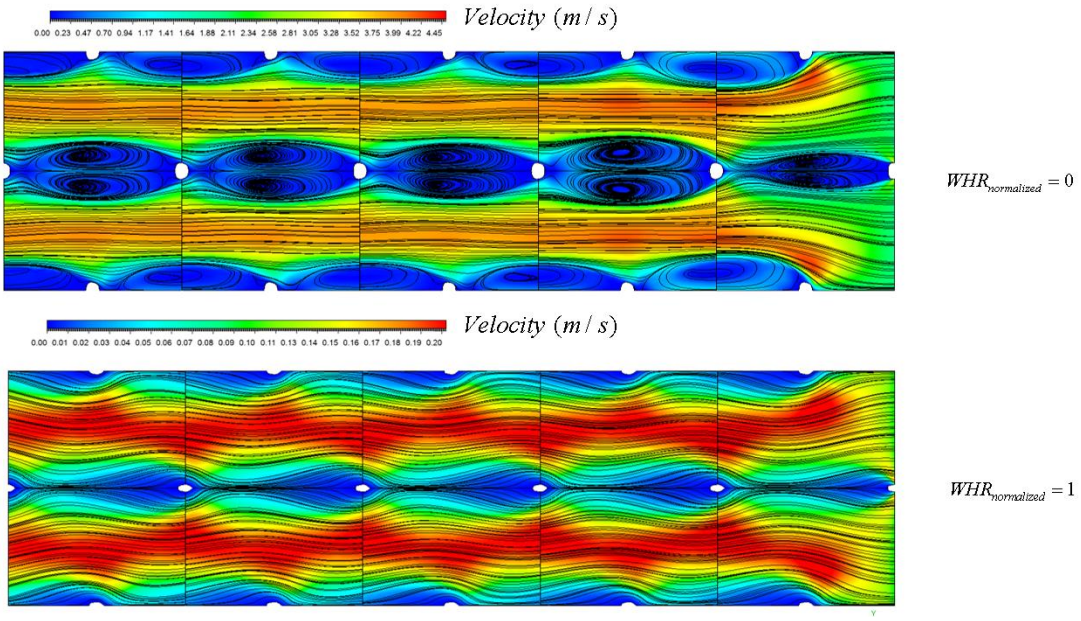

Figure 33: Velocity profile for different weld width-height ratio values.

5.6. Optimum Designs

A multi-objective genetic algorithm (MOGA) is run using the verified metamodel in order to optimize the thermal-hydraulic performance of NPPHX. The optimum NPPHX designs are presented in Figure 34 and Figure 35 compared to a baseline selected to be one of the optimum designs obtained for the PPHX with circular weld spot from the previous chapter. The baseline is given in Table 9. NPPHX Optimum designs dimensions are given in Appendix B. The most significant overall result that can be drawn from the NPPHX Pareto shown in Figure 34 and Figure 35 right away is that the maximum pressure drop of the optimum designs is now half of that of the optimum designs obtained previously for the PPHX optimization. As expected, the

more streamlined weld shape reduced the pressure drop significantly. The heat transfer coefficient on the other hand is either improved, or slightly affected by the change.

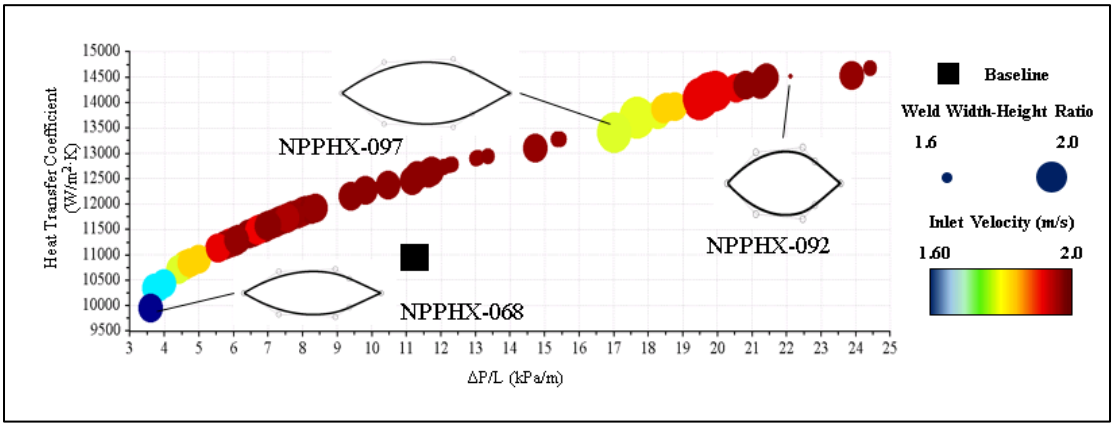

Figure 34: Optimum NPPHX designs at different weld width height ratios and inlet velocity.

The weld width height ratio (WHR) for the optimum designs ranges from 1.6 mm to 2.0 mm which means more streamlined weld shapes. While the ratio does not vary largely, smaller WHR mostly yield a lower heat transfer coefficient and a lower pressure drop. The effect of the inlet velocity, pitch ratio, and pillow height are all consistent with the results previously concluded from Figure 17. The pillow height and the inlet velocity for the optimum NPPHX designs are both in their respective high ranges of 11.45 mm to 12 mm, and 1.6 $m \cdot s^{-1}$ to 2 $m \cdot s^{-1}$, respectively, which is again quite expected as previously revealed in the sensitivity studies undertaken.

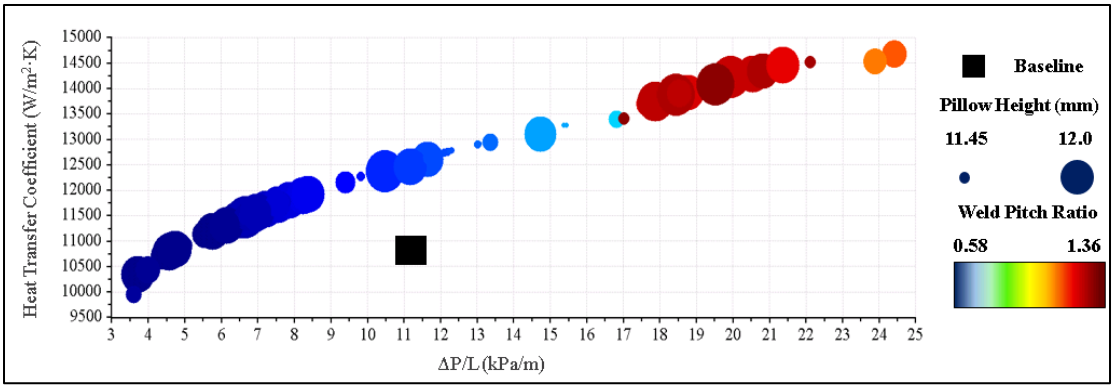

Figure 35: Optimum NPPHX designs at different pillow height and weld pitch ratio.

Table 9: NPPHX Optimization Baseline.

Baseline	$s_T / 2s_L$ (-)	h_i (mm)	d_{sp} (mm)	v_{in} (m/s)
PPHX-073	0.75	12.0	5.7	1.99

The optimization results show an improvement in the heat transfer coefficient ranging from at least 5% at moderate pressure drop values and up to 36% at high pressure drop values (about 24.4 kPa/m) with respect to the baseline. The highest pressure drop value in this case however is only 50% of the highest pressure value in the previous PPHX with circular spot weld optimization problem in Chapter 4. The optimization results also show a significant reduction in pressure drop per unit length ranging from at least 10% at moderate heat transfer coefficient values and up to 67% at lower heat transfer coefficient values relative to the baseline. This is a significant further improvement from the previous problem in Chapter 4.

5.7. Comparison of NPPHX with PPHX and Chevron PHX

Figure 36 shows a comparison between NPPHX optimum designs from the current study, PPHX optimum designs from Chapter 4, and optimum design obtained for Chevron PHXs by Saleh et al. [111] using offline AAO. Chevron PHXs have the highest pressure drop per unit length values overall, with the optimal designs having values up to 100 kPa/m. They are followed by PPHXs in which all of the optimal designs have pressure drop values of 50 kPa/m or less, which is effectively the half of chevron PHX values. Finally, NPPHXs optimal designs have pressure drop values lower than 25 kPa/m which is half of that of the PPHX with circular spot welds overall. The overall results show a significant lower pressure drop values in favor of NPPHXs.

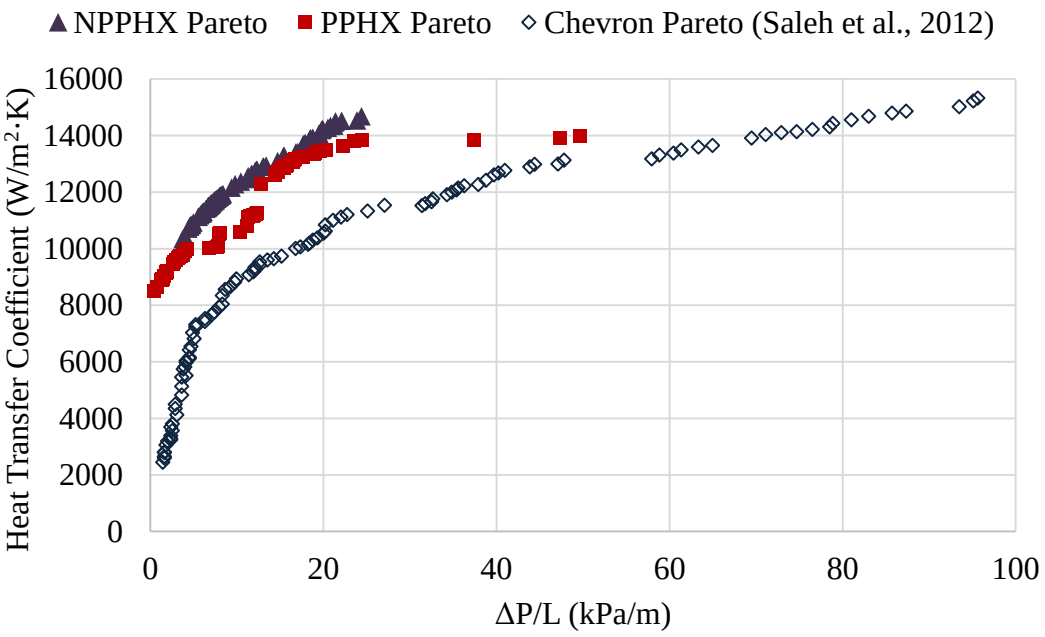

Figure 36: NPPHX optimum designs compared to PPHX and Chevron PHX optimum designs.

On the other hand, heat transfer coefficient is either slightly improved, or unaffected. At a heat transfer coefficient value of about 14,000 $W/m^2 \cdot K$, the pressure drop of NPPHX is 60% lower than that of the PPHX and 72% lower than that of the chevron PHX. At a lower heat transfer coefficient value of about 10,000 $W/m^2 \cdot K$, the pressure drop of NPPHX is 10% lower than that of the PPHX and 78.5% lower than that of the chevron PHX. On the other hand, at a pressure drop value of about 10.5 kPa/m, for example, the heat transfer coefficient of NPPHX is about 16% greater than that of the PPHX and about 38% greater than that of the chevron PHX. At a pressure drop value of 24 kPa/m, the heat transfer coefficient of NPPHX is about 5% greater than that of the PPHX, and about 28% greater than that of the chevron PHX. This is a further improvement compared to the optimization problem of Chapter 4 which places NPPHX in a further better competitive position as compared to chevron PHXs and gives it great potential to outperform thermal-hydraulic performance of chevron PHXs.

Chapter 6: Plate Heat Exchanger Solver Improvements

The challenges associated with PHXs modeling, as previously detailed in Section 1.2.4, can be summarized in the following points:

1. The complex nature of the plate heat exchanger problem with $2 \times (N-1) \times M$ unknowns, with interdependence between heat transfer and pressure drop calculations.
2. The flexibility of the model/tool such that it is able to handle different pass configurations, different number of fluids, different flow directions, a variety of heat transfer coefficient and pressure drop correlations or values, and different heat load sizes.
3. The robustness or the stability of the solution such that it accurately solves until convergence is reached.
4. The speed of solution should be convenient enough to allow for extensive modeling, design, and performance improvement for PHXs.
5. The flow maldistribution that takes place inevitably at the entrance and the exit of the PHX must be accounted for accurately modeling thermal-hydraulic performance of PHXs.

Qiao et al. [68] developed a model that addressed the first two challenges efficiently, as has been mentioned in Section 1.2.4. However, more effort is required in order to

address the other three challenges. The effort presented here is a continuation to the effort done by Qiao et al. [68]. The contribution to each of the other three challenges is addressed in the following sections.

6.1. Solver Robustness

In order to account for flow maldistribution, and improve the speed of the solution significantly, robustness must be vitally addressed first. The model developed by Qiao et al. [68] is a finite volume approach that divides the entire PHX into multiple slices, M . Each slice spans multiple channels and the performance is evaluated using wall temperature linked equations. At the heat exchanger level, all the slices are iterated upon using a successive substitution approach. .

6.1.1. Guess Wall Temperature

Qiao et al. [68] employs a quasi-Newton numerical method to solve for the unknowns in each slice. Although quasi-Newton methods are robust and have high rate of convergence. However, one of the very essential properties of quasi-Newton methods is that the initial guess value must be close enough to the final answer for the solution to converge. If an initial guess value is made far from the final answer, the solution will essentially diverge. Thus, in this problem, the initial guess wall temperatures must be carefully calculated in order to be close enough or in proximity to the final wall temperatures.

One approximation to obtain good initial guess wall temperatures could be to calculate them based on the inlet temperature and the heat transfer coefficient of the fluid associated with each channel. The following equation is applied

$$T_{wall,i} = \frac{U_{right,i-1} T_{in,i-1} + U_{left,i} T_{in,i}}{U_{right,i-1} + U_{left,i}} \tag{24}$$

where i is the channel number $i = 1, 2, \ldots, N$. The heat transfer coefficients in this equation are also pre-evaluated based on the inlet temperatures. Using this approximation, the overall success rate, stability, and convergence of the solution significantly improved and even the speed of the solution was slightly improved by up to 5% speed reduction.

6.1.2. Slice Routine

The model developed by Qiao et al. [68] is shown in Figure 37. The core of the model is the slice routine which solves for the wall temperatures in each iteration. The relative enthalpy and pressure residuals are then computed in order to decide if a solution is reached and convergence took place, otherwise the enthalpy and pressure values are updated and another iteration takes place. Divergence occurs frequently in this critical core part of the solver. Particularly, this usually take place when the solution jumps in a single iteration with a relatively large value which leads to a deviation in the solution path which leads to divergence. An updated model is developed to overcome some of the divergence that might take place in this part of the solver. The updated model is shown in Figure 38.

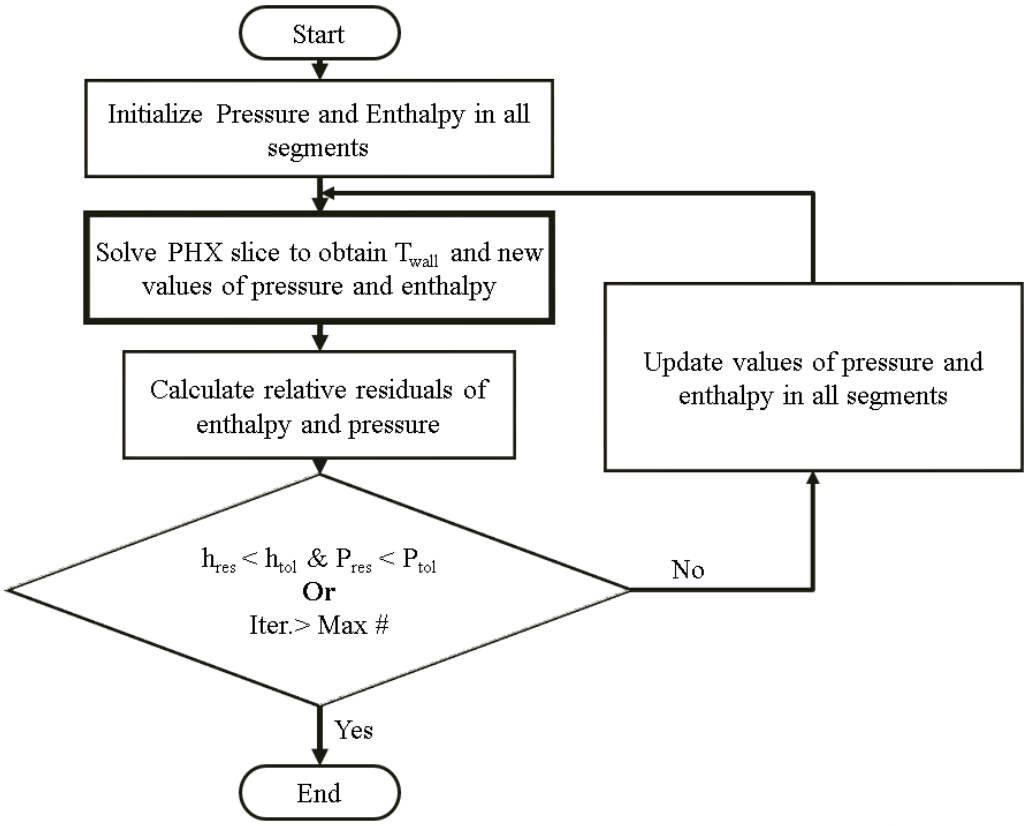

Figure 37: PHX model adapted from Qiao et al. [68].

In the updated model, first the initial guess wall temperature routine discussed in the previous section is added to each slice. Then, a check is made after solving each slice whether the solution step is outside the specified limits based on the inlet fluid temperatures given by

$$delta_{\max} = \frac{T_{in,\max} - T_{in,\min}}{T_{in,\min}}$$
$$delta_{\min} = \frac{T_{in,\min} - T_{in,\max}}{T_{in,\max}} \quad (25)$$

If the step in solution is within limits, the solution will continue. However, if the step is larger than the specified limits, the wall temperatures are re-evaluated using an explicit equation, using values from the previous iteration, given by

$$T_{wall,i} = \frac{U_{right,i} A_{right,i} T_{in,i} + U_{left,i+1} A_{left,i+1} T_{in,i+1}}{U_{right,i} A_{right,i} + U_{left,i+1} A_{left,i+1}} \quad (26)$$

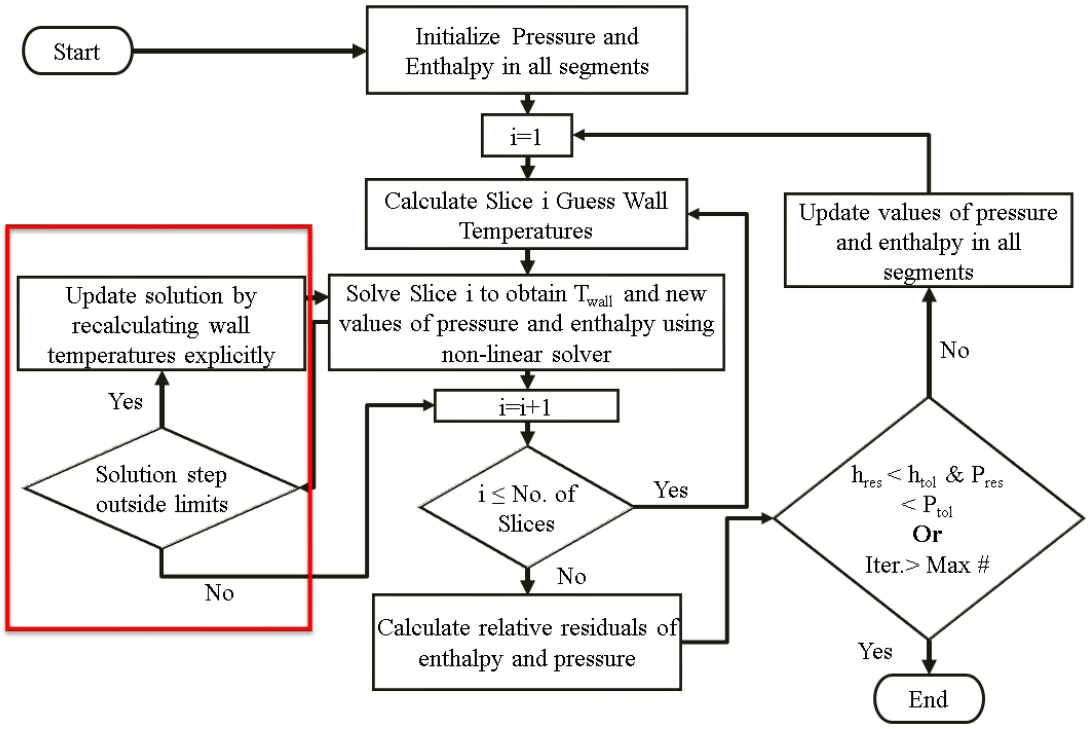

Figure 38: Updated PHX model.

A matrix of 3645 plate evaporators, and another matrix of 3645 plate condensers are used to evaluate the updated model and compare it against the base model developed by Qiao et al. [68]. The specifications of the matrices used are given in Table 10. Table 11 shows the result of running the matrices using the two models. The percentage of

cases that converged completely increased from 10.9% to 99.2% for plate evaporators, and from 43.3% to 99.1% for plate condensers, which is a significant improvement in the robustness of the model.

Table 10: Specifications of matrices used to evaluate updated model.

Parameter	Condenser Matrix	Evaporator Matrix
Number of slices	10-50	10-50
Plate Length (m)	0.4-0.6	0.4-0.6
Plate Width (m)	0.1-0.2	0.1-0.2
Hydraulic Diameter (m)	0.003-0.006	0.003-0.006
Chevron Angle (˚)	30˚, 45˚, 60˚	30˚, 45˚, 60˚
Fluid 1 Inlet Temperature (K)	300-310	318-325
Fluid 2 Inlet Temperature (K)	323-330	300-310

It must be noticed from the Table 11 that a significant number of cases with less number of slices solved successfully with the updated model. This shows that the updated model is more stable even for the cases with lower number of segments which usually take less time to solve completely as well. However, a significant increase in the solved cases also took place for cases with higher number of slices. It should be noted that the accuracy of the cases is not affected and consistent with the base model.

Table 11: Results of updated model evaluation.

		Evaporator		Condenser	
		Base [68]	Updated Model	Base [68]	Updated Model
Success (% of 3645 cases)		10.9%	99.2%	43.3%	99.1%
Cases solved with number of slices	10	0	703	27	703
	20	18	729	237	728
	30	86	729	423	726
	40	134	728	432	727
	50	159	726	459	729

6.2. Solver Speed

The robustness of the updated model is convenient enough to look into the next challenge which is the speed of the solution. As mentioned previously, the model introduced by Qiao et al. [68] adopts a successive substitution approach where the PHX is divided into a number of slices, M , of equal size and each slice can be solved individually. To solve each slice in a counter flow PHX, properties are calculated for each channel in each slice at the outlet and at the inlet in each iteration. Although the model is very accurate, this is very computationally expensive.

Solving the slices in parallel saves on computational time, however, this approach has a slow convergence and requires extensive thermophysical property calculations. Qiao et al. [68] employs an implicit quasi-Newton numerical method to solve for the unknowns in each slice. Another option is to employ explicit equations such as those in SEWTLE method [67]. However, implicit methods are more robust compared to explicit methods although computationally expensive. So it is required to maintain the robustness of the solution, while optimizing the number of thermophysical property calculations required and result in the same level of solution accuracy.

6.2.1. Model

An improved algorithm for the updated model, discussed in the previous section, is developed to improve the speed while maintaining the flexibility features required to develop any PHX design, while also maintaining the thermal-hydraulic accuracy and robustness of the model. The improved approach divides the flow in the PHX into two types according to the flow direction, namely: upward flow and downward flow irrespective of the kind of fluid in the channel or the phase of the fluid. As shown in Figure 39, one of the directions is the primary flow in a given iteration, and this is the solution direction in the current iteration. The properties are propagated in this direction for the primary flow, while the other flow is solved using the successive substitution approach.

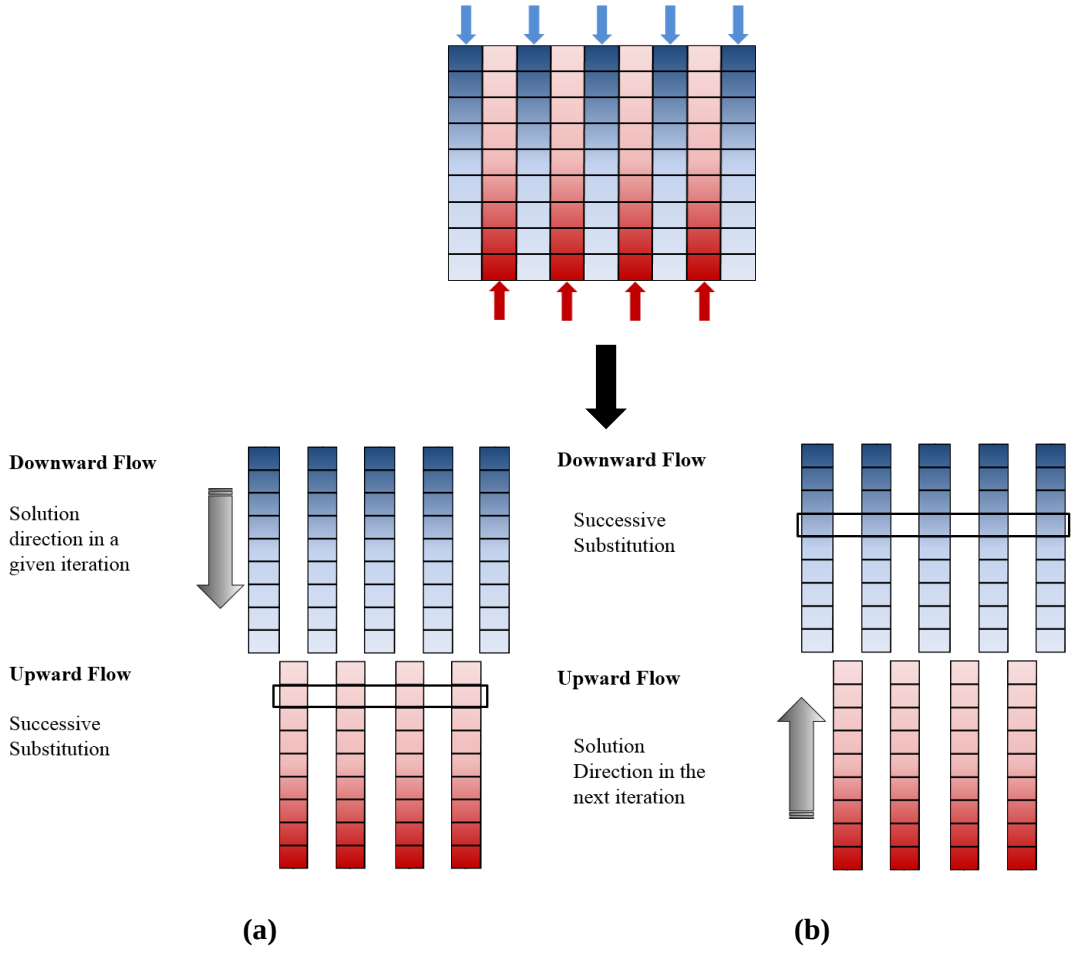

Figure 39: Improved solver outline (a) iteration in downward directions, (b) iteration in upward direction.

An example is given in Figure 39 (a). This will accelerate the solution in the direction of the primary flow. In the next iteration, as shown in Figure 39 (b), the directions are alternated such that the other direction becomes the primary flow. Then the properties propagate in this direction, while the other direction is solved using the successive substitution approach. This is alternated in the next iteration and so on.

One drawback in this approach is that the parallel calculation of the slices cannot take place anymore as the case in Qiao et al. [68]. However, the speed benefit from solving the PHX using this approach is much more significant than the benefit of the parallel calculation of the different segments.

To test the convergence of this improved approach, there are two aspects to look at. First, in terms of heat transfer, it is possible for temperature crossing to take place between the fluids or the numerical solution to diverge due to the acceleration of the solution in a certain direction. However, this is avoided as the initial guess wall temperatures are calculated the same way using Equation (26). Using this equation, the guess wall temperatures are well predicted to achieve numerical convergence as discussed in Section 6.1.1. Also, the temperature difference between the preceding and adjacent control volumes actually becomes smaller due to the accelerated solution, which makes the solution arguably more stable.

Second, numerically the solution must achieve convergence. The solution is said to reach final convergence when the state of the solution is correct and does not change. The "four basic rules", stated by Patankar [96], that promote convergence are as follows

1. Consistency at control volume faces: the wall of the PHX represents a common face for two adjacent channels. In each segment, the wall is the common face for two adjacent control volumes. The heat flux across the wall is represented by the same expression in the discretization equation for both control volumes [68]. This is the case in the base model, and the improved algorithm.

2. Positive coefficients in the iterative procedure: assumptions 2 to 4 in Qiao et al. [68] state that the plate surface temperature, the phase of the fluid, and the heat transfer coefficient are assumed to be constant within a segment. The same assumptions are maintained with the current approach. The assumptions guarantee that the coefficients of the iterative procedure within each segment will have the same sign, i.e. positive.
3. Negative slope linearization of the source term. In the PHX problem, there is a negative-slope relationship between the heat flux, which is the source term, and the dependent variable which is the wall temperature as the wall temperature decreases as heat is added to the control volume and vice versa. Therefore, this rule is applied as well.
4. Summation of neighboring coefficients. This rule implies that the center point temperature must be a weighted average of the neighbor temperature values which is applied, again due to the assumptions stated in 2.

Therefore, the current approach does not violate any of these rules. However, Patankar [96] also mentions that it is very difficult to always guarantee convergence with all the interlinkages present is such complicated problems. But by having the basic rules in place, and solving the correct problem, thermal and numerical convergence can be achieved, i.e. the solution will converge to the correct answer.

6.2.2. Validation

Experimental data sets that were previously used by Qiao et al. [68] and Eldeeb et al. [112] are used to validate the improved approach, in addition to few other data points. In this validation, all the thermodynamic properties are calculated based on NIST REFPROP 9.1 [113], the single-phase correlation developed by Yan and Lin [14] is used for single-phase heat transfer coefficient calculation, and the correlation developed by Muley and Manglik [114] is used for single-phase pressure drop calculation.

A single phase water-water data set is used with 22 data points. Using the improved approach, the heat capacity and the outlet temperatures of both streams are calculated and shown in Figure 40. The heat capacity for all cases is within 2% showing a very strong agreement with the experimental results. Most of the outlet temperatures for both streams are within 0.1 K, with very few points within 0.2 K.

Water-R134a condensation data set with 12 data points is used to validate the prediction of heat capacity using the new approach. The results from the improved approach versus the experimental results are shown in Figure 41. The heat capacity is within 5% for most data points with two data points within 7%. In this study, the condensation heat transfer coefficient correlation developed by Yan et al. [37] for plate heat exchangers, and the widely accepted [40] pressure drop correlation developed by Lockhart and Martinelli [115] are used.

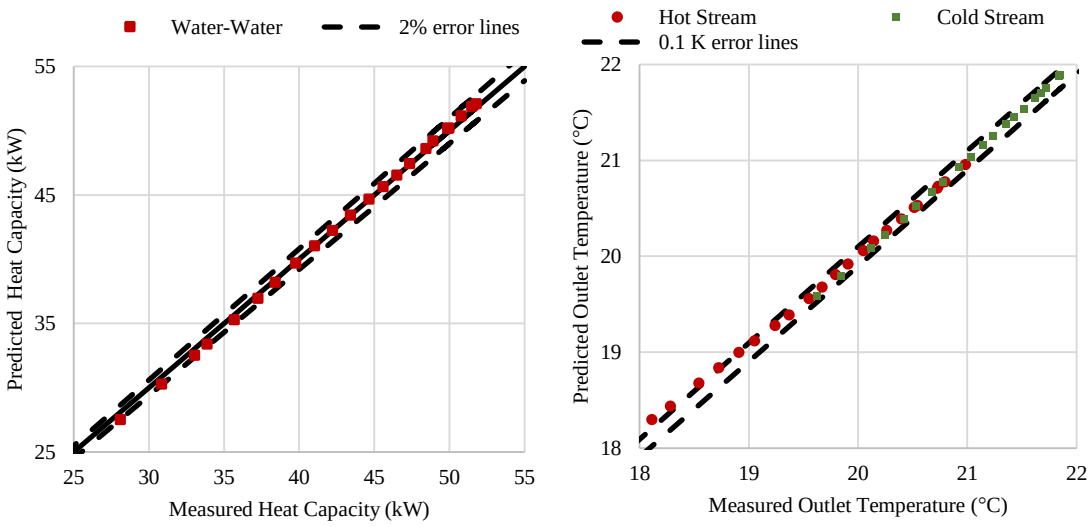

(a) **(b)**

Figure 40: Comparison between predicted and experimental (a) heat capacity, and (b) outlet temperature of improved solver for water-water single phase.

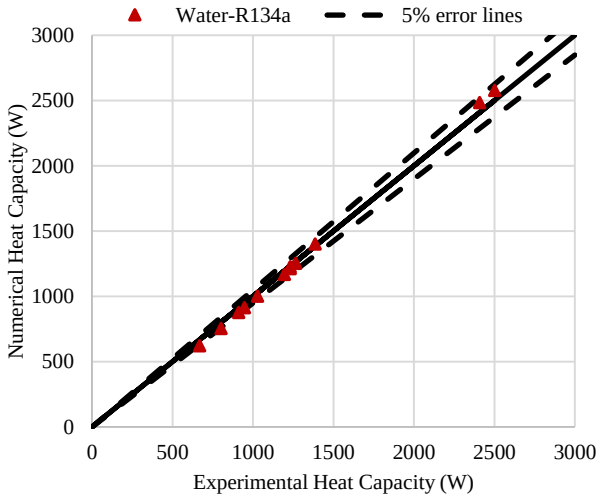

Figure 41: Comparison between predicted and experimental heat capacity of improved solver for water-R134a condensation.

Figure 42 shows the validation of the improved approach using experimental results of three datasets. The evaporation heat transfer coefficient and pressure drop correlations developed by Khan and Chyu [4] for plate heat exchangers are used in this study. Figure 42 (a) shows water-R22 predicted heat capacity using the improved approach against the experimental results. This data set has 58 data points with 49 points within 3% of the experimental results. The improved approach solved 15 cases which failed to solve using the approach presented in Qiao et al. [68].

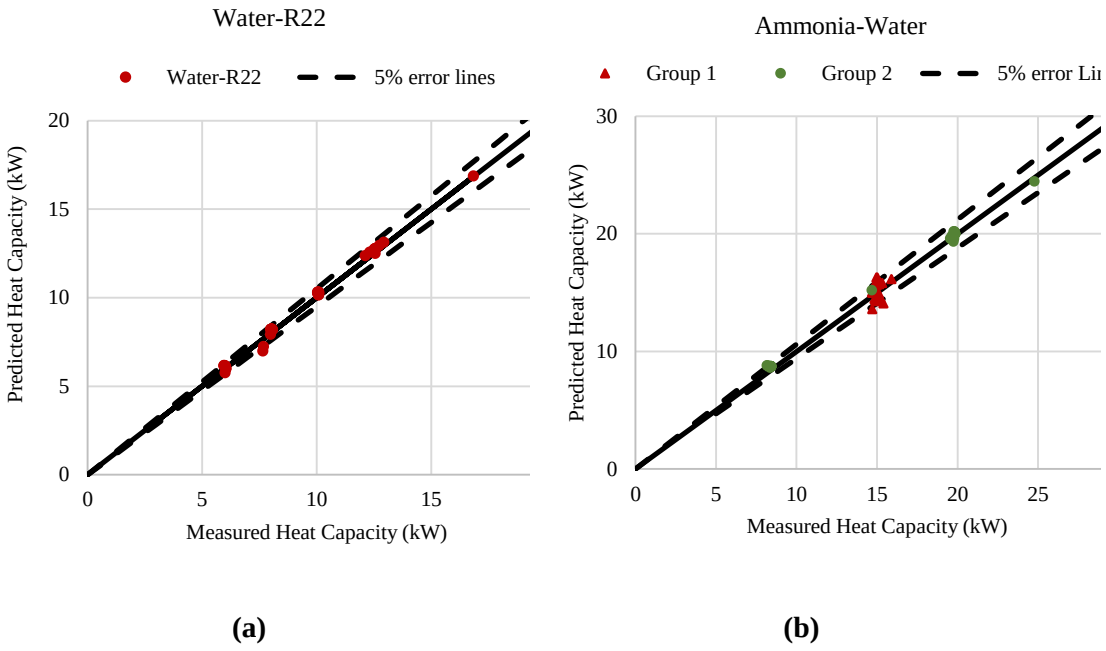

Figure 42: Comparison between predicted and experimental heat capacity for (a) water-R22, and (b) ammonia-water, of improved solver for evaporation.

Figure 42 (b) shows two data sets of ammonia-water evaporation. Group 1 contains 25 data points, with 19 points within 6% of the experimental results and the remaining points lie within 9%. In this data set, 8 cases that failed to solve by the current solver

and were not presented in Qiao et al. [68] are solved by the improved approach. Group 2 contains 32 data points with 28 of these points within 5% of the experimental results and the remaining points are within 8%. Qiao et al. [68] only presented 12 of these points. Generally, the improved approach is more robust than the model developed by Qiao et al. [68]. Finally, few data points using propylene glycol 30% and carbon dioxide PHX are also validated, with the heat load within about 3%.

On a system level, the improved model is employed as a component in a comprehensive steady state solver for vapor compression systems [116], in order to simulate a carbon dioxide two-stage refrigeration system shown in Figure 43 [117].

The system presented in Figure 43 constitute three PHXs: the subcooler, the medium temperature evaporator, and the low temperature evaporator. Table 12 shows the results for both the base model [68], and the improved model. The time reduction is about 92%.

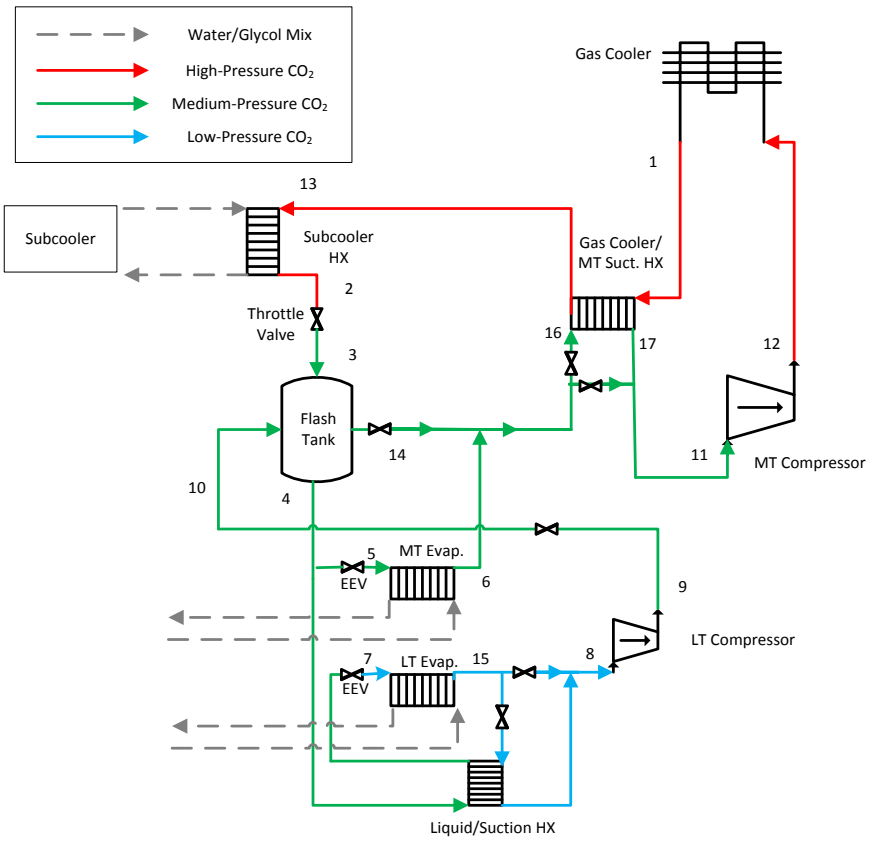

Figure 43: Carbon Dioxide two-stage refrigeration system from Beshr et al. [117].

Table 12: Results of base and improved models when employed in a system level.

Solver	COP	Total Capacity (kW)	Power Consumption (kW)	Time (min)
Base [68]	1.23	12.84	10.45	25.78
Improved Model	1.23	12.87	10.44	2.12

6.2.3. Verification

The improved approach is verified against the approach developed by Qiao et al. [68] using a test matrix containing 7246 PHX cases. The cases include condensers,

evaporators, and single-phase PHXs. The refrigerants used in the matrix include water, R410A, R134a, ammonia, R22, propylene glycol 30%, and carbon dioxide. The overall success rate of the improved approach is higher than 98%, which makes the solution very stable compared to about 40% success rate of Qiao et al. [68].

In the most trivial case of parallel flow in all channels, the PHX will simply solve in one iteration using the improved approach rather than M iterations using successive substitution, no matter how many segments are used in the PHX. This is four times faster in terms of simulation time. In a more complicated case where the flow is counter and phase change takes place in all channels at the same time, the number of iterations is 22 times faster and the solution speed is 5 times faster. For the test matrix developed, the improved approach proved to be more robust with 7% of the cases solving only with the new approach, especially for a lower number of segments. The new approach is at least 2-16 times faster than the approach developed by Qiao et al. [68]. For the 7246 cases, the solution is on average 7 times faster than the approach developed by Qiao et al. [68].

Finally, this developed model will make the simulation of PHXs easier and favorable, and thus allowing significant improvement of PHX design. More energy efficient PHX designs can potentially be the next generation of compact, highly energy efficient, heat exchangers which can have a lot of favorable implications such as significantly reducing the environmental impact.

6.3. Flow Maldistribution

The last challenge is to account for flow maldistribution in the inlet and the outlet of the PHX. Flow maldistribution occurs due to pressure drop that takes place as the fluid enters or exits from the PHX. Numerous studies in literature investigated flow maldistribution in PHXs for liquids (e.g. Bassiouny and Martin [118]). Jensen et al. [119] developed a numerical model for predicting flow maldistribution of two-phase flow in evaporators using a similar successive substitution approach. However, the improved algorithm discussed in the previous section is utilized as the base solver for estimating the flow maldistribution taking place for single and two-phase flows.

For a single fluid path, the main pressure drop takes place in the ports, manifolds due to contraction or expansion, header, and the channel. There are also gravitational and acceleration pressure drop.

$$\Delta P_{total} = \Delta P_{port,in} + \Delta P_{man,in} + \Delta P_{header,in} + \Delta P_{channel} + \Delta P_{header,out} \Delta P_{ports,out} + \Delta P_{man,out} \quad (27)$$

An algorithm using a non-linear numerical solver is developed to solve for the flow distribution according to pressure drop in different flow paths for each fluid given by Equation (27). An iterative procedure takes place in each iteration to calculate the charge distribution over the channels of each fluid according to the total pressure drop given in Equation (27). To verify the algorithm, a matrix of 7587 cases is studied including condensers, evaporators, and single-phase PHXs. The refrigerants used in the matrix include water, R410A, R134a, ammonia, R22, propylene glycol 30%, and carbon dioxide. The flow maldistribution solver is based on the improved faster solver

discussed in the previous section. Compared to the faster solver, the average time change is less than 3% increase in time, while the heat load within 2%, and the average pressure drop is within 13%.

Chapter 7: Conclusions

The first objective of this thesis is the optimization of PPHXs with circular spot welds using four design parameters, including basic geometrical parameters, in order to obtain a novel PPHX design that has a performance that is at least 50% better than existing designs. The second objective is to build on the improvements achieved from the first objective by performing a comprehensive optimization study using eleven design parameters including weld shape parameterization using NURBS to obtain a novel PPHX design with at least 20% or better thermal-hydraulic performance as compared to the optimal chevron PHXs designs present in literature. The third objective is to improve existing PHX modeling combining robustness, accuracy, flexibility, and convenient speed into a single model using a novel algorithm. All of the objectives are complete and the conclusions are presented for each objective in the following sections.

7.1. Optimization of Pillow Plate Heat Exchanger

- Comprehensive investigation of thermal-hydraulic performance of PPHXs is undertaken. In this optimization problem, four design parameters are investigated including the spot weld diameter, the pillow plate height, the weld pitch ratio, and the fluid inlet velocity. Computational challenges due to the 3D complex structure of PPHXs are solved and the whole simulation is

successfully automated through a PPCFD code which writes a python script, executed through an executable batch file, which in turn executes various JavaScript for the different CFD simulation components. Through reviewing the literature and to the best of my knowledge, this is the first work to successfully fully automate Static Structural (SS) CFD simulation linked with Finite Element Modeler (FEM) and Fluid Flow (FF) CFD simulation with all components in one ANSYS workbench using Python script and JavaScript automatically which are all generated using a PPCFD code. Previous work done either used a different geometry platform (such as Gambit), or the parametric study feature in ANSYS workbench. This can also aid in future investigation and optimization of complex heat exchanger surfaces especially complex geometries that cannot be generated by just changing a parameter value in a parametric set, but rather involving multiple processes.

- A metamodel is obtained using 408 CFD simulations and successfully verified using 103 random designs. The metamodel can be used to accurately predict the thermal-hydraulic performance of PPHXs without running full CFD simulations which is very computationally expensive. The metamodel is then used in a MOGA to obtain the optimal PPHX designs.
- The verified metamodel is also used to conduct a sensitivity analysis to investigate the effect of each of the four design parameters on the thermal-hydraulic performance of PPHXs. The analysis revealed that longitudinal pitch ratio is more favorable for the heat transfer coefficient, however yields higher

pressure drop than transverse patterns, while the pillow height has a desirable effect on both. The inlet velocity is found to be directly proportional to heat transfer and pressure drop as well with pressure drop increasing at a very higher rate at higher inlet velocity values. The analysis also shows that the weld diameter is the most promising parameter for thermal-hydraulic performance further improvement.

- The optimum designs obtained show a significant improvement in performance with at least 33.1% enhancement in heat transfer coefficient at high Reynolds numbers and up to the double with respect to the baseline. A significant reduction in pressure drop per unit length is realized as well ranging from at least 11% at low Reynolds numbers and up to 98% reduction relative to the baseline.
- The optimum designs obtained are also compared to the optimum designs of chevron PHXs obtained from literature [111]. PPHX optimum results show a range of 23% improvement in heat transfer coefficient at high pressure drop and up to three times improvement at lower pressure drop values. A pressure drop improvement is realized as well with 30% reduction at high heat transfer coefficient values. This places PPHXs in a very strong position as compared to chevron PHXs and gives them a great potential to outperform chevron PHXs.

7.2. Weld Shape Optimization of Pillow Plate Heat Exchanger

- Given the finding of the first objective that the weld size and shape have the most significant effect on the thermal-hydraulic performance of PPHX, it is decided to further improve their thermal-hydraulic performance. This is done by undertaking a more comprehensive optimization problem with a larger set of eleven design parameters. The problem include weld shape optimization using NURBS in addition to the other hydroforming and flow characteristic parameters as a part of a larger multi-scale analysis effort. A more streamlined weld shape leads to a smaller wake region behind the weld and thus improving the pressure drop significantly.
- The optimization problem has the same objectives of maximizing the heat transfer coefficient while minimizing the pressure drop per unit length. The set of eleven design parameters include shape variables that describe the weld shape and size in addition to design variables describing the pillow height, weld pitch ratios, and the inlet fluid velocity. The weld shape is defined and varied using NURBS curves. The CFD simulation is automated by a PPCFD code that is written with a similar procedure as the first optimization problem, using Python script for the workbench, JavaScript for the diiferent components, and reading NURBS curves coordinates from text files.

- A metamodel is developed using 1764 CFD simulations and verified using 354 random designs. The metamodel is used in a MOGA to obtain the optimal PPHX with NURBS weld shape designs.
- The optimal designs obtained show a significant improvement in performance as compared to a baseline, selected as one of the optimal designs obtained from the PPHX optimization problem in the first objective. Relative to the baseline, up to 36% improvement in heat transfer coefficient and up to 67% reduction in pressure drop is achieved. This is a huge further improvement in thermal-hydraulic performance.
- The optimal designs are compared to chevron PHX optimal designs from literature [111] as well. The results show a range of 28% improvement in heat transfer coefficient at high pressure drop and up to 38% improvement at lower pressure drop with respect to chevron PHX optimal designs. A significant pressure drop reduction is also realized with 72% reduction at high heat transfer coefficient values. This places PPHX with NURBS weld shape in a very strong position compared to chevron PHXs and gives it a great potential to outperform their thermal-hydraulic performance and to potentially lead to significant energy efficiency on the component level as well as the system level.

7.3. Improved modeling of Plate Heat Exchangers

- The model developed by Qiao et al. [68] is developed and improved significantly with respect to accuracy, robustness, and speed.

- Two routines are developed to improve the stability of the solver, namely: the guess wall temperature routine, and the slice routine. The solver robustness improved significantly increasing the success rate to more than 99% for two-phase flow.
- An improved algorithm to solve the PHX is developed in order to optimize the property calculation routines leading to significant time improvement by significantly reducing the number of iterations required for a simulation to completely solve. The time improvement is on average seven times faster and up to sixteen times faster. Thus, an existing accurate and flexible PHX design tool became more robust and computational efficient as well. This has a great impact on designing reliable PHX flexibly, accurately, and easily, and thus improving the performance of novel PHX designs in order to achieve optimum energy efficiency.
- A flow maldistribution solver is developed to account for the inevitable unequal charge distribution that takes place at the entrance of the PHX due to different pressure drop values that take place in each individual fluid path. The accurate prediction of the amount of charge in each channel leads to more accurate modeling of the total amount of heat transfer and pressure drop that takes place in the PHX and thus better design and modeling. This allows the proximity between modeling and practical industrial situations to enhance the accuracy of the model.

- The tool is used as a component in an existing steady-state vapor compression modeling tool [116] in order to optimize the performance on the system level as well in an accurate, and time efficient manner.

Chapter 8: List of Contributions and Future Work

8.1. Contributions

The list of contributions include:

- Optimization of PPHX using four design parameters resulted in optimal novel PPHX designs with enhanced heat transfer coefficient values that are up to the double at moderate inlet Reynolds number, and up to 98% reduction in pressure drop per unit length at low inlet Reynolds number as compared to an existing design in the literature [58]. This is very important to achieve high energy efficiency in a wide variety of applications on the component level and further translated into energy efficiency on the component level as well, thus reducing the negative environmental impact.
- A more comprehensive optimization of PPHX that include topology and shape optimization using NURBS weld shape to improve hydraulic performance and a total of eleven design parameters, including weld shape, hydroforming, and flow characteristic parameters, achieved novel optimal designs that have 28%-38% improvement in heat transfer coefficient and up to 72% reduction in pressure drop when compared to optimal chevron PHX designs in literature [111]. This places PPHX with NURBS weld shape in a very strong position compared to chevron PHXs in addition to the PPHX economic advantage. The

optimal PPHX with NURBS weld shape designs also achieved up to 36% improvement in heat transfer coefficient and up to 67% reduction in pressure drop per unit length when compared to optimal PPHX designs with circular spot welds obtained from the first contribution. This will translate to a further higher energy efficiency on both the component level and on the system level.

- The PHX computer model developed by Qiao et al. [68] is developed and improved significantly using two routines that improve the robustness of the solver increasing the two-phase solution success rate to up to 99%. A novel algorithm that improve the speed of the solver in terms of number of iterations as well as solution time by up to sixteen times faster is also developed. A flow maldistribution solver predicting the mass flow rate distribution over the different channels is developed to improve the accuracy of the solver. An already existing accurate solver is thus more stable, significantly faster, and even more accurate in order to be able to predict the performance of PHXs accurately, cheaply, and in a convenient time. This solver can be used both on the component level as well as on the system level, thus projecting the design benefits of individual PHX components towards energy efficiency on the overall system energy efficiency.

8.2. List of Publications

The following peer-reviewed journal papers are published or submitted as outcomes of this research.

1. R. Eldeeb, V. Aute and R. Radermacher, "Pillow Plate Heat Exchanger Optimization Using Approximation and Parallel Parameterized CFD", *International Journal of Refrigeration, submitted*.
2. R. Eldeeb, V. Aute and R. Radermacher, "Pillow Plate Heat Exchanger Weld Shape Optimization Using Non-Uniform Rational B-Splines", *International Journal of Refrigeration, submitted*.
3. R. Eldeeb, V. Aute and R. Radermacher, "A Survey of Correlations for Heat Transfer and Pressure Drop for Evaporation and Condensation in Plate Heat Exchangers", *International Journal of Refrigeration,* vol. 65, pp. 12-26, 2016.
4. A. Alabdulkarem, R. Eldeeb, Y. Hwang, V. Aute and R. Radermacher, "Testing, Simulation, and Soft-Optimization of R410A low-GWP Alternatives in Heat Pump System", *International Journal of Refrigeration,* vol. 60, pp. 106-117, 2015.

The following peer-reviewed conference papers are published or accepted as a result of this research.

1. R. Eldeeb, J. Ling, V. Aute and R. Radermacher, "Approximation Assisted Optimization of Pillow Plate Heat Exchangers", Proceedings of the 16th International Heat Transfer Conference, IHTC-16, August 10-15, Beijing, China, 2018, *submitted*.
2. R. Eldeeb, J. Ling, V. Aute and R. Radermacher, "Weld Shape Optimization for Pillow Plate Heat Exchangers", in *17th International Refrigeration and Air Conditioning Conference at Purdue, Paper 2642*, 2018, *submitted*.

3. R. Eldeeb, J. Ling, V. Aute and R. Radermacher, “Heat Transfer Enhancement Using Approximation Assisted Optimization for Pillow Plate Heat Exchanger”, in *17th International Refrigeration and Air Conditioning Conference at Purdue, Paper 2641*, 2018, *submitted*.
4. R. Eldeeb, V. Aute and R. Radermacher, "An Improved Approach for Modeling Plate Heat Exchangers Based on Successive Substitution in Alternating Flow Directions", in *16th International Refrigeration and Air Conditioning Conference at Purdue, Paper 2279*, 2016.
5. R. Eldeeb, V. Aute and R. Radermacher, "Investigation of Thermal-Hydraulic Characteristics of Pillow Plate Heat Exchangers Using CFD", in *16th International Refrigeration and Air Conditioning Conference at Purdue, Paper 2278*, 2016.
6. R. Eldeeb, V. Aute and R. Radermacher, "A Survey of Correlations for Heat Transfer and Pressure Drop During Evaporation in Plate Heat Exchanger", in *11th IIR Gustav Lorentzen Conference on Natural Refrigerants, Paper 99*, Hangzhou, China, 2014.
7. R. Eldeeb, V. Aute and R. Radermacher, “A Model for Performance Prediction of Brazed Plate Condensers and Alternative Lower GWP Refrigerant”, in *15th International Refrigeration and Air Conditioning Conference at Purdue, Paper 2276*, 2014.
8. Alabdulkarem, R. Eldeeb, Y. Hwang, V. Aute and R. Radermacher, "Evaluation and Soft-Optimization for R410A Low-GWP Replacement Candidates

Through Testing and Simulation", in *15th International Refrigeration and Air Conditioning Conference at Purdue, Paper 2256*, 2014.

8.3. Recommendations for Future Work

This work has placed PPHX in a distinct position and created an opportunity to great future advances on the component level and on the system level. Future researches can benefit from the contributions of this work by addressing the following:

- Leverage the information from the verified metamodels to predict the thermal-hydraulic performance of PPHXs in order to model a complete PPHX which can be employed on a system level modeling such as that developed by Beshr [116]. Testing the performance of the selected optimal PPHX designs on a system level can reveal the amount of improvement of the performance for the entire system. This can be done by developing a solver that combines the optimal designs obtained by the optimization studies with the improved solver model achieved from this work. The addition of a reliable model for PPHXs performance prediction can be used to design, model, and improve the performance of PPHX components as well as system level performance.
- Address other physical constraints that may have an impact on the manufacturing process, such as static and dynamic stress analysis, and vibration, and noise.
- Manufacture selected optimal designs and perform experimental validation in order to ensure the actual performance matches the numerical simulation.

- Investigate solutions to larger scale PPHX that may pose additional challenges such as overall PPHX volume or stacking welded plates together.
- Numerical and experimental investigation of the external channel, with the inlet wall being set at a constant temperature. This is especially important for two-phase applications as the condensing/evaporating fluid is usually in the internal channel.
- Use the developed metamodels to develop general heat transfer and pressure drop correlations that can be employed and used in the improved solver in order to predict the performance of the whole PPHX without having to go back to the metamodels as the correlations can be directly available for use in the PPHX solver model.

Appendices

Appendix A – PPHX Optimum Designs

Table 13: Optimum PPHX designs dimensions.

Design Tag	Pitch Ratio	Pillow Height	Spot Weld Diameter
	-	mm	mm
PPHX-001	0.6081	11.4458	9.3158
PPHX-002	1.4029	11.9912	3.9648
PPHX-003	1.4051	11.9560	3.9648
PPHX-004	0.5800	11.9912	9.2063
PPHX-005	1.4040	11.9384	3.9648
PPHX-006	0.7509	12.0000	7.3861
PPHX-007	0.6081	11.4458	9.3158
PPHX-008	0.7441	12.0000	7.4819
PPHX-009	0.6654	12.0000	7.5504
PPHX-010	1.4051	11.9912	3.0068
PPHX-011	0.6070	12.0000	9.2063
PPHX-012	1.4029	11.9384	3.9648
PPHX-013	0.5800	11.9912	9.1515
PPHX-014	0.6070	12.0000	9.2063
PPHX-015	1.3995	11.9560	4.3343
PPHX-016	0.5800	11.9208	9.1515
PPHX-017	0.6081	12.0000	9.1789
PPHX-018	0.6081	12.0000	9.2063
PPHX-019	0.6081	12.0000	9.2063
PPHX-020	0.6081	12.0000	9.1515
PPHX-021	0.6081	12.0000	9.1926
PPHX-022	0.6070	12.0000	8.4399
PPHX-023	0.6081	11.4545	9.2063
PPHX-024	0.5800	12.0000	9.1926
PPHX-025	0.6081	12.0000	9.2063

Design Tag	Pitch Ratio	Pillow Height	Spot Weld Diameter
	-	mm	mm
PPHX-026	0.6081	12.0000	9.1926
PPHX-027	0.6081	12.0000	9.2063
PPHX-028	1.3894	11.9384	6.0724
PPHX-029	1.3984	11.9736	3.2258
PPHX-030	0.7351	12.0000	7.4682
PPHX-031	0.6070	12.0000	9.2063
PPHX-032	1.3894	11.9736	4.7585
PPHX-033	0.6070	12.0000	9.2063
PPHX-034	1.4051	11.9384	3.4585
PPHX-035	0.6070	12.0000	9.2063
PPHX-036	1.3905	11.9384	4.1017
PPHX-037	1.3905	11.9560	5.1965
PPHX-038	0.6081	12.0000	9.2063
PPHX-039	1.4040	11.9560	3.4721
PPHX-040	1.3894	11.9824	4.9775
PPHX-041	1.3905	11.9912	4.1564
PPHX-042	0.7531	12.0000	7.4682
PPHX-043	0.7531	12.0000	7.4545
PPHX-044	1.3714	11.9912	5.9081
PPHX-045	0.7441	12.0000	7.4682
PPHX-046	0.5800	11.9912	9.1515
PPHX-047	0.6081	12.0000	9.2063
PPHX-048	0.6070	12.0000	8.4399
PPHX-049	1.3905	11.8681	3.9648
PPHX-050	0.6081	12.0000	9.1926
PPHX-051	0.6081	12.0000	9.2063
PPHX-052	1.3894	11.9824	4.9775
PPHX-053	0.6070	12.0000	9.3020
PPHX-054	1.3905	11.9560	4.1017
PPHX-055	0.6531	12.0000	5.6344
PPHX-056	0.6699	11.9824	9.1789
PPHX-057	1.4029	11.9560	4.3891
PPHX-058	1.3174	11.9824	9.1515
PPHX-059	1.3714	12.0000	5.9081

Design Tag	Pitch Ratio	Pillow Height	Spot Weld Diameter
	-	mm	mm
PPHX-060	0.6070	12.0000	9.2063
PPHX-061	0.7531	12.0000	7.4409
PPHX-062	0.6081	12.0000	9.1926
PPHX-063	0.7576	12.0000	7.4409
PPHX-064	0.6699	11.9912	9.1378
PPHX-065	0.6609	11.9912	7.6872
PPHX-066	0.6070	11.9912	9.1378
PPHX-067	1.4040	11.9560	4.7585
PPHX-068	0.5811	12.0000	9.1926
PPHX-069	1.3118	12.0000	9.6442
PPHX-070	1.3894	12.0000	9.3568
PPHX-071	1.3894	11.9736	3.1026
PPHX-072	0.7509	11.9912	5.6891
PPHX-073	0.6104	11.9912	9.1515
PPHX-074	0.7441	12.0000	7.4409
PPHX-075	0.7509	12.0000	7.4409
PPHX-076	1.4029	11.9384	3.0890
PPHX-077	0.6081	12.0000	9.1926
PPHX-078	1.4040	11.9736	3.9169
PPHX-079	0.6081	12.0000	9.2063
PPHX-080	0.6070	12.0000	9.2063
PPHX-081	1.3894	11.9912	5.6344
PPHX-082	1.4040	11.9384	3.9648
PPHX-083	0.6081	12.0000	9.2063
PPHX-084	0.6070	12.0000	9.2063
PPHX-085	1.3894	11.9824	4.9775

Appendix B - NPPHX Optimum Designs

Table 14: Optimum NPPHX designs dimensions.

Design Tag	Pitch Ratio	Pillow Height	WHR	Weld Height	Weld Width	x_1	x_2	x_3	y_1	y_2	y_3
	-	mm	-	mm	mm	mm	mm	mm	mm	mm	mm
NPPHX-001	0.756	11.455	1.746	4.204	7.340	1.851	4.889	5.534	2.247	2.475	1.5
NPPHX-002	1.337	11.859	1.995	4.232	8.443	2.126	5.623	6.624	2.059	2.330	1.5
NPPHX-003	1.310	11.771	1.998	4.193	8.377	2.115	5.585	6.573	2.090	2.348	1.5
NPPHX-004	0.580	11.930	1.875	4.075	7.641	1.949	5.094	5.910	2.247	2.492	1.5
NPPHX-005	0.755	11.507	1.746	4.204	7.340	1.851	4.889	5.525	2.248	2.482	1.5
NPPHX-006	0.739	11.455	1.745	4.193	7.316	1.845	4.872	5.516	2.247	2.498	1.5
NPPHX-007	0.688	11.543	1.869	4.122	7.704	1.941	5.136	5.962	2.249	2.500	1.5
NPPHX-008	0.608	11.683	1.871	4.114	7.698	1.956	5.127	5.957	2.247	2.500	1.5
NPPHX-009	0.616	11.648	1.874	4.083	7.651	1.945	5.101	5.909	2.249	2.500	1.5
NPPHX-010	1.346	11.789	1.997	4.224	8.435	2.125	5.624	6.619	2.090	2.348	1.5
NPPHX-011	0.617	11.648	1.869	4.083	7.631	1.940	5.088	5.883	2.249	2.492	1.5
NPPHX-012	0.733	11.507	1.746	4.107	7.169	1.822	4.780	5.546	2.247	2.498	1.5
NPPHX-013	0.805	11.472	1.746	4.216	7.361	1.856	4.907	5.694	2.247	2.500	1.5
NPPHX-014	0.599	11.930	1.873	4.114	7.706	1.958	5.137	5.943	2.249	2.500	1.5
NPPHX-015	0.608	11.789	1.870	4.103	7.672	1.955	5.115	5.935	2.247	2.498	1.5
NPPHX-016	0.581	11.930	1.875	4.099	7.685	1.998	5.123	5.924	2.247	2.492	1.5
NPPHX-017	0.580	11.789	1.871	4.114	7.698	1.961	5.132	5.957	2.249	2.500	1.5
NPPHX-018	0.581	11.648	1.844	4.107	7.571	1.971	5.042	5.837	2.247	2.492	1.5
NPPHX-019	0.626	11.930	1.875	4.099	7.685	1.961	5.123	5.944	2.247	2.500	1.5
NPPHX-020	1.328	11.789	1.875	4.208	7.890	1.982	5.255	6.198	2.122	2.346	1.5
NPPHX-021	1.319	12.000	1.993	4.193	8.356	2.110	5.571	6.470	2.122	2.348	1.5
NPPHX-022	0.761	11.648	1.748	4.114	7.191	1.828	4.794	5.544	2.249	2.475	1.5
NPPHX-023	0.616	11.648	1.875	4.099	7.685	1.961	5.123	5.934	2.249	2.484	1.5
NPPHX-024	0.617	11.648	1.875	4.099	7.685	1.961	5.123	5.924	2.247	2.500	1.5
NPPHX-025	0.626	11.613	1.844	4.107	7.571	1.932	5.047	5.846	2.247	2.500	1.5
NPPHX-026	0.644	11.578	1.871	4.095	7.661	1.952	5.108	5.926	2.249	2.500	1.5
NPPHX-027	0.643	11.718	1.869	4.114	7.690	1.954	5.127	5.933	2.249	2.492	1.5

Design Tag	Pitch Ratio	Pillow Height	WHR	Weld Height	Weld Width	x_1	x_2	x_3	y_1	y_2	y_3
	-	mm	-	mm	mm	mm	mm	mm	mm	mm	mm
NPPHX-028	0.805	11.455	1.746	4.204	7.340	1.851	4.889	5.534	2.247	2.482	1.5
NPPHX-029	0.643	11.507	1.871	4.075	7.625	1.940	5.083	5.898	2.249	2.496	1.5
NPPHX-030	0.733	11.507	1.713	4.099	7.020	1.789	4.675	5.430	2.248	2.498	1.5
NPPHX-031	0.616	11.789	1.871	4.075	7.625	1.945	5.083	5.958	2.249	2.500	1.5
NPPHX-032	0.580	11.930	1.871	4.099	7.669	1.952	5.112	5.912	2.247	2.500	1.5
NPPHX-033	0.616	11.648	1.871	4.099	7.669	1.949	5.112	5.922	2.249	2.484	1.5
NPPHX-034	0.607	12.000	1.873	4.114	7.706	1.958	5.137	5.943	2.249	2.492	1.5
NPPHX-035	0.643	11.648	1.873	4.114	7.706	1.958	5.137	5.946	2.249	2.492	1.5
NPPHX-036	0.581	11.930	1.875	4.099	7.685	2.001	5.123	5.924	2.247	2.500	1.5
NPPHX-037	0.581	11.648	1.875	4.075	7.641	1.949	5.094	5.910	2.249	2.492	1.5
NPPHX-038	1.364	11.859	1.995	4.103	8.185	2.062	5.451	6.332	2.184	2.330	1.5
NPPHX-039	1.308	11.912	1.875	4.067	7.626	1.921	5.084	5.884	2.122	2.484	1.5
NPPHX-040	0.707	12.000	1.873	4.107	7.691	1.957	5.122	5.952	2.249	2.500	1.5
NPPHX-041	0.652	11.930	1.875	4.087	7.663	1.950	5.103	5.907	2.249	2.492	1.5
NPPHX-042	0.617	11.930	1.875	4.099	7.685	1.961	5.123	5.944	2.249	2.492	1.5
NPPHX-043	0.634	11.930	1.873	4.099	7.677	1.999	5.118	5.923	2.247	2.500	1.5
NPPHX-044	0.616	11.718	1.873	4.114	7.706	1.964	5.137	5.941	2.249	2.500	1.5
NPPHX-045	0.617	11.930	1.872	4.067	7.614	1.943	5.076	5.870	2.247	2.469	1.5
NPPHX-046	0.589	11.894	1.873	4.114	7.706	1.958	5.137	5.943	2.249	2.492	1.5
NPPHX-047	0.635	11.648	1.874	4.122	7.725	1.971	5.150	5.955	2.249	2.500	1.5
NPPHX-048	0.581	11.789	1.875	4.114	7.714	1.966	5.143	5.970	2.249	2.500	1.5
NPPHX-049	0.608	11.648	1.840	4.103	7.548	1.926	5.032	5.838	2.247	2.500	1.5
NPPHX-050	0.626	11.648	1.875	4.069	7.630	1.947	5.086	5.882	2.247	2.500	1.5
NPPHX-051	0.800	11.912	1.875	4.099	7.685	1.961	5.123	5.924	2.247	2.500	1.5
NPPHX-052	0.644	11.930	1.871	4.095	7.661	1.955	5.108	5.906	2.247	2.498	1.5
NPPHX-053	0.652	11.930	1.874	4.091	7.666	1.951	5.106	5.920	2.249	2.500	1.5
NPPHX-054	1.301	11.648	1.875	4.193	7.861	2.046	5.240	6.147	2.216	2.348	1.5
NPPHX-055	0.739	11.455	1.745	4.200	7.329	1.848	4.881	5.526	2.247	2.498	1.5
NPPHX-056	0.589	11.648	1.873	4.114	7.706	1.966	5.132	5.941	2.247	2.492	1.5
NPPHX-057	1.364	12.000	1.998	4.204	8.400	2.121	5.595	6.504	2.184	2.346	1.5
NPPHX-058	1.328	11.982	1.873	4.193	7.852	1.980	5.235	6.079	2.122	2.367	1.5

Design Tag	Pitch Ratio	Pillow Height	WHR	Weld Height	Weld Width	x_1	x_2	x_3	y_1	y_2	y_3
	-	mm	-	mm	mm	mm	mm	mm	mm	mm	mm
NPPHX-059	0.616	11.648	1.875	4.099	7.685	1.958	5.123	5.924	2.249	2.484	1.5
NPPHX-060	0.599	11.648	1.875	4.099	7.685	1.956	5.123	5.944	2.247	2.492	1.5
NPPHX-061	0.733	11.578	1.873	4.122	7.721	1.962	5.147	5.972	2.249	2.473	1.5
NPPHX-062	1.319	11.930	1.868	4.193	7.832	1.998	5.221	6.058	2.247	2.492	1.5
NPPHX-063	1.337	11.912	1.873	4.193	7.852	2.003	5.235	6.084	2.247	2.359	1.5
NPPHX-064	1.204	11.789	1.748	4.075	7.123	1.794	4.748	5.514	2.090	2.355	1.5
NPPHX-065	0.581	11.789	1.875	4.114	7.714	1.966	5.143	5.967	2.247	2.500	1.5
NPPHX-066	0.625	11.648	1.875	4.107	7.699	1.964	5.133	5.941	2.247	2.492	1.5
NPPHX-067	0.581	11.930	1.871	4.107	7.683	1.960	5.122	5.943	2.249	2.500	1.5
NPPHX-068	0.599	11.648	1.871	4.107	7.683	1.955	5.122	5.923	2.247	2.500	1.5
NPPHX-069	0.616	11.578	1.875	4.114	7.714	1.961	5.143	5.947	2.249	2.500	1.5
NPPHX-070	0.589	11.648	1.869	4.099	7.661	1.952	5.107	5.926	2.249	2.500	1.5
NPPHX-071	0.733	11.912	1.871	4.240	7.932	1.998	5.288	6.141	2.247	2.484	1.5
NPPHX-072	1.299	11.718	1.875	4.075	7.641	1.924	5.094	5.910	2.122	2.363	1.5
NPPHX-073	1.337	12.000	1.870	4.103	7.672	1.952	5.115	5.935	2.122	2.457	1.5
NPPHX-074	0.617	11.930	1.875	4.075	7.641	1.989	5.094	5.910	2.247	2.500	1.5
NPPHX-075	0.836	11.648	1.625	4.064	6.602	1.665	4.397	5.115	2.247	2.498	1.5
NPPHX-076	0.590	11.789	1.875	4.067	7.626	1.946	5.084	5.899	2.249	2.500	1.5
NPPHX-077	0.724	11.648	1.871	4.095	7.661	1.950	5.108	5.926	2.247	2.490	1.5
NPPHX-078	0.625	11.648	1.870	4.083	7.635	1.941	5.090	5.886	2.247	2.500	1.5
NPPHX-079	0.586	11.930	1.875	4.083	7.655	1.991	5.104	5.902	2.249	2.492	1.5
NPPHX-080	0.590	11.930	1.875	4.087	7.663	1.950	5.103	5.907	2.249	2.492	1.5
NPPHX-081	0.737	11.472	1.750	4.122	7.213	1.833	4.809	5.579	2.247	2.498	1.5
NPPHX-082	0.608	11.718	1.875	4.091	7.670	1.949	5.108	5.936	2.249	2.500	1.5
NPPHX-083	1.175	11.771	1.875	4.099	7.685	1.953	5.123	5.927	2.249	2.500	1.5
NPPHX-084	0.581	11.648	1.870	4.107	7.679	1.959	5.114	5.940	2.247	2.492	1.5
NPPHX-085	0.581	11.930	1.874	4.064	7.615	1.940	5.076	5.890	2.247	2.469	1.5
NPPHX-086	0.733	11.472	1.748	4.216	7.369	1.873	4.913	5.700	2.247	2.475	1.5
NPPHX-087	0.724	11.930	1.875	4.232	7.934	2.024	5.289	6.140	2.216	2.371	1.5
NPPHX-088	0.679	11.718	1.869	4.247	7.938	1.997	5.292	6.120	2.249	2.477	1.5
NPPHX-089	1.310	11.455	1.868	4.099	7.657	1.926	5.104	5.763	2.249	2.455	1.5

Design Tag	Pitch Ratio	Pillow Height	WHR	Weld Height	Weld Width	x_1	x_2	x_3	y_1	y_2	y_3
	-	mm	-	mm	mm	mm	mm	mm	mm	mm	mm
NPPHX-090	0.733	11.648	1.869	4.114	7.690	1.942	5.127	5.948	2.247	2.500	1.5
NPPHX-091	1.328	11.789	1.873	4.208	7.882	1.980	5.249	6.192	2.122	2.346	1.5
NPPHX-092	1.346	11.578	1.620	4.071	6.595	1.661	4.396	5.101	2.122	2.457	1.5
NPPHX-093	0.656	11.930	1.875	4.107	7.699	1.964	5.133	6.016	2.247	2.500	1.5
NPPHX-094	0.635	11.648	1.874	4.122	7.725	1.971	5.150	5.960	2.249	2.500	1.5
NPPHX-095	0.580	11.789	1.875	4.067	7.626	1.943	5.084	5.901	2.247	2.492	1.5
NPPHX-096	0.608	11.789	1.870	4.103	7.672	1.955	5.115	5.935	2.247	2.498	1.5
NPPHX-097	1.364	11.578	1.995	4.110	8.201	2.063	5.451	6.354	2.247	2.469	1.5
NPPHX-098	0.805	11.472	1.746	4.216	7.361	1.847	4.907	5.694	2.247	2.500	1.5
NPPHX-099	0.616	11.648	1.874	4.083	7.651	1.945	5.101	5.909	2.249	2.500	1.5
NPPHX-100	0.617	11.930	1.874	4.107	7.695	1.963	5.130	5.933	2.247	2.500	1.5
NPPHX-101	0.739	11.455	1.745	4.193	7.316	1.845	4.872	5.516	2.247	2.498	1.5
NPPHX-102	1.299	11.930	1.875	4.224	7.919	1.992	5.279	6.128	2.218	2.371	1.5
NPPHX-103	0.739	11.490	1.746	4.200	7.333	1.849	4.884	5.529	2.247	2.490	1.5
NPPHX-104	0.589	11.894	1.873	4.114	7.706	1.958	5.137	5.963	2.249	2.492	1.5
NPPHX-105	0.635	11.789	1.871	4.103	7.676	1.958	5.117	5.938	2.247	2.498	1.5
NPPHX-106	0.616	11.789	1.871	4.075	7.625	1.945	5.083	5.958	2.249	2.500	1.5

Bibliography

[1] U. E. I. Adminstration, "Annual Energy Outlook 2016 with Projections to 2040," U.S. Department of Energy, Washington, DC, 2016.

[2] R. K. Shah and D. P. Sekulic, Fundamentals of Heat Exchanger Design, New Jersey: John Wiley & Sons, Inc., 2003.

[3] Z. H. Ayub, "Plate Heat Exchanger Literature Survey and New Heat Transfer and Pressure Drop Correlations for Refrigerant Evaporators," *Heat Transfer Engineering*, vol. 24, no. 5, pp. 3-16, 2003.

[4] M. Khan and M. Chyu, "Evaporation in Flooded Corrugated Plate Heat Exchangers with Ammonia and Ammonia/Miscible Oil, RP-1352," American Society of Heating, Refrigerating and Air-Conditioning Engineers, Inc., Atlanta, GA, USA, October, 2010.

[5] B. Palm and J. Claesson, "Plate Heat Exchangers: Calculation Methods for Single- and Two-Phase Flow," *Heat Transfer Engineering*, vol. 27, no. 4, pp. 88-98, 2006.

[6] G. A. Longo and A. Gasparella, "Heat Transfer and Pressure Drop during HFC Refrigerant Vaporisation Inside a Brazed Plate Heat Exchanger," *International Journal of Heat and Mass Transfer*, vol. 50, no. 25-26, pp. 5194-5203, 2007.

[7] D. Han, K. Lee and Y. Kim, "Experiments on the Characteristics of Evaporation of R410A in Brazed Plate Heat Exchangers with Different Geometric Configurations," *Applied Thermal Engineering,* vol. 23, no. 10, pp. 1209-1225, 2003.

[8] H. Arima, J. H. Kim, A. Okamoto and Y. Ikegami, "Local Boiling Heat Transfer Characteristics of Ammonia in a Vertical Plate Evaporator," *International Journal of Refrigeration,* vol. 33, pp. 359-370, 2010.

[9] Y. Y. Hsieh and T. F. Lin , "Saturated Flow Boiling Heat Transfer and Pressure Drop of Refrigerant R-410A in a Vertical Plate Heat Exchanger," *International Journal of Heat and Mass Transfer,* vol. 45, no. 5, pp. 1033-1044, 2002.

[10] C. B. Panchal, D. L. Hillis and A. Thomas, "Convective Boiling of Ammonia and Freon 22 in Plate Heat Exchangers," 1983.

[11] F. Táboas, M. Vallès, M. Bourouis and A. Coronas, "Flow Boiling Heat Transfer of Ammonia/Water Mixture in a Plate Heat Exchanger," *International Journal of Refrigeration,* vol. 33, no. 4, pp. 695-705, 2010.

[12] B. Thonon, R. Vidil and C. Marvillet, "Recent Research and Developments in Plate Heat Exchangers," *Journal of Enhanced Heat Transfer,* vol. 2, no. 1-2, pp. 149-155, 1995.

[13] S. Palmer, W. Payne and P. Domanski, "Evaporation and Condensation Heat Transfer Performance of Flammable Refrigerants in a Brazed Heat Exchanger," NISTIR 6541, Gaithersburg, MD, 2000.

[14] Y. Y. Yan and T. F. Lin, "Evaporation Heat Transfer and Pressure Drop of Refrigerant R-134a in a Plate Heat Exchanger," *Journal of Heat Transfer,* vol. 121, no. 1, pp. 118-127, 1999.

[15] Y. Y. Hsieh, L. J. Chiang and T. F. Lin, "Subcooled Flow Boiling Heat Transfer of R-134a and the Associated Bubble Characteristics in a Vertical Plate Heat Exchanger," *International Journal of Heat and Mass Transfer,* vol. 45, no. 9, pp. 1791-1806, 2002.

[16] Y. Y. Hsieh and T. F. Lin , "Evaporation Heat Transfer and Pressure Drop of Refrigerant R-410A Flow in a Vertical Plate Heat Exchanger," *Journal of Heat Transfer, ASME Transactions,* vol. 125, no. 5, pp. 852-857, 2003.

[17] J. H. Park and Y. S. Kim, "Experimental Study on R-134a Evaporation Heat Transfer Characteristics in Plate and Shell Heat Exchanger," in *The 4th International Symposium on HVAC,* Beijing, China, October 9-11, 2003.

[18] I. Kim, J. Park, Y. Kwon and Y. Kim, "Experimental Study on R-410A Evaporation Heat Transfer Characteristics in Oblong Shell and Plate Heat Exchanger," *Heat Transfer Engineering,* vol. 28, no. 7, pp. 633-639, 2007.

[19] M. G. Cooper, "Heat Flow Rates in Saturated Pool Boiling – A Wide Ranging Examination using Reduced Properties," Orlando, Florida, 1984.

[20] G. A. Longo, "Vaporisation of the Low GWP Refrigerant HFO1234yf Inside a Brazed Plate Heat Exchanger," *International Journal of Refrigeration,* vol. 35, no. 4, pp. 952-961, 2012.

[21] G. A. Longo, S. Mancin, G. Righetti and C. Zilio, "A New Model for Refrigerant Boiling Inside Brazed Plate Heat Exchangers," *International Journal of Heat and Mass Transfer*, vol. 91, pp. 144-149, 2015.

[22] D. Sterner and B. Sunden, "Performance of Plate Heat Exchangers for Evaporation of Ammonia," *Heat Transfer Engineering*, vol. 27, no. 5, pp. 45-55, 2007.

[23] B. Ouazia, "Evaporation Heat Transfer and Pressure Drop of HFC-134 Inside a Plate Heat Exchanger," New York, NY, November 11-16, 2001.

[24] E. Djordjevic and S. Kabelac, "Flow Boiling of R134a and Ammonia in a Plate Heat Exchanger," *International Journal of Heat and Mass Transfer*, vol. 51, no. 25-26, pp. 6235-6242, 2008.

[25] M. S. Khan, T. S. Khan, M. C. Chyu and Z. H. Ayub, "Evaporation Heat Transfer and Pressure Drop of Ammonia in a Mixed Configuration Chevron Plate Heat Exchanger," *International Journal of Refrigeration*, vol. 41, pp. 92-102, 2014.

[26] J. Huang, T. J. Sheer and M. Bailey-McEwan, "Heat Transfer and Pressure Drop in Plate Heat Exchanger Refrigerant Evaporators," *International Journal of Refrigeration*, vol. 35, pp. 325-335, 2012.

[27] F. Táboas, M. Vallès, M. Bourouis and A. Coronas, "Assessment of Boiling Heat Transfer and Pressure Drop Correlations of Ammonia/Water Mixture in a

Plate Heat Exchanger," *International Journal of Refrigeration,* vol. 35, no. 3, pp. 633-644, 2012.

[28] E. Lee, H. Kang and Y. Kim, "Flow Boiling Heat Transfer and Pressure Drop of Water in a Plate Heat Exchanger with Corrugated Channels at Low Mass Flux Conditions," *International Journal of Heat and Mass Transfer,* vol. 77, pp. 37-45, 2014.

[29] R. L. Amalfi, F. Vakili-Farahani and J. R. Thome, "Flow Boiling and Frictional Pressure Gradients in Plate Heat Exchangers: Part 2, Comparison of Literature Methods to Database and New Prediction Methods," *International Journal of Refrigeration,* vol. 61, pp. 185-203, 2016.

[30] D. Lee, D. Kim, S. Park, J. Lim and Y. Kim, "Evaporation Heat Transfer Coefficient and Pressure Drop of R-1233zd(E) in a Brazed Plate Heat Exchanger," *Applied Thermal Engineering,* vol. 130, pp. 1147-1155, 2018.

[31] W. Nusselt, "The Condensation of Steam on Cooled Surfaces," *Z. Ver. Deutsch. Ing.,* vol. 60, pp. 541-546, 569-575 (Translated into English by D.Fullarton, Chemical Engineering Fundamentals, vol. 1, no. 2, pp. 6-19, 1982)., 1916.

[32] L. Bromley, "Effect of Heat Capacity of Condensate," *Industrial Engineering Chemistry,* vol. 44, no. 12, pp. 2966-2969, 1952.

[33] W. Rohsenow, "Heat Transfer and Temperature Distribution in Laminar-Film Condensation," *Transactions of the ASME,* vol. 79, pp. 1645-1648, 1956.

[34] M. Chen, "An Analysis Study of Laminar Film Condensation, Part I - Flat Plates," *ASME Journal of Heat Transfer,* vol. 83, pp. 48-55, 1961.

[35] M. Shah, "A General Correlation for Heat transfer during Film Condensation Inside Pipes," *International Journal of Heat and Mass Transfer,* vol. 22, no. 3, pp. 547-556, 1979.

[36] L. Wang, B. Sundén and R. M. Manglik, Plate Heat Exchangers: Design, Applications, and Performance, Ashurst Lodge: WIT Press, 2007.

[37] Y. Yan, H. Lio and T. Lin, "Condensation Heat Transfer and Pressure Drop of Refrigerant R-134a in a Plate Heat Exchanger," *International Journal of Heat and Mass Transfer,* vol. 42, pp. 993-1006, 1999.

[38] W. Kuo, Y. Lie, Y. Hsieh and T. Lin, "Condensation Heat Transfer and Pressure Drop of Refrigerant R-410A Flow in a Vertical Plate Heat Exchanger," *International Journal of Heat and Mass Transfer,* vol. 48, pp. 5205-5220, 2005.

[39] S. J. Eckels and M. B. Pate, "An Experimental Comparison of Evaporation and Condensation Heat Tranfer Coefficients for HFC-134a and CFC-12," *Inernational Journal of Refrigeration*, vol. 14, pp. 70-77, 1991.

[40] L. Wang, R. Christensen and B. Suden, "An Experimental Investigation of Steam Condensation in Plate Heat Exchangers," *International Journal of Heat Exchangers,* vol. 1, no. 2, pp. 125-150, 2000.

[41] L. Boyko and G. Kruzhilin, "Heat Transfer and Hydraulic Resistance during Condensation of Steam in HorizontalTube and in a Bundle of Tubes," *International Journal of Heat and Mass Transfer*, vol. 10, no. 2, pp. 361-373, 1967.

[42] B. Thonon and A. Bontemps, "Condensation of Pure and Mixture of Hydrocarbons in a compact Heat Exchanger: Experiments and Modelling," *Heat Transfer Engineering*, vol. 23, no. 6, pp. 3-17, 2002.

[43] D. Han, K. Lee and Y. Kim, "The Characteristics of Condensation in Brazed Plate Heat Exchangers With Different Chevron Angles," *Journal of the Korean Physical Society*, vol. 43, no. 1, pp. 66-73, 2003.

[44] G. Longo, "Refrigerant R134a Condensation Heat Transfer and Pressure Drop Inside a Small Brazed Plate Heat Exchanger," *International Journal of Refrigeration*, vol. 31, pp. 780-789, 2008.

[45] G. Longo, "R410A Condensation Inside a Commercial Brazed Plate Heat Exchanger," *Experimental Thermal and Fluid Science*, vol. 33, pp. 284-291, 2009.

[46] G. Longo, "Heat Transfer and Pressure Drop During Hydrocarbon Refrigerant Condensation Inside a Brazed Plate Heat Exchanger," *International Journal of Refrigeration*, vol. 33, pp. 944-953, 2010.

[47] G. Longo, "Heat Transfer and Pressure Drop During HFC Refrigerant Saturated Vapour Condensation Inside a Brazed Plate Heat Exchanger," *International Journal of Mass and Heat Transfer*, vol. 53, no. 5-6, pp. 1079-1087, 2010.

[48] G. Longo and C. Zilio, "Condensation of low GWP Refrigerant HFC1234yf Inside a Brazed Plate Heat Exchanger," *International Journal of Refrigeration,* vol. 36, pp. 612-621, 2013.

[49] G. Longo, C. Zilio and G. Righetti, "Condensation of the low GWP Refrigerant HFC1234ze(E) Inside a Brazed Plate Heat Exchanger," *International Journal of Refrigeration*, vol. 38, pp. 250-259, 2013.

[50] G. A. Longo, S. Mancin, G. Righetti and C. Zilio, "HFC404A Condensation Inside a Small Brazed Plate Heat Exchanger: Comparison with the Low GWP Substitutes Propane and Propylene," *International Journal of Refrigeration,* vol. 81, pp. 41-49, 2017.

[51] G. Longo, G. Righetti and C. Zilio, "A New Model for Refrigeration Condensation Inside a Brazed Plate Heat Exchanger (BPHE)," in *Proceedings of the 15th International Heat Transfer Conference, IHTC-15*, Kyoto, Japan, 2014.

[52] G. A. Longo, G. Righetti and C. Zilio, "A New Computational Procedure for Refrigerant Condensation Inside Herringbone-type Brazed Plate Heat Exchangers," *Intenational Journal of Heat and Mass Transfer*, vol. 82, pp. 530-536, 2015.

[53] S. Mancin, D. Del Col and L. Rossetto, "Condensation of Superheated Vapour of R410A and R407C Inside Plate Heat Exchangers: Experimental Results and Simulation Procedure," *International Journal of Refrigeration,* vol. 35, no. 7, pp. 2003-2013, 2012.

[54] S. Mancin, D. Del Col and L. Rossetto, "R32 Partial Condensation Inside a Brazed Plate Heat Exchanger," *International Journal of Refrigeration,* vol. 36, no. 2, pp. 601-611, 2013.

[55] J. Mitrovic and R. Peterson, "Vapor Condensation Heat Transfer in a Thermoplate Heat Exchanger," *Chemical Engineering & Technology,* vol. 30, no. 7, pp. 907-919, 2007.

[56] J. Mitrovic and B. Maletic, "Numerical Simulation of Fluid Flow and Heat Transfer in Thermoplates," *Chemical Engineering & Technology,* vol. 34, no. 9, pp. 1439-1448, 2011.

[57] M. Piper, A. Olenberg, J. M. Tran and E. Y. Kenig, "Determination of the Geometric Design Parameters of Pillow-Plate Heat Exchangers," *Applied Thermal Engineering,* vol. 91, pp. 1168-1175, 2015.

[58] M. Piper, A. Olenberg, J. M. Tran and E. Y. Kenig, "Numerical Investigation of Turbulent Forced Convection Heat Transfer in Pillow Plates," *International Journal of Heat and Mass Transfer,* vol. 94, pp. 516-527, 2016.

[59] M. Piper, A. Zibart and E. Y. Kenig, "New Design Equations for Turbulent Forced Convection Heat Transfer and Pressure Loss in Pillow-Plate Channels," *International Journal of Thermal Sciences*, vol. 120, pp. 459-468, 2017.

[60] J. M. Tran, M. Linnemann, M. Piper and E. Y. Kenig, "On the Coupled Condensation-Evaporation in Pillow-Plate Condensers: Investigation of Cooling Medium Evaporation," *Applied Thermal Engineering*, vol. 124, pp. 1471-1480, 2017.

[61] V. Gullapalli, Estimation of Thermal and Hydraulic Characterisitcs of Compact Brazed Plate Heat Exchangers, Lund, Sweden: Doctoral Thesis, Department of Energy Sciences, Faculty of Engineering, Lund University, 2013.

[62] S. G. Kandlikar and R. K. Shah, "Asymptotic Effectiveness-NTU Formulas for Multipass Plate Heat Exchangers," *Journal of Heat Transfer*, vol. 111, pp. 314-321, 1989.

[63] T. Zaleski and K. Klepacka, "Approximate Method of Solving Equations for Plate Heat Exchangers," *International Journal of Heat and Mass Transfer* , vol. 35, no. 5, pp. 1125-1130, 1992.

[64] M. C. Georgiadis and S. Macchietto, "Dynamic Modelling and Simulation of Plate Heat Exchangers under Milk Fouling," *Chemical Engineering Science*, vol. 55, no. 9, pp. 1605-1619, 2000.

[65] C. Ribeiro and M. Andrade, "An Algorithm for Steady-State Simulation of Plate Heat Exhcnagers," *Journal of Food Engineering*, vol. 53, pp. 59-66, 2002.

[66] J. A. Gut and J. M. Pinto, "Modeling of Plate Heat Exchangers with Generalized Configurations," *International Journal of Heat and Mass Transfer,* vol. 46, pp. 2571-2585, 2003.

[67] J. M. Corberán, P. Fernandez De Cordoba, S. Ortuna, V. Ferri and P. Montes, "Detailed Modelling of Evaporators and Condensers," International Refrigeration and Air Conditioning Conference at Purdue, July 25-28, paper #485, 2000.

[68] H. Qiao, V. Aute, H. Lee, K. Saleh and R. Radermacher, "A New Model for Plate Heat Exchangers with Generalized Flow Configurations and Phase Change," *International Journal of Refrigeration,* vol. 36, no. 2, pp. 622-632, 2013.

[69] R. Shah, "Advances in science and technology of compact heat exchangers," *Heat Transfer Engineering,* vol. 27, no. 5, pp. 3-22, 2006.

[70] O. Abdelaziz, V. Aute, S. Azarm and R. Radermacher, "Approximation-Assisted Optimization for novel compact heat exchangers," *HVAC&R Research,* vol. 16, no. 5, pp. 707-728, 2010.

[71] T. Xioping, L. Huahe and L. Xiangfei, "CFD simulation and experimental study on airside performance for MCHX," in *International Refrigeration and Air Conditioning Conference,* Lafayette, IN, 2010.

[72] D. Taler and P. Oclon, "Thermal contact resistance in plate fin-and-tube heat exchangers, determined by experimental data and CFD simulations," *International Journal of Thermal Sciences*, vol. 84, pp. 309-322, 2014.

[73] D. Bacellar, O. Abdelaziz, V. Aute and R. Radermacher, "Novel heat exchanger design using Computational Fluid Dynamics and Approximation Assisted Optimization," in *ASHRAE Winter Conference*, Chicago, 2015.

[74] A. Gholami, M. A. Wahid and H. A. Mohammed, "Heat transfer enhancement and pressure drop for fin-and-tube compact heat exchangers with wavy rectangular winglet-type vortex generators," *International Communications in Heat and Mass Transfer*, vol. 54, p. 132–140, 2014.

[75] L. Li, X. Du, L. Yang, Y. Xu and Y. Yang, "Numerical simulation on flow and heat transfer of fin structure in air-cooled heat exchanger," *Applied Thermal Engineering*, vol. 59, pp. 77-86, 2013.

[76] V. Singh, O. Abdelaziz, V. Aute and R. Radermacher, "Simulation of air-to-refrigerant fin-and-tube heat exchanger with CFD-based air propagation," *Internationa Journal of Refrigeration*, vol. 34, pp. 1883-1897, 2011.

[77] H. Wu, Y. Gong and X. Zhu, "Air flow and heat transfer in louver-fin round-tube heat exchangers," *Journal of Heat Transfer*, vol. 129, pp. 200-300, 2007.

[78] J. Wu and W. Tao, "Investigation on laminar convection heat transfer in fin-and-tube heat exchanger in aligned arrangement with longitudinal vortex

generator from the viewpoint of field synergy principle," *Applied Thermal Engineering,* vol. 27, pp. 2609-2617, 2007.

[79] O. Abdelaziz, Development of multi-scale, multi-physics, analysis capability and its application to novel heat exchanger design and optimization, College Park, MD: PhD Thesis presented to the Department of Mechanical Engineering at the University of Maryland, 2009.

[80] R. Hilbert, G. Janiga, R. Baron and D. Thevenin, "Multi-objective shape optimization of a heat exchanger using parallel genetic algorithms," *International Journal of Heat and Mass Transfer,* vol. 49, p. 2567–2577, 2006.

[81] D. H. Fax and J. R. R. Mills, "Generalized Optimal Heat-Exchanger Design," *Americation Society of Mechanical Engineers Transactions,* vol. 79, no. 3, pp. 653-658, 1957.

[82] C. Hedderich, M. Kellher and G. Vanderplaats, "Design and optimization of air-cooled heat exchangers," *Journal of Heat Transfer,* vol. 104, no. 4, pp. 683-690, 1982.

[83] L. Huang, V. Aute and R. Radermacher, "A survey of optimization formulations and techniques for the design of heat exchangers using lower GWP refrigerants," in *ASHRAE Winter Conference*, Chicago, IL, 2015.

[84] M. Hestenes, "Multiplier and gradient methods," *Journal of Optimization, Theory and Applications,* vol. 4, no. 5, pp. 303-320, 1969.

[85] V. Aute, "Editorial, Topical Section on Optimization in HVAC&R, Mathematical Optimization - The Systematic Approach to Finding Low-Cost and Energy-Efficient System Designs," *HVAC&R Research,* vol. 18, no. 5, pp. 831-833, 2012.

[86] K. Deb, "Genetic algorithms for optimization," KanGAL Report No. 2001002, Kanpur, India, 2001.

[87] D. E. Goldberg, Genetic Algorithms in Search Optimization and Machine Learning, Addison-Wesley Publishing Company Inc., 1989.

[88] Y. Jaluria, Design and Optimization of Thermal Systems, Taylor & Francis Group., 2007.

[89] J. Arora, Introduction to Optimum Design, 3rd Ed., Academics Press., 2011.

[90] N. Cressie, Statistics for Spatial Data, New York: John Wiley & Sons, 1993.

[91] M. McKay, R. Beckman and W. Conover, "A comparison of three methods for selecting values of input variables in the analysis of output from a computer code," *Technometrics,* vol. 21, pp. 239-245, 1979.

[92] M. Shewry and H. Wynn, "Maximum entropy sampling," *Journal of Applied Statistics*, vol. 14, no. 2, pp. 165-170, 1987.

[93] K. Saleh, V. Aute, R. Radermacher and S. Azarm, "Chevron Plate Heat Exchanger Optimization Using Efficient Approximation-Assisted Multi-

Objective Optimization Techniques," *HVAC&R Research,* vol. 19, no. 7, pp. 788-799, 2013.

[94] ASME, Standard for verification and validation in Computational Fluid Dynamics and heat transfer - ASME V&V 20-2009, New York: ASME, 2009.

[95] F. Incropera, D. Dewitt, T. Bergman and L. A.S., Fundamental of heat and mass transfer, Wiley, 2011.

[96] S. V. Patankar, Numerical Heat Transfer and Fluid Flow, Hemisphere Publishing Corporation, 1980.

[97] ANSYS Inc., *ANSYS 17.0,* www.ansys.com, 2016.

[98] T. Shih and J. Zhu, "A new Reynolds stress algebraic equation model," NASA Lewis Research Center, Cleveland, OH, 1994.

[99] T. Shih, W. Liou, A. Shabbir, Z. Yang and J. Zhu, "A new k-e eddy viscosity model for high Reynolds number turbulent flows - model development and validation," NASA Lewis Research Center, Cleveland, OH, 1994.

[100] U. Schumann, "Realizability of Reynolds-stress turbulence models," *Physics of Fluids,* vol. 20, no. 5, pp. 721-725, 1977.

[101] P. J. Roache, Verification and Validation in Computational Science and Engineering, Hermosa Publishers, 1998.

[102] W. Oberkampf and G. Trucano, "Verification and Validation in Computational Fluid Dynamics," *Progress in Aerospace Sciences,* vol. 38, pp. 209-272, 2002.

[103] L. Eca and M. Hoekstra, "An Evaluation of Verification Procedures for CFD Applications," in *24th Symposium on Naval Hydrodynamics*, Fukuoka, Japan, 8-13 July, 2002.

[104] D. Pelletier and P. J. Roache, Verification and Validation of Computational Heat Transfer, Second Edition ed., Wiley , 2006.

[105] P. J. Roache, "Error Bars for CFD," in *AIAA Paper 2003-0408, AIAA 41st Aerospace Sciences Meeting*, Reno, Nevada, 2003.

[106] L. Piegl and W. Tiller, The NURBS book, New York: Springer, 1995.

[107] D. Bacellar, Airside Passive Heat Transfer Enhancement, using Multi-scale Analysis and Shape Optimization, for Compact Heat Exchangers with Small Characteristic Lengths, PhD Thesis: University of Maryland, USA, 2016.

[108] H. Hamad, "A new metric for measuring metamodels quality-to-fit for deterministic simulations," in *Proceedings of the 2006 Winter Simulation Conference*, 2006.

[109] F. Dittus and L. Boelter, "Heat Transfer in Automobile Radiators of The Tubular Type," *International Communications in Heat and Mass Transfer,* vol. 12, no. 1, pp. 3-22, 1985.

[110] T. W. Simpson, J. D. Peplinski, P. N. Koch and J. K. Allen, "Metamodels for Computer-based Engineering Design: Survey and Recommendations," *Engineering with Computers,* vol. 17, no. 2, pp. 129-150, 2001.

[111] K. H. Saleh, V. Aute, R. Radermacher and S. Azarm, "Plate Heat Exchanger Optimization Using Different Approximation Assisted Multiobjective Optimization Techniques," Purdue, 2012.

[112] R. Eldeeb, V. Aute and R. Radermacher, "A Model for Performance Prediction of Brazed Plate Condensers and Alternative Lower GWP Refrigerants," West Lafayette, Indiana, USA, 2014.

[113] E. W. Lemmon, M. L. Huber and M. O. McLinden, "NIST Standard Reference Database 23: Reference Fluid Thermodynamic and Transport Properties-REFPROP, Version 9.1," National Institute of Standards and Technology, 2013.

[114] A. Muley and R. M. Manglik, "Experimental Study of Turbulent Flow Heat Transfer and Pressure Drop in a Plate Heat Exchanger with Chevron Plates," *Journal of Heat Transfer,* vol. 121, no. 1, pp. 110-117, 1999.

[115] R. Lockhart and R. Martinelli, "Proposed Correlation of Data for Isothermal Two-Phase, Two-Component Flow in Pipes," *Chemical Engineering Progress,* vol. 45, no. 1, pp. 39-48, 1949.

[116] M. Beshr, Steady State Modeling and Optimization for Performance and Environmental Impact of Advanced Vapor Compression Systems, PhD Thesis: University of Maryland, USA, 2016.

[117] M. Beshr, J. Bush, V. Aute and R. Radermacher, "Steady State Testing and Modeling of a CO2 Two-Stage Refrigeration System with Mechanical

Subcooler," in *12th IIR Gustav Lorentzen Conference on Natural Refrigerants*, UK, 2016.

[118] M. K. Bassiouny and H. Martin, "Flow Distribution and Pressure Drop in Plate Heat Exchangers - I," *Chem. Eng. Sci.,* vol. 39, pp. 693-700, 1984.

[119] J. K. Jensen, M. R. Kaern, T. S. Ommen, W. B. Markussen, L. Reinholdt and B. Elmegaard, "Effect of Liquid/Vapour Maldistribution on the Performance of Plate Heat Exchanger Evaporators," in *Proceedings of the 24th IIR International Congress of Refrigeration*, Yokohama, Japan, 2015.

[120] B. Maletic, Modelling and Numerical Analysis of Fluid Flow and Heat Transfer in Thermoplates, Paderbon (PhD Thesis): University of Paderborn, 2009.

[121] L. Huang, V. Aute and R. Radermacher, "A model for air-to-refrigerant microchannel condensers with variable tube and fin geometries," *International Journal of Refrigeration*, vol. 40, pp. 269-281, 2014.

[122] T. H. Shih, W. W. Liou, A. Shabbir, Z. Yang and J. Zhu, "A new Eddy Viscosity Model for High Reynolds Number Turbulent Flows," *Computers and Fluids*, vol. 24, no. 3, pp. 227-238, 1995.